A Study Investigating Copper Smelting Remains From San Bartolo, Chile

by

Antonella I. Alunni

Submitted to the Department of Materials Science and Engineering in Partial Fulfillment of the Requirements for the Degree of

Bachelor of Science

at the

Massachusetts Institute of Technology

June 2006

Signature of Author .....
Department of Materials Science and Engineering
May 18, 2006

Certified by .....
Heather N. Lechtman
Professor of Archaeology and Ancient Technology
Thesis Supervisor

Accepted by .....
Caroline A. Ross
Professor of Materials Science and Engineering
Chair, Departmental Undergraduate Committee

Table of Contents

LIST OF FIGURES AND TABLES

Figure 14. Site map of El Establecimiento in San Bartolo. Pieces of slag and the portion of furnace wall were collected from Sector Cementerio Histórico, and pieces of ore were collected from Sector de las *Qollqas* (after Castro et al. 2003).

Figure 15. MIT 5313. Four views of the object, showing bulbous and knobby components with cavities in between the contiguous globular parts.

Figure 16. MIT 5313. Two views, showing the pale green color of the object.

Figure 17. MIT 5313. Line drawing showing four views.

Figure 18. MIT 5313. Line drawing showing locations and orientations of samples removed.

Figure 19. MIT 5313-A. Photomicrograph of ore sample taken with a metallurgical microscope, 200x, etched with K_2CrO_7. Cross-polarized light; arrows point to red cuprous oxide grains.

Figure 20. MIT 5313-A. Photomicrograph of ore sample taken with a metallurgical microscope, 500x, etched with K_2CrO_7. Copper grains displaying annealing twins.

Figure 21. MIT 5313-A. Photomicrograph of ore sample taken with a metallurgical microscope, 500x, etched with K_2CrO_7. Copper grain exhibiting slip planes.

Figure 22. MIT 5313-A. Photomicrograph of ore sample taken with a metallurgical microscope, 500x, etched with K_2CrO_7. Copper grain exhibiting a double-grain boundary, as indicated by the arrow.

Figure 23. MIT 5313-A. Color image analysis with an electron microanalyzer identifying an assemblage of granitic grains, copper, and pores.

Figure 24. MIT 5319. Two views of the object, which is subrounded, trapezoidal, and generally flat, except for a few bumps and bulges on Face A.

Figure 25. MIT 5319. Two views, showing the green color of the object.

Figure 26. MIT 5319. Line drawing showing sandy accretions that were removed.

Figure 27. MIT 5319. Line drawing showing locations and orientations of samples removed for electron microanalysis.

Figure 28. MIT 5319-A and MIT 5319-B. Line drawing of the two specimens, showing the samples divided into zones. Zone 1: lustrous veins of primary copper sulfide containing some cuprous oxide weathering product, intergrowth of copper sulfide and copper sulfate, and lead sulfide. Zone 2: intergrowth of copper sulfide and

barium-strontium sulfate. Zone 3: chloride weathering product of the primary copper sulfide vein.

Figure 29. MIT 5318. Two views of the object, showing rounded surfaces, chipped surfaces, and vesicles; arrow points to corroded copper prill.

Figure 30. MIT 5318. Two views showing green, corroded copper prills and red oxide material.

Figure 31. MIT 5318. Line drawing showing red oxide material and relatively large, exposed copper prills.

Figure 32. MIT 5318. Line drawing showing location and orientation of samples removed.

Figure 33. MIT 5318-A. Polished cross-section; sample exhibits four zones. Going from Zone 1 to Zone 4, pore size decreases, but quantity and size of copper prills increase.

Figure 34. MIT 5318-A. Photomicrograph of slag sample taken with a metallurgical microscope, 200x, cross-polarized light. Zone 1 (see Fig. 33). Inclusion of cuprous oxide, located on edge of large pore, appears red.

Figure 35. MIT 5318-A. Photomicrograph of slag sample taken with a metallurgical microscope, 50x, as-polished. Copper prill and the phases surrounding it: (a) copper, (b) thin cuprous oxide "rind," (c) copper sulfide matte, and (d) glassy matrix.

Figure 36. MIT 5316. Two views, showing the burnt sienna and dark brown colors of the object.

Figure 37. MIT 5316. Two views of the object, showing conchoidal features at the top, fused rocky material in the center, and rounded features at the bottom.

Figure 38. MIT 5316. Side view of the object, showing conchoidal features on top, fused rocky material in the center, and rounded features on the bottom.

Figure 39. MIT 5316. Line drawing showing three views of the object and location of the band of earthy material.

Figure 40. MIT 5316. Line drawing showing location and orientation of samples removed.

Figure 41. MIT 5316-A. Photomicrograph of slag sample taken with a metallurgical microscope, 100x, as-polished. Bright orange, copper prill surrounded by a thin rind of cuprous oxide, which is in turn surrounded by a region of bright blue copper sulfide matte. The prill formed within a glassy matrix.

Figure 42. MIT 5316-A. Photomicrograph of slag sample taken with a metallurgical microscope, 500x, as-polished, plane-polarized light. At this magnification, copper sulfide prills appear as tiny white specks scattered in a glassy matrix. The matrix is characterized by alternating bands of red and dark blue color.

Figure 43. MIT 5316-B4. Thermal alteration test: standard sample, not subjected to heat, exhibiting sharp and angular edges.

Figure 44. MIT 5316-C3. Thermal alteration test: sample held at 800 degrees C for 10 minutes, resulting in loss of luster on the surfaces but no gross morphological changes.

Figure 45. MIT 5316-B1. Thermal alteration test: sample held at 900 degrees C for 10 minutes, resulting in dramatic wrinkling on the surfaces of the sample.

Figure 46. MIT 5316-D3. Thermal alteration test: sample held at 1000 degrees C for 10 minutes, resulting in continued wrinkling on the surfaces of the sample.

Figure 47. a. MIT 5316-C1. Thermal alteration test: sample held at 1050 degrees C for 10 minutes, at which point surface sweating occurred. Sample displays continued wrinkling.
b. MIT 5316-B3. Thermal alteration test: sample held at 1075 degrees C for 10 minutes, at which point the sample slumped. As a result, the sample buckled in on itself, and its edges became rounded.

Figure 48. a. MIT 5316-E1. Thermal alteration test: sample held at 1100 degrees C for 5 minutes, at which point the sample slumped completely.
b. MIT 5316-D2. Thermal alteration test: sample held at 1125 degrees C for 10 minutes, at which point the sample melted.

Figure 49. Ternary phase diagram of system MnO-Al_2O_3-SiO_2 (Snow 1943). The composition of the once-molten slag (MIT 5316; see Table 2) is plotted in red. The concentrations of Fe_2O_3, MgO, CaO, Na_2O, K_2O, TiO_2, and P_2O_5 were added to the concentration of Al_2O_3. Using this bulk value for the component oxides, the melting point of the slag is 1168 degrees C.

Figure 50. MIT 5320. Two views of the object. Face A displays the slag-coated interior of the furnace wall, and Face B displays the ceramic exterior of the furnace wall.

Figure 51. MIT 5320. Two side views of the object, exhibiting three zones. Zone A is a largely unaltered ceramic zone that corresponds with the exterior of the furnace wall, zone B is a partially heat-altered intermediate zone, and zone C is a highly heat altered zone that corresponds with the interior of the furnace wall.

Figure 52. MIT 5320. A top view of the object on the left, and a bottom view of the object on the right. Both views exhibit three zones. Zone A is a largely unaltered

ceramic zone that corresponds with the exterior of the furnace wall, zone B is a partially heat-altered intermediate zone, and zone C is a highly heat altered zone that corresponds with the interior of the furnace wall.

Figure 53. MIT 5320. Face A, the black interior of the furnace wall with white arrows pointing at copper prills. Face B, the earth-colored exterior of the furnace wall.

Figure 54. MIT 5320. Top view, showing the black, highly heat-altered interior (zone C) and the exterior (zone A) of the furnace wall.

Figure 55. MIT 5320. Line drawing showing locations and orientations of samples removed.

Figure 56. MIT 5320-B. As-polished. Furnace wall showing progression of heat alteration, where zone C appears most affected and zone A appears to be least affected by heat.

a. Photomicrograph taken with a metallurgical microscope, 50x, as-polished. Unaltered zone.
b. Photomicrograph taken with a metallurgical microscope, 50x, as-polished. Intermediate zone.
c. Photomicrograph taken with a metallurgical microscope, 50x, as-polished. Strongly heat-altered zone.

Figure 57. MIT 5320-A. Photomicrograph taken with a metallurgical microscope, 200x, as-polished. Interior of the furnace wall, zone C. Copper prill surrounded by a copper oxide rind, which is in turn surrounded by a copper sulfide matte. In the upper right corner, a prill of copper sulfide matte.

Table 1. Metal assay results for two pieces of ore and two pieces of slag.

Table 2. ICP-OES results for two pieces of ore and two pieces of slag.

Table 3. INAA results for two pieces of ore and two pieces of slag.

Table 4. Electron beam microprobe identification of various colored features observed with the petrographic microscope.

Table 5. Results of heating samples of glassy slag from MIT 5316.

INTRODUCTION

Research on the metallurgy of archaeological artifacts has focused primarily on the examination of objects to reveal their design, their composition, the properties of the material people selected to achieve the design, and the fabrication processes used in managing the metal to produce the end product. Recently that focus has begun to broaden, and archaeologists are taking a step back to investigate the earliest stages of prehistoric metal processing that precede object manufacture, namely ore mining and extractive metallurgy. However, little archaeological work on mining and extraction has been accomplished to date, in part because so few metal processing sites have been identified. These sites are very difficult to find because of the lack of standing architecture, particularly smelting installations. Prehistoric smelting furnaces tend to be small and are either excavated beneath the ground surface or are above ground but made of impermanent materials.

I was fortunate to obtain a small corpus of surface-collected smelting materials from the Inka copper smelting site of San Bartolo, Chile, even though this site has not undergone excavation or systematic surface collection. Despite these constraints, this thesis provides significant results about Inka extractive metallurgy that took place at San Bartolo.

Problem Statement

This thesis examines a corpus of material associated with metallurgical processes recovered from the archaeological site of San Bartolo, Chile. The site was utilized by the Inka

prior to the Spanish invasion of the Andes in the third decade of the sixteenth century. This corpus includes: small, smooth, gray, heat-altered artifacts, containing bits of metal and charcoal, that resemble metallurgical slag; small, brown, glassy artifacts, with bits of metal, that resemble metallurgical slag; small, green, rock-like artifacts that resemble metallic ore; and a small block of heat-altered, pink clay that might be a section of furnace wall. Analyses of these materials have led to hypotheses regarding copper smelting technologies that are revealed in the archaeological remains generated by metalworkers at this site. This is the first study carried out on surface-collected material from San Bartolo that investigates site data and archaeological evidence from a metallurgical standpoint.

Research Goals

The fundamental goal of this research is to understand the metallurgical processes carried out by the Inka at San Bartolo through study of an assortment of surface-collected artifacts that include slags of various compositions and morphologies, metallic ore, and heat-altered clay resembling a portion of furnace wall. The artifacts in this corpus are all likely features of a smelting furnace site. This research focuses on the analysis of these remains to establish whether smelting took place at the site and, if so, to characterize this stage of metal production.

Extractive Metallurgy: Smelting

Smelting is a form of extractive metallurgy that proceeds through several stages (which may vary depending on the types of ore that are smelted) and ultimately results in the winning of the particular metal contained in the ore being smelted. Mined ore is percussively crushed to a

size that facilitates liberation of the metallic mineral component from the rock gangue. During ore processing, the gangue is discarded while the valuable mineral is separated manually. In some circumstances, a preliminary heat treatment, roasting, may follow to render the ore more friable, to chemically convert sulfides, chlorides, and carbonates to oxides while driving off water, and ultimately to reduce the energy input needed in smelting. This is followed by the smelting operation.

Smelting refers to the chemical reduction of a metallic ore and to the physical separation of the won metal from slag, the smelting waste product that comprises fused silica that originates from remnants of the gangue, and metallic oxides. The slag serves to collect impurities such as minor elements in the ore, gangue (rocky, non-metallic mineral), furnace lining inclusions, charcoal and ash. In furnace smelting, fuel, usually charcoal, is charged into the furnace and burned to generate carbon monoxide, which is necessary to create the needed reducing environment. Ore, which is mixed with the charcoal, is introduced to the furnace with or without flux. Flux, such as hematite or limonite, is a component of the charge that facilitates slag formation. The direct smelting process may be illustrated through the reduction reaction of copper carbonate to copper metal, which is represented by the following equation:

$$\underset{\text{copper carbonate}}{CuCO_3} + \underset{\text{carbon monoxide}}{CO\uparrow} \xrightarrow{\text{heat}} \underset{\text{copper metal}}{Cu} + \underset{\text{carbon dioxide gas}}{2CO_2\uparrow}$$

The temperature and reducing conditions are maintained throughout the smelting process by adding fuel and ore (and flux) in the proper ratio as well as by adjusting air supply via natural draft, blowpipes, or bellows. The won metal subsequently coalesces into droplets (known as prills) that sink through the layer of slag and collect at the base of the furnace to form an ingot.

Since most ores contain metallic mineral in close association with undesirable earthy material and gangue, slag must be produced to remove these components. For instance, earthy, iron oxide (Fe_2O_3) present in a copper ore and gangue (largely SiO_2) need to be eliminated when smelting the ore. Heating the earthy material in an environment rich in carbon monoxide yields wüstite, FeO, which subsequently fuses with the silica (SiO_2) present in the rocky gangue to form the slag fayalite, $FeO.SiO_2$. The following equations illustrate the slag formation described above:

$$\underset{\text{iron oxide}}{Fe_2O_3} + CO \rightarrow \underset{\text{wüstite}}{FeO} + CO_2\uparrow \quad \text{and}$$

$$\underset{\text{wüstite}}{2FeO} + \underset{\text{silica}}{SiO_2} \rightarrow \underset{\text{fayalite}}{2FeO.SiO_2}$$

Carbon monoxide will not reduce the sulfur in a sulfide mineral, yet the vast majority of metallic ores in the earth's crust are sulfides. Until recently, many scholars have argued that prehistoric peoples were unable to smelt sulfide ores to extract the metallic components. Clair Patterson (1971), a geologist, claimed that Andean communities never smelted sulfide ores of copper or of copper sulfarsenides. Historians of metallurgy, geologists, and archaeologists of the Old World assumed that in western Asia and in Europe the only option available to early metalworkers for extracting metal from sulfide ores was to use a two-step process: (1) roast the ore to drive off the sulfur as SO_2; (2) direct smelt the oxide ore produced during roasting, using a fuel that would produce CO (see Lechtman and Klein 1999 for a review of this literature).

Recent experiments have demonstrated that a straightforward process for extracting metal from sulfide ores is to cosmelt the sulfide with an oxide ore (Lechtman and Klein 1999;

Rostoker, Pigott and Dvorak 1989). In this process, the sulfur acts as the reducing agent, as illustrated in the following equation:

$$\underset{\text{copper carbonate}}{8\ CuCo_3} + \underset{\text{enargite}}{Cu_3AsS_4} \xrightarrow{\text{heat}} \underset{\text{Cu-As alloy}}{Cu,\ As} + \underset{\text{gas}}{4\ SO_2\uparrow} + \underset{\text{gas}}{8\ CO_2\uparrow}$$

The sulfur is oxidized and is eliminated as SO_2 gas.

Cosmelting is a one-step, direct smelting regime. It is highly likely that it was used in the Andes and elsewhere, since in mining the weathered products of primary sulfide ores, i.e., the oxides, mixtures of oxide and sulfide ore invariably and frequently occur. The two mineral types are charged together into the furnace. Metalworkers accustomed to direct smelting their ores would have approached cosmelting in the same way that they traditionally smelted oxide ores.

Smelting efficiency depends on the fluidity of the slag. Metal in the form of prills may become trapped in a highly viscous slag, whereas prills sink freely through a slag of low viscosity (Fig. 1). Fayalite melts at the lowest temperature of all the $FeO.SiO_2$ combinations that form on smelting (Fig. 2). Thus it is an important slag because of both its low melting point and its low viscosity, which allows the denser metal to descend and form a pool or ingot of metal at the bottom of the crucible or furnace. The metal is easy to remove physically from the fayalite slag, which floats above it. When prills become trapped in viscous slag after solidification, the slag is crushed, and the metallic prills are separated, then melted together to form ingots. At this point, the metal can be further alloyed and shaped into objects by means of casting and/or cold or hot working.

The characterization of ore minerals and slag remains from San Bartolo will help reconstruct the prehistoric, copper smelting process that took place at the site.

ORE GEOLOGICAL CONTEXT

The Andean region is subdivided into several archaeological zones, three of which include: the northern Andes, comprising Venezuela, Colombia, and northern Ecuador; the central Andes, extending from central Ecuador to the southern limits of Peru; and the south-central Andes, which includes Bolivia, northern Chile, and northwest Argentina. The Andes is a rich, metallic ore-bearing region, which, to this day, provides a variety of minerals for gold, silver, copper, and tin production. Because this study focuses on copper smelting and Andean extractive metallurgy is based largely on copper, the mining and production of gold and silver will not be discussed.

Andean ore deposits are distributed throughout the central and south-central Andes (Fig. 3). The north coast of Peru within the central Andean Zone is replete with metallic ore deposits, particularly copper oxides and carbonates, which are easy to smelt. The highlands are rich in copper sulfide ores, including the sulfarsenides that are arsenic-rich. The region extending from Pilzhum, Ecuador, to the southern limits of Peru, and especially the central Peruvian sierra, is characterized by extensive and dense enargite deposits (Fig. 4), which are some of the richest deposits of copper sulfarsenide ore mineral in the world (Lechtman 2005).

In the Lambayeque Valley of northern coastal Peru, there are many small mines that were exploited for extractive metallurgical practices at Batán Grande (Fig. 5), a large, prehistoric smelting site on the Peruvian north coast (Lechtman 1976). These mines contain chalcopyrite, sphalerite, galena, oxides of copper, as well as cuprite veins (Lechtman 1976). The area between the Lambayeque Valley in the north and the Chao Valley further south is rich in copper mineral with deposits that contain malachite and cuprite ores (Lechtman 1976). The Virú Valley

abounds in malachite, chrysocolla, and copper sulfides (Lechtman 1976). There are more valleys along the north coast of Peru that are rich in copper oxides and carbonates, arsenopyrite, chalcopyrite, chrysocolla, and malachite. Prehistoric coastal miners exploited these plentiful oxide ore deposits as well as complex copper minerals containing arsenic.

The south-central Andean zone contains tin-rich ore deposits as well as some scattered and poor deposits of nickel ore (Fig. 3 and 4). The central Andes are characterized by igneous rocks, which produced tin-rich magmas as a result of geological processes in the area (Lechtman 2003). Consequently, some regions in the far south of Peru, northern Bolivia, and northwest Argentina are rich in cassiterite (SnO_2). In fact, some of the richest cassiterite deposits in the world are located in the tin fields of Bolivia and NW Argentina, which are the only significant sources of tin in the Andes (Lechtman 2003).

In the Lake Titicaca basin *altiplano*, native copper, cuprite, and malachite are abundant in mines (Lechtman 1976). Northern Chile is rich in copper deposits, and coastal areas tend to concentrate native copper. Small, sporadic ore deposits near La Paz, Bolivia, and at Copiapó, Chile, contain copper, arsenic, and nickel minerals, such as nickeline, gersdorffite, domeykite, and rammelsbergite (Lechtman 2003).

METALLURGY IN THE ANDEAN WORLD

Exploitation of Metallic Ores

Pre-hispanic metallurgy in the Andean region involved the extraction of metal from a variety of ores to produce copper, silver, and lead and a wide variety of alloys including copper-silver, copper-gold, copper-silver-gold, copper-arsenic bronze, and copper-tin bronze. Gold was mined from veins or placer deposits. Metallurgy in the New World first appeared in the central Andean zone, which includes the region from the present border of Colombia and Ecuador to the southern limit of Peru (Lechtman 1988). All Andean alloys were based on the metal copper, and its alloys with arsenic or tin (the bronzes) were the most prominent alloys during the later periods, from the Middle Horizon (ca. 800-1000 C.E.) to the period of Inka hegemony (ca. 1450-1532 C.E.). Fragments of thin copper foil excavated in the Lurín Valley, Peru, that date to the Initial Period (ca. 1800 B.C.E. to 800 B.C.E.) suggest that copper metallurgy began during the second millennium B.C.E. (Burger and Gordon 1998). Though few smelting sites have been studied in the south-central Andes, the earliest evidence of copper smelting in northern Chile has been found to date back to the Late Formative period, as early as 500 B.C.E. (Graffam et al. 1994).

The particular types of metal produced in any region of the Andes depended on the resources locally available as well as on the composition of the ores. Sulfidic ores of copper containing silver occur in the central Andes and were smelted initially to produce copper-silver alloys. Later copper-silver alloys were produced by melting together metallic copper and metallic silver. These alloys, developed during the Early Intermediate Period (ca. 0-800 C.E.),

were used because they were tough and because they developed enriched silver surfaces upon hammering and annealing, conferring a silver color to objects made from them (Lechtman 1988).

Copper-gold alloys, termed *tumbaga*, also developed during the Early Intermediate Period in northern Peru, were made by melting copper and gold together to form alloys of desired compositions (Lechtman 1988). Gold rich *tumbaga* was gold in color; copper-rich *tumbaga* was pink in color. Both alloy types retained flexibility after hammering—more so than the copper-silver alloys. In addition, copper-rich *tumbagas* developed an enriched gold surface upon chemical treatment so that objects made of such alloys appeared golden. Copper-gold alloys were used throughout the Andean zone for sheet metal, solder, and weld metal (Lechtman 1988).

Copper sulfarsenide ores, which are abundant in the north Peruvian highlands, were heavily utilized in the entire region north of Lake Titicaca and into Ecuador by 800 C.E., during the Middle Horizon (Lechtman 1988; Lechtman and Klein 1999; Shimada 1994) and continued in use even after the Inka conquest of this zone. These ores provided a convenient source of copper and arsenic with which to produce copper-arsenic alloys, or arsenic bronze. Arsenic bronze was the exclusive type of bronze produced in the central Andes prior to the Inka hegemony, and this variety of bronze alloy characterized bronze production in the central Andes for over 650 years (Lechtman 2003).

The south-central Andes, at the latitude, roughly, coincident with the southern shores of Lake Titicaca and comprising present-day Bolivia and northwest Argentina, is a region that contains some of the richest deposits of cassiterite ore in the world. These ores were smelted to produce tin, which was subsequently melted with metallic copper to yield copper-tin alloys (Graffam et al. 1994; Lechtman 1988; Shimada 1994). By the end of the Middle Horizon,

copper-tin bronze became the distinguishing alloy of the south-central Andes. Used for the production of ornaments, implements, and staffs of office, copper-tin bronze later became the favored alloy of the Inka state. The Inka disseminated tin bronze objects throughout their empire, including to the northern regions of Peru and Ecuador (Lechtman 1988). The Inka allowed some local production of copper-arsenic bronze to continue in the north, especially at Batán Grande (Shimada 1994), but production of arsenic bronze in the central Andes diminished during the Inka hegemony (Lechtman 1988).

It is important to note that the type of copper alloy produced in any region within the Andes varies with the specific ore minerals that the metalworkers had at their disposal, given geographic limitations. Thus, arsenic bronze was produced in the central Andes while tin bronze and tertiary (arsenic-nickel-tin) bronze were produced in the south-central zone (Fig. 4; Lechtman 2005). Until the establishment of the Inka Empire, there do not appear to have been long-distance exchanges of metallic ore minerals or of ingots between the central and the south-central regions (Lechtman and Macfarlane 2004).

Prehistoric Andean Extractive Metallurgy

The Central Andes

Evidence of prehistoric mining and ore smelting is difficult to find in the Andes, hence archaeologists have uncovered and studied only a limited number of extractive metallurgical sites. Two of the most thoroughly investigated and, thus, informative sites are Batán Grande in Peru and Ramaditas in Chile (Fig. 5).

Batán Grande was once a large Middle Horizon (ca. 850-1000 C.E.) smelting center for the production of copper-arsenic alloys (see Fig. 5) and is now a modern village in the La Leche Valley, just north of the Lambayeque Valley on the far north coast of Peru (Shimada et al. 1982). Archaeologists have reconstructed the primary prehistoric extractive metallurgical practices carried out there—copper-prill extraction and the smelting of copper ores and arsenic-rich ores—on the basis of evidence of furnace charging, slag grinding, prill extraction, and ingot production.

The mining-metallurgical complex of Cerro Blanco and Cerro de los Cementerios, which lies within the Batán Grande region, has been extensively studied by Izumi Shimada (Shimada 1994; Shimada and Merkel 1991; Shimada et al. 1982). Based on previous studies suggesting that the location of prehistoric Andean smelting sites was influenced more by the strength and direction of the wind than by the proximity of ore or fuel (Lechtman 1976), Shimada determined that the installations at this complex were well-suited for smelting because of the regularity of the wind, which blows hard enough in a constant direction to increase furnace draft and disperse noxious smelting fumes (Shimada et al. 1982). Metalworkers at Batán Grande had reasonable access to copper ore and fuel. A large prehistoric mine, yielding copper-lead-zinc oxides and sulfides is located at nearby Cerro Blanco, and the archaeologists found five copper ore mines in Cerro de los Cementerios (Shimada et al. 1982). Shimada and his crew also found a major prehistoric road that leads from Cerro de los Cementerios to the north highlands, a possible source for the arsenical ores that were crucial smelting additives (Shimada et al. 1983). The site is near a subtropical thorny forest that may have supplied charcoal used to fuel the smelting furnaces (Shimada et al. 1982).

More than 50 pear-shaped bowl furnaces (Fig. 6), with a primitive chimney and refractory mud lining, were partially or entirely excavated at Batán Grande (Shimada and Merkel

1991). Excavations revealed remains of large-scale and long-term metallurgical activity that lasted from 900 to 1532 C.E. Studies of ore remains suggest that the smelting charge was composed of a mixture of arsenic, copper, and iron ores (Shimada and Merkel 1991). The abundance of small pieces of hematite and limonitic concretions found in association with the furnaces are evidence of fluxes that served to facilitate the separation of metal and slag. Whole and fragmented refractory ceramic blowtube tips (Fig. 7) indicate that blowtubes, blown by lung power, were used to regulate the furnace temperature during smelting (Shimada et al. 1982).

Large quantities of finely crushed, prill-containing slag that accumulated in deep lenses indicate that the slag (Fig. 8) was typically highly viscous so that the copper-arsenic alloy prills were unable to sink to the bottom of the furnace to form ingots (Shimada et al. 1982). Evidence of *batanes*, large concave stone anvils, and *chungos*, dioritic, ovoid, rocking stones, which are characteristic of prehistoric slag crushing processes at Batán Grande, further suggest that smelting regularly involved prill-extraction from crushed, solid slag (Shimada et al. 1982). The metalworkers at Batán Grande used batán-chungo sets to crush slags produced during the smelting operations in order to remove manually metal prills trapped in the slag. The prills were then remelted to form ingots or castings (Shimada and Merkel 1991). The presence of arsenic in the copper prills confirms that arsenic-bearing compounds were not added at a later stage but rather incorporated in the initial charge, as mentioned above (Shimada et al. 1982).

The Moche were the first people to produce copper-arsenic alloys in the Andes by the first few centuries C.E. (Lechtman 1988), though the Sicán initiated the large-scale production of copper-arsenic alloys at Batán Grande circa 850-900 C.E. (Shimada and Merkel 1991). The Chimú conquered the Sicán around 1375 but maintained the Sicán mining and metal refinement activities in their preexisting locations (Shimada and Merkel 1991). The Chimú established the

largest coastal state in the Andes before they were conquered in 1476 by the Inka, who also decided to continue copper-arsenic alloy production in the Sicán metallurgical tradition (Shimada and Merkel 1991). The Sicán approach to smelting was indeed labor-intensive, but it was in the best interests of the Chimú and the Inka to maintain their extractive metallurgical practices. Human labor was a characteristic part of the economy throughout Andean history; access to labor supply for metal production was not a problem (Shimada and Merkel 1991).

The South-Central Andes

More recently, the smelting site of Ramaditas in the south-central Andes has been excavated and studied (Graffam et al. 1994). Ramaditas, located in the Guatacondo Valley of the Atacama desert in northern Chile (Fig. 5), was a small (ca. 3 hectares) early copper smelting site dating to 500 B.C.E., during the Late Formative Period (Graffam et al. 1994). Thus the activities at Ramaditas occurred approximately 1350 years prior to the establishment of the copper-arsenic smelting site at Batán Grande. Extractive metallurgy at Ramaditas was carried out on a small scale, and smelting was performed on a periodic basis (Graffam et al. 1994). However, metalworkers achieved such low slag viscosities that there was good separation of metal from slag during the smelting process. Upon analysis, low percentages of high-purity, metallic copper were found in the Ramaditas slags, as well as a near-optimum silica to iron ratio, a factor that confers fluidity to slags. Both these characteristics are indicators of efficient smelting (Graffam et al. 1994). The excavators suggest (Graffam et al. 1994) that the efficiency of extraction is likely to be attributable to the high quality of copper ore in the dry Atacama desert as well as to the possible use of the *huayra*, or natural draft furnace, examples of which are shown in Figures

9 and 12. The prehistoric furnaces at the site have been destroyed over time, and their original form cannot be reconstructed.

Though extractive metallurgy at Ramaditas was dispersed and episodic as compared with the near-industrial scale of activity at Batán Grande in the north, the evidence suggests that people in the Atacama desert had developed an efficient copper smelting technology in northern Chile in the Late Formative Period which eventually became the preferred tradition of smelting in the south-central Andes. It was the established tradition that the Inka encountered and maintained when they conquered the southern region of Andean America.

Extractive Metallurgy in the Inka Context

When the Inka came to power in 1450, all supplies of natural resources and labor became property of the state. The Inka adopted silver and gold as resources that became symbols of the royal lineages, and these metals were mined exclusively for the Inka state (Murra 1980). However, copper-tin bronze was the most widely used metal that the Inka disseminated throughout the empire, and it became one of the standard emblems of Inka domination (Lechtman 1976).

Copper-tin bronze along with copper-arsenic and copper-arsenic-nickel bronzes were alloys yielded from extractive metallurgical practices that predated the Inka. It was during the Middle Horizon (600-1000 C.E.) that new technology, such as bronze metallurgy, developed. It was at this time that the long-distance, north-south interchange of extractive metallurgical knowledge was made possible with the onset of long-distance communication and exchange throughout most of the central and south-central Andes (Lechtman 1976, 2003). As previously

mentioned, in the central Andes, around 850-900 C.E., the Sicán significantly developed the technology the Moche had used to make copper-arsenic alloys (Shimada and Merkel 1991). At this time also, in the Bolivian *altiplano* and regions in northern Chile and northwest Argentina, people within the Tiwanaku domain developed copper-arsenic-nickel bronze and copper-tin bronze (Lechtman 2003). By the time the Inka became the ruling authority in the Andes, the production of copper-arsenic-nickel bronze had waned, possibly because of a diminishing supply of arsenic and nickel ores, but copper-arsenic alloys continued to be produced, and copper-tin bronze became the imperial bronze (Lechtman 2003).

Few Inka smelting sites have been found. Located in northwest Argentina, one Inka smelting site, Quillay Wayras (Fig. 5), is associated with an Inka tambo that may have housed about 40-50 people (Raffino et al. 1996). The pottery found at the site suggests that the houses were inhabited by a labor force of *mitimaes* (groups of workers relocated by the state) from the nearby Haulfín Valley (Raffino et al. 1996). The site is located on the sides and upper reaches of gullies and is near the Khapaq Ñan (Fig. 10), the royal Inka highway (Raffino et al. 1996). Quillay Wayras consists of fourteen *huayras* (natural draft wind furnaces) made from adobe walls that were 10 cm in thickness (Raffino et al. 1996). Slag is dispersed throughout the surface of the site, and remains of native copper encrusted in gangue are also present (Raffino et al. 1996). Thick layers of carbon have accumulated at the bases of the furnaces, and radiocarbon analyses of the carbon determined dates between 1490 and 1560 C.E., which correspond to the Inka horizon (Raffino et al. 1996).

The *huayras* are only partially preserved. There is no complete *huayra* remaining in Quillay Wayras. The bases of all the furnaces have been conserved, but only half of the *huayras* preserve the lower half and center of the furnace (Raffino et al. 1996). Figure 11 is a

reconstruction drawing of the presumed size and shape of an intact furnace, made on the basis of measurements taken of the standing remains (Raffino et al. 1996, fig. 7). Raffino supposes that the *hauyras* were shaped like arched towers and had a diameter of 4 m and height of 2.2 m (Raffino et al. 1996, fig. 7). Despite the natural draft that was present at the site, Raffino believes that air introduced through blowtubes inserted into orifices in the upper third of the *huayras* maintained temperature and reducing conditions while chimneys allowed fumes to escape (Raffino et al. 1996).

Unlike the *huayras* that Raffino describes, ethnohistoric sources suggest that *huayras* were cylindrical or upward-flaring in shape, and holes in the clay walls allowed wind to enter and contribute oxygen to the charge (Fig. 9). Colonial chronicler Alvaro Alonso Barba illustrated the traditional huayra, with an open, not arched, top and flames, not blowtubes, coming out of the holes (Fig. 12). Although the furnaces at Quillay Wayras are indeed Inka smelting installations, they are probably not *huayra* furnaces (González 2004).

The only other large, Inka smelting site in the south-central Andes is Viña del Cerro, located in the Copiapó valley of Chile (Fig. 5). The Inka conquered the Copiapó valley between 1471 and 1480 C.E. (Niemeyer et al. 1991). They exploited the region's rich ores of copper, silver, and gold, which were relatively easy to extract, and metalworkers produced a variety of everyday tools and decorative items from smelted copper-tin bronze (Niemeyer et al. 1991). Viña del Cerro is a copper smelting site divided into four units, one of which is a metallurgical installation, Unidad C (Fig. 13). Although no furnaces remain there, Niemeyer found the remains of the stone foundations of 26 *huayra* furnaces in Unidad C, which are between 2 and 3 m in diameter, on a hill that is exposed to large volumes of wind (Niemeyer et al. 1991).

Though the Inka technical successes with extractive metallurgy were based on the

accomplishments of previous societies, the Inka brought metallurgical production to a new level in the Andes. The Inka state maintained existent smelting and production methods but reorganized the labor force in order to accommodate the shift to large-scale production of copper alloys (González 2004, Lechtman 1993). The Inka operated as managers who broke down smelting and production processes into tasks to be carried out on a large scale by different communities dispersed throughout the Andes (González 2004). This had never been done before, and as a result of this social change imposed by the Inka, the state was able to distribute copper-tin bronze tools and weapons throughout its vast empire (Lechtman 2003). The social system that the Inka established to oversee the metallurgical production process was so effective that, from their capital in Cuzco to the north, the Inka were able to greatly increase copper-tin bronze production, once exclusive to the Bolivian *altiplano*, northern Chile, and northwest Argentina, and extend it from the south-central Andes to the north.

Since the Spanish presence was very limited in the south-central Andes compared to the central Andean zone, regions dominated by the Inka empire as far south as Chile and Argentina provide good sites to study, because they exhibit pre-Hispanic traditions largely unaffected by European practices. For this reason, the present study of metallurgical remains from San Bartolo may yield important information in regards to Inka extractive metallurgy.

SAN BARTOLO

San Bartolo is an abandoned mining village located approximately 22 km north of the town of San Pedro de Atacama, just east of the Atacama Desert in northern Chile (Fig. 5). It lies approximately 3,000 meters above sea level on the Rio Grande. The geological setting of San Bartolo is primarily calcium sulfate. The stratigraphy of the site belongs to the mid-Tertiary Pacencia Group, which is composed of more than 2km of continental sediments that lie to the west of the Salar de Atacama. This group is correlated with the Corocoro Group located in Bolivia, which is characterized by its copper ore deposit (Flint 1985). Three copper mines—El Abra mine, Artola mine, and Almeyda mine—as well as *qollqas,* typical Inka storehouses that, in this case, kept copper mineral, have been identified at San Bartolo (Castro et al. 2003). This thesis will provide additional data regarding the ore species collected in the San Bartolo region.

In the latter half of the 15th century, the Inka moved south from their capital at Cuzco, Peru, and conquered vast territories in the south-central Andes, including large portions of present-day Bolivia, northern Chile, and northwest Argentina. They exploited sources of silver, gold, tin, and copper whose metallic ores abounded in these areas (Moseley 2001). They developed mining towns, such as San Bartolo, and exploited the local ore deposits until the 16th century, when the Spanish invasion ended the Inka Empire. San Bartolo has been identified as one of the key suppliers of smelted copper to the Inka (Castro et al. 2003).

The archaeological evidence suggests that mining in San Bartolo was abandoned between the 16th and 19th centuries. However, San Bartolo was utilized again by Chilean miners from the 1850s to the 1970s (Castro et al. 2003). Since there was no mining activity between the Inka occupation and the modern occupation of San Bartolo, any metallurgical debris associated with

the material from the Inka period should reveal details of Inka metallurgical technology uninfluenced by Spanish practices.

Chilean archaeologists Victoria Castro Rojas, Carlos Aldunate del Solar, and Varinia Varela Guarda have visited, mapped, and begun to investigate San Bartolo since January 2003, with the goal of reconstructing the copper smelting process used by prehistoric San Bartolo metalworkers. The artifacts examined in this study were surface-collected by this archaeological team come from El Establecimiento, an Inka establishment located in the valley of San Bartolo (Fig.14). At present, El Establecimiento consists of an Inka cemetery, a 20th century cemetery, two modern farms, and a number of *qollqas.* Upon evaluating the site, the team of archaeologists identified the following areas within El Establecimiento: Sector Cementerio Inka (an Inka cemetery), Sector Cementerio Histórico (a 20th century cemetery), Sector de las *Qollqas* (Inka storehouses), and Sector de la Planta (Fig. 14). They found an array of slag thinly distributed on the surface of the ground in an area measuring approximately 400 m^2 in Sector Cementerio Histórico. In Sector de las *Qollqas*, they found an abundance of copper ore in three separate *qollqas* as well as in a contiguous pre-Hispanic dump. They also collected copper mineral from deposits located in Sector de la Planta.

The Chilean archaeologists—Castro Rojas, Aldunate del Solar, and Varela Guarda—who recovered the San Bartolo artifacts, provided Professor Lechtman (DMSE, CMRAE) with a total of eighteen artifacts for laboratory analysis: eight pieces of slag (one of which is attached to a piece of what may be furnace wall) and ten pieces of copper mineral. We have no data at present on the total number of artifacts the team collected at the site.

METHODOLOGY AND ANALYTICAL RESULTS

Of the archaeological materials retrieved at San Bartolo, five artifacts were thoroughly examined for this study. As previously mentioned, this corpus includes small, green, rock-like artifacts (MIT 5313 and MIT 5319), which I determined to be pieces of copper ore. This corpus also includes a small, gray, heat-altered artifact (MIT 5318), which my study identified as a copper smelting slag and a small, brown, vitrified artifact (MIT 5316), which my analyses indicate is a glassy copper smelting slag. The corpus lastly comprises a ceramic artifact (MIT 5320), which I identified as a portion of a smelting furnace wall.

The following section discusses the results of the materials analyses carried out on each one of the artifacts. These analytical procedures included: (1) image documentation by conventional photography; (2) metallography and petrography; (3) electron microbeam probe qualitative energy-dispersive X-ray spectroscopy (EDS); (4) quantitative wavelength-dispersive spectrum (WDS) electron microanalysis; (5) metal assay; (6) inductively coupled plasma optical emission spectroscopy (ICP-OES); and (7) instrumental neutron activation analysis (INAA).

MIT 5313

MIT 5313 (Fig. 15) was surface-collected at Sector de las *Qollqas* in San Bartolo (Fig. 14). The object weighs 15.5 g and has a density of 3.44 g/cc. The length, width-1, width-2 and depth of the object, respectively, are: 3.73 cm, 2.34 cm, 1.36 cm, and 1.41 cm. MIT 5313 exhibits a multi-globular morphology (Fig. 15). When the artifact arrived at MIT, it was covered with sand and earth accretions. With these mineral accretions removed, the surface is pale green

with a granular texture (Fig. 16). Low-power magnification (7x-30x) reveals many major and minor indentations as well as hairline cracks. Image documentation by conventional photography, metallography, electron microbeam probe analysis, and bulk chemical analysis were used to examine the object both qualitatively and quantitatively.

Documentation

Different forms of visual documentation were carried out in order to offer the greatest range of information possible. Features such as overall shape and color are compromised when views are magnified, while the smallest details can be illustrated only at high magnification. Together, the combination of line drawings, photomacrographs, and photomicrographs provided the most complete visual representation of the artifact.

The line drawings of MIT 5313 show four views (Fig. 17). After initial cleaning with a toothbrush and water to remove the sandy accretions, macro scale photographs of MIT 5313 were taken with a Nikon Coolpix 5400 digital camera, and these images were processed in grayscale as well as color using Adobe Photoshop, Version 8 software (Fig. 15 and 16). 35 mm color slides were taken with a Nikon FM2 camera with a 55 mm macro lens using Kodak Elite Chrome 100 daylight film.

Photomicrographs (100x-500x) of a cross section through the artifact were taken with a Leica DMLM metallurgical microscope outfitted with a Leica DC300 digital camera, and these images were processed using Leica IM50 software. These images will be described in more detail in the following section.

Metallography

A cross section (MIT 5313-A) was cut diagonally across the top third of the artifact (Fig. 18) using a Raytech JemSaw with rotating diamond saw blade. The section was washed with water and rinsed with ethanol and then acetone to expedite the drying and minimize oxidation of the sample. The section was subsequently hot mounted in Mark V Laboratory Fina-Met phenol-formaldehyde resin, ground, and polished with a sequence of increasingly fine diamond pastes to a final one-micron grit.

Prior to etching (i.e., in the as-polished state), the polished surface of MIT 5313-A was observed with the unaided eye and examined with an American Optical 569 low-power binocular microscope (7x-30x) with raking incident light. These observations revealed a significant amount of pink metal (copper) in the section with a thin corrosion crust on the exterior of the section, which corresponds to the surface of the artifact. When viewing the specimen with a Leitz HM-LUX metallurgical microscope at a magnification of 200, the section showed a sponge-like metallic matrix with large quantities of small, colorless mineral grains and small, opaque, red, non-metallic material surrounding the metallic matrix.

The polished section was subsequently etched for five seconds using potassium dichromate in order to reveal the metal microstructure more clearly. When examined with crossed-polarized light at magnifications of 50-200, the etched section exhibited brilliant red, cuprous oxide (Cu_2O) grains in the non-metallic zones (Fig. 19). Under plane-polarized light, the microstructure in the metallic zones revealed by the potassium dichromate etch exhibits many different sized grains with annealing twins (Fig. 20). Some of the metallic zones have a higher density of annealing twins than others. Grain boundaries in these zones define grains with a large range of sizes. The grains are randomly dispersed, rather than forming a pattern. Some

grains exhibit slip planes, indicative of shear stress (Fig. 21). At least one metal grain exhibits a double-grain boundary (Fig. 22), indicating that the boundary has moved slightly from its original position.

The prominent features of the metallic microstructure — grains of many different sizes containing annealing twins, grains exhibiting slip planes, and the presence of double grain boundaries — together with the high purity of the copper (see section on Bulk Chemical Analysis) indicate that the ore is largely a weathered native copper. The copper in the ore is therefore present as native copper and as cuprous oxide.

Electron Microbeam Probe Analysis

An electron microbeam probe in the Department of Earth, Atmospheric and Planetary Science (EAPS) at MIT, JEOL SuperProbe 733, operated by Dr. Nilijan Chatterjee in EAPS of MIT, was used for qualitative and quantitative analysis of the composition of MIT 5313-A and to generate scanning electron microscope (SEM) images for further examination and documentation. Color image analysis of SEM images was performed with ImagePro software in the Ceramics Facility of the Center for Materials Research in Archaeology and Ethnology (CMRAE).

Energy-dispersive X-ray spectrum (EDS) analysis of the non-metallic zones identified an assemblage of granitic mineral grains, illustrated in the color image analysis in Figure 23. These granitic grains include quartz, plagioclase feldspar (Ca-Na-Al silicate), and Potassium-feldspar (K-Al silicate), with minor amounts of epidote (Ca-Al-Fe silicate), biotite mica (K-Fe-Mg-Al silicate), and muscovite mica (hydrous K-Al silicate). EDS data are presented in Appendix A.

Wavelength-dispersive quantitative spectral (WDS) analysis of the metallic zones of MIT 5313-A indicates that the metal is composed of pure copper. No trace elements were detected at the operating sensitivity of the probe. WDS data are presented in Appendix A.

Bulk Chemical Analysis

Another sample from the same artifact (MIT 5313-1) was removed with a rotating diamond saw blade (see Fig. 18) for bulk chemical analysis in order to determine the relative composition, in weight percent, of copper and the major oxides. The section, weighing 1.030 g, was submitted to Activation Laboratories in Ontario, Canada, where it underwent an assay for metallic copper content, analysis by inductively coupled plasma optical emission spectroscopy (ICP-OES) to determine the proportion, by weight, of the major oxides, and instrumental neutron activation analysis (INAA) for determination of trace element content in the bulk sample.

For the metallic copper analysis, the sample was crushed and screened through a 100 mesh (149 μm) screen. Table 1 shows the weight percent composition of copper in the sample to be 58.2%. Table 2 gives the weight percent compositions of the major oxides found in the sample as analyzed by ICP-OES. The major oxides include SiO_2, Al_2O_3, CaO, and Na_2O. Taken together, the oxides comprise 34.8% of the sample, by weight. Table 3 gives the trace elements, in parts per million and parts per billion, that were determined in the sample, as analyzed by INAA.

MIT 5319

MIT 5319 was surface-collected at Sector *La Planta* in San Bartolo (see Fig. 14). The artifact weighs 34.5 g with a density of 3.14 g/cc. The length, width, and thickness of the artifact, respectively, are: 4.15 cm, 3.50 cm, and 1.45 cm. The artifact is visibly subrounded, trapezoidal in shape, and thin. The front and back faces of the artifact (Fig. 24) (Faces A and B, respectively) are mostly flat. Less than 20% of the surface was covered with sand and clay. With the sand and clay removed, the artifact appears green (Fig. 25). Image documentation by conventional photography, metallography, electron microbeam probe analysis, and bulk chemical analysis were used to examine MIT 5319 both qualitatively and quantitatively.

Documentation

Line drawings of MIT 5319 (Fig. 26) illustrate two views of the artifact. These drawings show where the sandy accretions were located before they were removed. They also provide a sense of the overall flatness of the artifact; it's only 1.45 cm thick compared to its length of 4.15 cm and width of 3.50 cm.

After initial cleaning, macro scale photographs of MIT 5319 were taken with a Nikon Coolpix 5400 digital camera, and these images were processed in grayscale as well as color using Adobe Photoshop, Version 8 software (see Fig. 24 and 25). 35 mm color slides were taken with an Olympus C-35DA-2 camera using Kodak Elite Chrome 160T film. These images highlight the grainy surface texture that remained after cleaning.

Photomicrographs (50x-500x) of sections cut through the artifact were taken with a Leica DMLM metallurgical microscope outfitted with a Leica DC 300 digital camera, and these images

were processed using Leica IM50 software. These images are discussed in the following section.

Metallography and Petrography

Two sections (MIT 5319-A and MIT 5319-B) were cut from opposite ends of the artifact using a Raytech JemSaw with rotating diamond saw blade (Fig. 27). Each of these sections was washed with water and rinsed with ethanol and then acetone to expedite the drying and minimize oxidation of the samples. The sections were subsequently mounted in Mark V Laboratory Fina-Met phenol-formaldehyde resin, ground, and polished with a sequence of increasingly fine diamond pastes to one-micron grit. A final polish was achieved with alpha-alumina suspension in distilled water.

When sections MIT5319-A and MIT 5319-B are viewed with the unaided eye or with an American Optical 569 low-power binocular microscope (7x-30x) with raking incident illumination, three distinct materials are visible—a green material, a dark gray material, and a lustrous material that is dark gray in color and appears in the form of veins within the non-lustrous dark gray material. These materials are located in distinct zones within the cross section, as shown in Figure 28.

In MIT 5319-A, Zone 1 consists of a green material that occupies approximately 20% of the section area; Zone 2, a dark gray material, comprises approximately 70% of the area of the section; and Zone 3, a lustrous vein that intersects Zone 2, occupies approximately 10% of the section. Table 4 presents the analyses of the various materials found in MIT 5319-A and B. Examination of MIT 5319-A, Zone 1, with a Leitz HM-LUX metallurgical microscope at 50x and with plane-polarized light, reveals gray, equiaxed grains of different shapes and sizes.

Zone 2 reveals a slightly different composition. Under plane-polarized light and at 100x, gray, equiaxed grains (similar to those seen in Zone 1) occur within a pale green, amorphous matrix. In the lustrous vein, Zone 3, light blue crystals inside the same pale green matrix are revealed under plane-polarized light. With a petrographic microscope under cross-polarized light and at 100x-200x, Zone 3, corresponding to the vein, shows yellow and red crystals in addition to a few dark green crystals within a gray matrix. When the polarizing lenses are crossed, all zones across the entire section show green, brown, white, and gray areas with indistinct boundaries.

The section view of MIT 5319-B (Fig. 28) reveals that it is also visibly divided into three zones: Zone 1 contains green material (approximately 20% of the section); Zone 2 contains dark gray material (approximately 60% of the section); and Zone 3 contains lustrous veins within the dark gray material (approximately 20% of the section). Under both plane- and cross-polarized light and at 50x, Zone 1 of MIT 5319-B is identical to Zone 1 of MIT 5319-A. With a metallurgical microscope under plane-polarized light, it reveals gray, equiaxed grains of varying shapes and sizes and, with a petrographic microscope under cross-polarized light, it reveals green, brown, white, and gray areas with indistinct boundaries. With a metallurgical microscope under plane-polarized light and at 50x, Zone 2 of MIT 5319-B is similar to Zone 1 except that its equiaxed crystals are enclosed in a pale green matrix. With the polarizing lens fully crossed, all of the material in Zone 2 is extinguished except for a scattering of yellow specks that appear randomly dispersed in the matrix. Under plane-polarized light and at 100x-200x, Zone 3 of MIT 5319-B appears identical to Zone 2 of MIT 5319-A. It shows gray, equiaxed grains within a pale green, amorphous matrix along with light blue crystals inside the same pale green matrix but located within the lustrous vein. With a petrographic microscope under cross-polarized light, the area outside the vein in Zone 3 contains hazy patches of green, brown, white, and gray, while the

area corresponding to the vein roughly consists of 78% gray matrix, 10% yellow crystals, 5% red crystals, 5% dark green crystals and 2% pale green crystals. Under the same lighting conditions, the red crystals are extinguished when the petrographic microscope stage is rotated through 40 degrees. When the stage is rotated another 25 degrees, these same crystals turn buff in color.

Electron Microbeam Probe Analysis

An electron microbeam probe, JEOL SuperProbe 733, operated by Dr. Nilijan Chatterjee in EAPS of MIT, was used for the qualitative analysis of the composition of the various zones in MIT 5319-B.

Energy-dispersive X-ray spectral (EDS) analysis identified the composition of Zone 1 to be a combination of SiO_2 grains with a nearly pure copper-chloride phase. The probe showed no trace of sulfur in Zone 1. Zone 1 is a chloride weathering product of the primary copper sulfide vein in the ore. An intergrowth of copper sulfide (Cu_2S) and barium-strontium sulfate [(Ba, Sr)SO_4] was identified in Zone 2. No chlorine was identified in Zone 2. EDS analysis detected three phases in Zone 3: chalcocite (Cu_2S); an intergrowth of Cu_2S and copper sulfate (Cu_2SO_4); and lead sulfide (PbS), which appeared to be a very minor phase. Wavelength-dispersive X-ray spectral (WDS) analysis of MIT 5319-B indicated that the composition of the lustrous vein is Cu_2S and that the Cu_2S phase is a primary sulfide that contains some cuprous oxide (Cu_2O) weathering product. EDS and WDS data are presented in Appendix A. EDS and WDS analysis with corresponding metallurgical and petrographic analysis are presented in Table 4.

Bulk Chemical Analysis

Another sample (MIT 5319-1) was removed from the artifact with a rotating diamond saw blade (see Fig. 27) for bulk chemical analysis in order to determine the weight percent composition of copper and oxides present. The section, weighing 2.0 g, was submitted to Activation Laboratories in Ontario, Canada, where it was assayed for metallic copper content, analyzed by inductively coupled plasma optical emission spectroscopy (ICP-OES) to determine the major oxides, and by instrumental neutron activation analysis (INAA) for overall trace element content.

For metallic copper analysis, the sample was crushed and screened through a 100 mesh (149 μm) screen. Table 1 shows the composition of copper in the sample to be 24.2%, by weight. Table 2 shows the relative abundance of the major oxides found in the sample as analyzed by ICP-OES. These oxides include SiO_2, Al_2O_3, CaO, Na_2O, and K_2O. Together, all the oxides present account for 61.0 weight percent of the sample. The total weight of metallic copper and oxides is 85%. Sulfur, which was not analyzed, undoubtedly accounts for most of the remaining weight that was left unaccounted. Table 3 shows the trace elements, in parts per million (or billion), that were found in the sample analyzed by INAA.

Thus the ore sample 5319 is a weathered copper sulfide ore. It contains veins of unaltered, primary copper sulfide mineral as well as weathering products consisting of copper oxide, copper chloride, and copper sulfate.

MIT 5318

MIT 5318 was surface-collected at Sector *Cementerio Histórico* in San Bartolo (see Fig. 14). The artifact weighs 56.8 g with a density of 2.84 g/cc. The length, width, and thickness of the artifact, respectively, are: 5.25 cm, 3.95 cm, and 3.3 cm. The artifact has an irregular shape with rounded edges. The surface is interrupted by tiny vesicles and is weathered and smooth except for several small chipped areas of less than 1 cm (Fig. 29). An abundance of corroded copper prills with diameters smaller than 0.5 cm are distributed throughout the surface. Some of these prills reveal exposed copper metal, others exhibit green corrosion products of copper (Fig. 30). After the removal of pink sandy accretions, which covered less than 10% of the surface, the artifact appeared dark grey with less than 20% red oxide material visible on the surface (Fig. 30 and Fig. 31). Image documentation by conventional photography, metallography, electron microbeam probe analysis, and bulk chemical analysis were used to examine MIT 5318 both quantitatively and qualitatively.

Documentation

The line drawings of MIT 5318 (Fig. 31) illustrate two views of the artifact. These drawings indicate where areas of red oxide material and relatively large, exposed copper prills are located on the surface of the specimen.

After initial cleaning to remove the sandy accretions, macro scale photographs of MIT 5318 were taken with a Nikon Coolpix 5400 digital camera, and these images were processed in grayscale as well as color using Adobe Photoshop, Version 8 software (see Fig. 29 and 30).

These images emphasize the artifact's smooth rounded features as well as its grainy and chipped surfaces.

Photomicrographs (50x-200x) of a section of the object were taken with a Leica DMLM metallurgical microscope outfitted with a Leica DC 300 digital camera, and these images were processed using Leica IM50 software. Photomicrographs of the artifact were also taken with a Wild M-420 Makroskop camera using TMAX 100 film. These images will be described in more detail in the following section.

Metallography

A cross section (MIT 5318-A) was cut through MIT 5318 using a Raytech JemSaw with rotating diamond saw blade (Fig. 32). The section was washed with water and rinsed with ethanol and then acetone to expedite the drying and minimize oxidation of the sample. The section was subsequently cold mounted in Buehler Epoxide resin, ground, and polished with a sequence of increasingly fine diamond pastes to a one-micron grit. A final polish was completed with alpha-alumina suspension in distilled water.

When section MIT 5318-A is viewed with the unaided eye or with an American Optical 569 low-power binocular microscope (7x-30x) with raking incident illumination, four distinct zones are visible (Fig. 33): Zone 1, which has a black matrix; Zone 2, which has a gray matrix; Zone 3, which has a pink matrix; and Zone 4, which has a red matrix.

When viewed, as-polished, with a Leitz HM-LUX metallurgical microscope at 50x-200x and with plane-polarized light, four phases are visible in Zone 1: Phase (a), a copper phase that appears orange; Phase (b), a cuprous oxide phase that appears speckled blue; Phase (c), a copper sulfide phase that appears green; and Phase (d), the glassy gray matrix. The copper occurs in the

form of prills. The cuprous oxide occurs as random inclusions, and the copper sulfide is present in the form of prills and also as random inclusions. Zone 1 contains three extremely large pores (approximately 0.2 cm in diameter), one of which contains three inclusions of cuprous oxide that appear red-orange under cross-polarized light (Fig. 34). Less than 5 vol. % of the copper prills (which measure less than 0.1 cm in diameter) that are distributed throughout the sample 5318-A is present in Zone 1. This zone consists of many medium-sized pores (approximately 0.01 cm in diameter) and inclusions of copper sulfide within the matrix.

Observed at 100x-200x with plane-polarized light, Zone 2 exhibits many small (less than 0.01 cm in diameter) and medium-sized pores (about 0.01 cm in diameter). Less than 5 vol. % of the copper prills (which measure less than 0.1 cm in diameter) in sample 5318-A appear in Zone 2, and nearly all of these prills are surrounded by a thin, uniform "rind" of cuprous oxide which is surrounded by an irregular mass of copper sulfide (see Fig. 35). This pattern of circumferential zoning around the prill [i.e. Phase (a) surrounded by a rind of Phase (b), which is surrounded by Phase (c)] is characteristic of the some of prills throughout Zones 2 and 3, and it is characteristic of the majority of prills in Zone 4. Few copper prills contain inclusions of cuprous oxide or copper sulfide. In Zone 2, prills of copper sulfide also occur in about 30 vol. % of the matrix.

At 50x-200x and with plane-polarized light, Zone 3 reveals many small pores (less than 0.01 cm in diameter). Less than 25 vol. % of the copper prills in the section, with sizes varying from small (less than 0.01 cm in diameter) to medium (about 0.01 cm in diameter), are located in Zone 3. Most of these prills are surrounded by a rind of cuprous oxide, and about 25% of these are also surrounded by copper sulfide.

Observed at 100x with plane-polarized light, Zone 4 shows many small (less than 0.01 cm in diameter) pores. The majority of the copper prills (more than 75 vol. %) in the section occur in Zone 4, with sizes varying from small to large (0.05 cm in diameter). Most of the prills are surrounded by a cuprous oxide rind, and more than 75% of these prills are also surrounded by a mass of copper sulfide.

The fact that the pore size increases dramatically, from less than 0.01 cm in diameter in Zone 4 to 0.2 cm in diameter in Zone 1, indicates that the orientation of sample MIT 5318 during cooling was such that Zone 1 was vertically higher than Zone 4. The high density of copper prills in Zone 4 (approximately 15 vol. %) as compared with their low density (approximately less than 5 vol. %) in Zone 1 confirms this assessment of the sample's orientation during cooling, since the heavy copper metal would have migrated down from Zone 1 to Zone 4 as the material—glass plus metal — solidified.

Electron Microbeam Probe Analysis

An electron microbeam probe, JEOL SuperProbe 733, operated by Dr. Nilijan Chatterjee in EAPS at MIT, was used for qualitative analysis of the composition of MIT 5318-A.

Energy-dispersive X-ray spectral (EDS) and wavelength-dispersive spectral (WDS) analyses of MIT 5318-A show that the sample has a glassy matrix composed of SiO_2, Al_2O_3, CaO, Na_2O, and K_2O (see Appendix A). The pores in the sample appear in this glassy matrix. Scanning electron microscopy (SEM) images and WDS show that same copper sulfide appears as crystalline regions within the glassy matrix. EDS also indicates that the sample contains Cu-Fe sulfide inclusions within the glassy matrix. SEM images indicate that the crystalline regions comprise varying types of gray crystals. WDS analysis shows that: dark gray crystals are

composed of SiO_2, Al_2O_3, Na_2O, and K_2O; moderately gray crystals are composed of SiO_2, MnO, MgO, and CaO; and light gray crystals are composed of SiO_2, FeO, MnO, and Na_2O. EDS suggests that Phase (b) is Cu_2O and that Phase (c) is Cu_2S.

The copper prills in the sample are pure copper, according to the WDS data (EDS and WDS data are presented in Appendix A). The copper prills [Phase (a)] often contain inclusions of cuprous oxide (Cu_2O) and copper sulfide (Cu_2S) (see Fig. 35). The surfaces of the prills are covered with a thin, uniform layer of Cu_2O [Phase (b)], clearly an oxidation product of the copper that formed during cooling. Another layer [Phase (c)] has formed in contact with Phase (b). This outer layer surrounding the copper core of the prill was analyzed as Cu_2S. Phase (c), therefore, consists of a thin layer of copper sulfide matte. The small concentrations of sulfur within the glassy matrix have concentrated in a fine zone to surround each prill.

Bulk Chemical Analysis

Another sample, MIT 5318-1, was removed from the artifact with a rotating diamond saw blade (Fig. 32), for bulk chemical analysis in order to determine the weight percent composition of copper and oxides in the sample. The section, weighing 0.6 g, was submitted to Activation Laboratories in Ontario, Canada, where it was assayed for metallic copper content, analyzed by inductively coupled plasma optical emission spectroscopy (ICP-OES) to determine the major oxides present, and by instrumental neutron activation analysis (INAA) for overall trace element content.

For metallic copper analysis, the sample was crushed and screened through a 100 mesh (149 μm). Table 1 shows that the copper content of this sample was determined as 27.7 weight

percent. Table 2 shows the compositions, in weight percent, of the major oxides found in the sample as analyzed by ICP-OES. All the major oxides that occur in the two ore samples (MIT 5313 and 5319)—SiO_2, Al_2O_3, Fe_2O_3, CaO, Na_2O, K_2O—are also present in sample MIT 5318, but two other oxides also appear in the category of major oxides: MnO (4.1%) and MgO (1.0%). In addition, the proportion, by weight, of SiO_2 in MIT 5318 has doubled over its presence in MIT 5313 (49.3 : 23.8) and the weight of SiO_2 is 1.6 times as great as in MIT 5319 (49.3 : 31.1). The level of Al_2O_3 is also somewhat higher in MIT 5318 than in either of the two ore samples. The total weight of all the oxides was determined as 75.9 weight percent. Table 3 shows the trace elements, in parts per million and per billion, that were found in the sample as analyzed by INAA.

The microstructural and compositional analyses indicate that MIT 5318 is a copper slag. It has the vitrified, glassy matrix, with pores and vesicles, expected of a smelting slag. Metallic copper prills are embedded in the glass. The appreciably higher level of MnO in the slag than in the ore samples may indicate that MnO_2 was added to the smelting charge as a flux, although the high concentration of copper prills in the sample suggests that the slag was never sufficiently fluid to allow the prills to sink through it.

MIT 5316

MIT 5316 was surface-collected at Sector *Cementerio Histórico* in San Bartolo (see Fig. 14). The artifact weighs 96.4 g with a density of 3.0125 g/cc. The length, width, and depth of the object, respectively, are: 6.35 cm, 4.25 cm, and 3.10 cm. The artifact is highly reflective, and its color ranges from burnt sienna to dark brown (Fig. 36).

The artifact displays three physically distinct morphologies at the top, center, and bottom as shown on Face B in Figure 37 and Face C in Figure 38. The top is characterized by multiple conchoidal fractures that vary in size and result in the irregular topography of the material (Fig. 37, Face A). The planes resulting from the conchoidal fracture contain stress lines that are generally parallel to each other. The presence of these conchoidal fractures indicates that the top portion is likely composed of a glassy material.

The center of the artifact consists of gray, rocky material that forms a wide band across the center (Fig. 37, Face B and Fig. 38). The surfaces of the material have fused with the surrounding glassy matrix. Both regions contain shiny gray as well as transparent mineral grain inclusions. The upper boundary, where the earthy material and the conchoidal material come into contact, is clearly visible in Figure 37, Face B. The lower boundary cannot be distinguished clearly, since the two regions gradually blend into one another.

The bottom of the artifact (Fig. 37, Face B and Fig. 38) consists of brown, once-molten material and contains no fractures, which suggests that this unbroken area may correspond to the original surface of the artifact. The entire bottom face has a rounded and smooth texture. Image documentation by conventional photography, metallography, electron microbeam probe analysis, bulk chemical analysis, and thermal experiments were used to examine MIT 5316 both quantitatively and qualitatively.

Documentation

Line drawings of MIT 5316 illustrate three views of the artifact (Fig. 39). These drawings show clearly the location of the band of earthy material surrounded by the once-molten glass. They also illustrate the stress lines in Face A of the artifact.

After initial cleaning, macro scale photographs of MIT 5316 were taken with a Nikon Coolpix 5400 digital camera, and these images were processed in grayscale as well as color using Photoshop, Version 8 software (see Fig. 36-38). These images illustrate the artifact's conchoidal and rounded features.

Photomicrographs (50x-200x) of a cross section of the artifact were taken with a Leica DMLM metallurgical microscope outfitted with a Leica DC 300 digital camera. These images were processed using Leica IM50 software. They are described in more detail in the following section.

Metallography

A cross section (MIT 5316-A) was cut through MIT 5316 using a Raytech JemSaw with rotating diamond saw blade (Fig.40). The section was washed with water and rinsed with ethanol and then acetone to expedite the drying and minimize oxidation of the sample. The section was subsequently cold mounted in Buehler Epoxide resin, ground, and polished with a sequence of increasingly fine diamond pastes to a one-micron grit. A final polish was completed with alpha-alumina suspension in distilled water.

When section MIT 5316-A is viewed with the unaided eye or with an American Optical 569 low-power binocular microscope (7x-30x) with raking incident illumination, the entire cut and polished section, except for the rocky material, appears glassy and reveals very small (less than 0.01 cm diameter), circular, reflective particles that are pale blue (copper sulfide prills) and orange metallic (copper prills) as well as black voids that are scattered across the sample's surface. When observed with a Leitz HM-LUX metallurgical microscope at a magnification of

100 with plane-polarized light, some of the bright orange prills are revealed as surrounded by a thin rind, which is in turn surrounded by a region of bright blue material (Fig. 41). The top half of the section reveals relatively more of the smallest bright orange and blue prills while the bottom half shows fewer but slightly larger reflective orange and blue prills. The glassy matrix material is characterized by thin bands of red alternating with thin bands of dark blue (Fig. 42). These bands are straight in some areas and bent in others. The region of the matrix material at the very bottom of the section is primarily red.

A very thin region of the earthy material described above is located at the extreme left of the section. When viewed with a Leitz HM-LUX metallurgical microscope at 50x-500x and with plane-polarized light, this region shows pale orange, grey, and white vertical bands. The pale orange and gray bands contain angular inclusions of varying sizes, which suggests that the earthy material was never molten; the white bands contain small, circular, pale blue inclusions. When the sample is viewed with a petrographic microscope in cross-polarized light, crystallization within these three bands is visible. The glassy matrix immediately to the right of the orange, grey, and white bands contains a lamellar structure that corresponds to the alternating red and dark blue bands that characterize the glassy material. These lamellae are continuous throughout the section but are most concentrated at the bottom.

Electron Microbeam Probe Analysis

An electron microbeam probe, JEOL SuperProbe 733, operated by Dr. Nilijan Chatterjee in EAPS at MIT, was used for qualitative analysis (EDS) and quantitative analysis (WDS) of the composition of MIT 5316-A.

WDS analysis identified the pale blue prills as Cu_2S. The orange prills are copper metal, while the black features revealed by metallography are identified as pores. Both EDS and WDS analyses of MIT 5316-A show that the bands in the glassy matrix of the slag have a homogenous silica composition with about 20 weight percent MnO and less than 15 weight percent of Al_2O_3, CaO, Na_2O, K_2O, and FeO, combined (see Appendix A). The presence of a high concentration of MnO may account for the reddish banding. The earthy material appears to be crystalline and is composed of epidote (Ca-Fe silicate), plagioclase feldspar (Al-Ca silicate), and ilmenite ($FeTiO_3$). These analyses, together with the metallographic examination of the band of earthy material, which revealed the presence of angular inclusions, indicate that this is a rocky material and that its bulk was never molten.

Bulk Chemical Analysis

Another sample, MIT 5316-1, was removed from the artifact with a rotating diamond saw blade (see Fig. 40), for bulk chemical analysis in order to determine the weight percent composition of copper and oxides in the sample. The section, weighing 2.8 g, was submitted to Activation Laboratories in Ontario, Canada, where it was assayed for metallic copper content, analyzed by inductively coupled plasma optical emission spectroscopy (ICP-OES) to determine the major oxides, and by instrumental neutron activation analysis (INAA) for overall trace element content.

For the metallic copper analysis, the sample was crushed and screened through a 100 mesh (149 μm). Table 1 indicates that copper is present in the glassy matrix in a concentration of 1.4 weight percent. Table 2 indicates that 93 weight percent of the glassy material is composed of oxides, as determined by ICP-OES. All the oxides present in the slag artifact MIT

5318 are also present in MIT 5316, but the concentration of MnO in MIT 5316 is dramatically higher (at 31.2 weight percent), and the concentration of CaO is 1.4% higher (at 5.1 weight percent). Table 3 shows the trace elements, in parts per million and parts per billion, that were found in the sample as analyzed by INAA.

MIT 5316 is a once-molten, glassy slag artifact that contains a small amount of rocky material that was never molten and may have once belonged to the furnace wall. As expected for a copper smelting slag, this artifact has a relatively low concentration of copper (1.4%) in the form of copper metal and copper sulfide prills dispersed in the glassy matrix. The matrix is composed mostly of silica but also contains a high concentration of MnO (31.2%), which was likely added to the charge as a flux during the smelting operation in view of the absence of MnO in both of the ore samples (MIT 5313 and 5319). The higher level of MnO found in MIT 5316 compared to 5318 (31.2 weight percent versus 4.1 weight percent) suggests that MnO played a more significant role as a fluxing agent for 5316 than it did for 5318. As a result, MIT 5316 was a much more fluid slag than 5318. When the temperature was high enough in the smelting furnace, MIT 5316 melted to liquid, allowing the copper metal to sink through it, leaving a low concentration of metallic copper in the solidified glass. By contrast, MIT 5318 remained viscous, causing many prills to remain trapped in the slag.

Thermal Alteration Tests

Thermal alteration tests were carried out on a series of samples cut from artifact MIT 5316 in order to determine the temperature at which the slag became molten. That temperature would also indicate the approximate furnace temperature at which the smelting of copper ore

took place. After loose dirt was removed from the artifact with an electric hand drill and dremel bit, 12 small samples (2.8-5.5 g) were cut from MIT 5316 (Table 5). A standard sample, MIT 5316-B4, was left untreated (Fig. 43)

Sample MIT 5316-E1 was used to find the temperature at which the onset of slumping began. It is the temperature at which the slag becomes viscous and "rubbery" but is not liquid. The "slumping temperature" is related to T_g, the glass transition temperature of a glassy material. Below T_g the material is a rigid solid, and above T_g, it is a supercooled liquid. Elastic deformation occurs below T_g and viscous deformation, including slumping, occurs within a range of temperatures above T_g. The melting range is the temperature range at which the viscosity of the material is so low that the material becomes fluid (Shackelford 1988).

The sample was placed in an alundum refractory boat located on a firebrick set inside a CM Inc. Rapid Temperature Furnace (muffle-type). A Type-K thermocouple suspended directly above the sample and a Type-R thermocouple located at the rear roof of the furnace chamber measured both the temperature at the sample and the chamber temperature. Temperature readings were recorded from the Type-K thermocouple. At ambient temperature, nitrogen was introduced to the furnace and was kept flowing continuously during the experiments in order to prevent the slag samples from oxidizing excessively. After increasing the furnace temperature to 800°C, the sample was allowed to soak for ten minutes. The furnace was then turned off, and the sample was observed for evidence of slumping, such as a molten surface appearance or fluidity. Since the surface of the sample experienced no gross morphological changes at 800°C (Fig. 44), the sample was replaced in the furnace, and this procedure was repeated at temperatures of 900°C (Fig. 45), 950°C, 1000°C (Fig. 46), 1050°C (Fig. 47a), 1075°C (Fig. 47b), and finally at

1100°C (Fig. 48a). Slight slumping was observed at 1000°C. After five minutes at 1100°C the sample completely lost its shape.

Using 1100°C as an approximate temperature for the onset of fluidity, a phase change experiment was performed on a total of ten samples removed from the glassy portion of artifact MIT 5316. Each sample was placed inside a boat and on a firebrick inside the preheated (800°C) furnace, which maintained an almost oxygen-free environment from a continuous supply of nitrogen. The furnace temperature was increased to a given temperature; the sample was soaked for approximately ten minutes at that temperature; it was then removed from the furnace and subsequently observed and photographed as soon as it cooled. The experimental results for each sample are given in Table 5.

The sweating temperature, the temperature at which the sample experienced marked surface sweating, was found to be 1050°C, but the surfaces had begun to flow and to conform to the contour of the ceramic boat by 850-900°C. The bulk melting and running temperature, the temperature at which the sample became completely liquid, was determined to be 1125°C (Fig.48b). This temperature suggests that the metalworkers conducting the San Bartolo smelting operations achieved a smelting furnace temperature of at least 1125°C. In fact, the temperature within the smelting furnaces at San Bartolo needed to surpass this temperature in order for smelting to proceed successfully. The smelting furnace temperature was clearly high enough to form a fluid slag and to melt completely any smelted copper, whose temperature of fusion is 1083°C. The formation of the fluid slag allowed the smelted copper metal to sink through the slag and, presumably, to collect as a pool of liquid copper at the bottom of the furnace.

The theoretical melting temperature of a slag with the composition of MIT 5316 was determined from a ternary phase diagram for MnO-Al_2O_3-SiO_2. Though other oxides (including

CaO, Na_2O, K_2O, Fe_2O_3, and MgO) are present in the slag, their concentrations, in weight percent, were added to the concentration of Al_2O_3 because a ternary phase diagram that included some of these other oxides was not available. According to the ternary phase diagram (Fig. 49), a slag with composition of 31.2 weight percent MnO, 41.4 weight percent SiO_2, and 26.4 weight percent Al_2O_3 should melt at 1168°C. It was experimentally determined that the melting temperature of MIT 5316 is 1125°C, 43°C lower than the melting temperature given by the phase diagram. The difference between these temperature values is most likely due to the presence of other oxides in MIT 5316 that affected its thermal behavior.

Hence, this artifact, which is a glassy slag containing a small amount of copper metal and copper sulfide prills, has a relatively low melting temperature that is likely attributable to its high concentration of manganese oxide that served as a fluxing agent.

MIT 5320

MIT 5320 was surface-collected at Sector *Cementerio Histórico* in San Bartolo (see Fig. 14). The artifact weighs 326.2 g with a density of 1.677 g/cc. The length, width, and depth of the object, respectively, are: 7.6cm, 6.4 cm, and 4.0 cm. The artifact is visibly trapezoidal in shape (Fig. 50)

The object has three visible zones (Fig. 51 and 52). Zone A is a ceramic zone that corresponds with the exterior of the furnace. This zone is largely unaltered by heat, though it contains many cracks and, at low-power magnification (7x-30x), it displays microcracks all over its surface. This zone, earthy in color (Fig. 53 and 54), resembles the sandy accretions that once

covered the surfaces of MIT 5313 (native copper ore), MIT 5319 (weathered sulfide ore), and MIT 5318 (copper slag). Zone B is a gray, intermediate zone that was partially heat-altered. Zone C is a black, highly heat-altered zone that corresponds with the interior of the furnace wall. This zone is porous and contains globular features ranging from 1 to 4 mm in diameter, including one globule that contains an exposed copper prill that is 2 mm in diameter (see Fig. 53, Face A). The dark color of zone B and part of zone C may have resulted from exposure to a reducing environment during heating. Image documentation by conventional photography, metallography, and electron microbeam probe analysis were used to examine the object both qualitatively and quantitatively.

Documentation

Macro scale photographs of MIT 5320 were taken with a Nikon Coolpix 5400 digital camera, and these images were processed in grayscale as well as color using Adobe Photoshop, Version 8 software (see Fig. 50-54). Photomicrographs (50x-200x) of the sections cut through the object were taken with a Leica DMLM metallurgical microscope outfitted with a Leica DC 300 digital camera, and these images were processed using Leica IM50 software. These images are discussed in the following section.

Metallography

Two sections (MIT 5320-A and 5320-B) were cut from the bottom end of the artifact using a Raytech JemSaw with rotating diamond saw blade (Fig. 55). These sections were rinsed with water, dried, and subsequently cold mounted in Buehler Epoxide resin, ground, and

polished with a sequence of increasingly fine diamond pastes to a one-micron grit. A final polish was completed with alpha-alumina suspension in distilled water.

When section MIT 5320 is viewed with the unaided eye or with an American Optical 569 low-power binocular microscope (7x-30x) with raking incident illumination, the cut and polished section clearly reveals zones A, B, and C described above (Fig. 56).

When observed with a Leitz HM-LUX metallurgical microscope at a magnification of 50 with plane-polarized light, zone A is characterized as an assortment of different-sized crystals, ranging from very large laths to very fine crystals (Fig. 56a). Zone B (Fig. 56b) is characterized by approximately equal amounts of the aforementioned crystals and a glassy matrix. Zone C is characterized by a glassy matrix (Fig. 56c) in which a few copper prills and copper sulfide prills are embedded (Fig. 57). The copper prills are similar to those identified in the previous slags; that is, they display the same pattern of circumferential zoning where a core of metallic copper is surrounded by a thin cuprous oxide rind, which in turn is surrounded by a region of copper sulfide matte.

Electron Microbeam Probe Analysis

An electron microbeam probe, JEOL SuperProbe 733, operated by Dr. Nilijan Chatterjee in EAPS at MIT, was used for qualitative analysis (EDS) and quantitative analysis (WDS) of the composition of MIT 5320-A.

According to WDS analysis, the exterior of the furnace wall (zone A) contains crystals of Ca, Fe, Mg silicate in a glassy matrix consisting of the feldspar, Ca-K-Al silicate. The intermediate zone B contains glassy matrix material, fine crystals, and some large quartz and

feldspar inclusions which sloughed off the ceramic wall in zone A. Conditions in zone B were hot enough that the quartz and feldspar partially fused with the glassy matrix (see Fig. 56b).

WDS analysis identified a thin crust of calcium sulfate covering the surface of the interior furnace wall (zone C). The calcium may have migrated to the surface of zone C, where it contacted the slag, from the ceramic fabric in zone A, either during smelting or subsequent to the smelting alteration of the surface of zone C. Beneath the crust is a glassy matrix with microcrystals which are composed of oxides of Mn, Fe, and Cu and Ca-K-Al silicate. Copper prills and sulfide matte prills, described above (see Fig. 57), are embedded in this glassy matrix, and electron microprobe measurements show that the prills prenetrated the wall of the furnace to a depth of 2 mm from the surface.

These analyses indicate that this ceramic artifact was at one time part of a smelting furnace. The furnace wall was in contact with a high-temperature molten slag that contained copper prills and copper sulfide prills. The furnace wall melted to a depth of 2 mm, which allowed the prills to pass through the slag and into the ceramic fabric.

DISCUSSION

Copper smelting was essential during the Inka hegemony as demonstrated by the deliberate use of copper for the empire's most important alloys, which included copper-silver, copper-gold, copper-silver-gold, copper-arsenic bronze, and copper-tin bronze. Sixteenth century Spanish documents suggest that gold and silver mining and smelting were at the core of Inka metallurgy when, in reality, these Spanish chronicles indicate the intense interest of the *conquistadores* in gold and silver. It was the search for those two metals that motivated the European voyages to the Americas and that provoked Francisco Pizarro, in 1532, to assassinate Atawalpa, the reigning Inka emperor. The Inka sought sources of copper understanding that metal alloy systems based on copper provided the properties they required of metal: toughness, malleability, and the generation of specific colors.

Unfortunately, there exists a paucity of Inka smelting sites. Only three studies have been published on the archaeological remains of Inka copper smelting installations, all in the provinces of the Inka empire. Izumi Shimada has researched Inka bowl furnaces at one site, Batán Grande, located on the far north coast of Peru (Shimada 1994; Shimada et al. 1982, 1991). When the Inka came to power, they maintained the preexisting extractive metallurgical practices of the local communities at Batán Grande. These practices were initiated by the Sicán (ca. 850 C.E.) before they were conquered by the Chimú (ca. 1375), who also preserved the Sicán large-scale production of copper-arsenic alloys. The other two copper smelting sites are located in northwest Argentina, a south-central Andean province of the Inka empire. Luis Gonazález has carried out an extensive site investigation at Rincón Chico (González 2004). The Inka

introduced a few minor changes to the preexisting metallurgical technology that existed at this bronze production site. However, in order to produce bronze tools and ornaments at a large scale, the state reconfigured the organization of the labor force. Rodolfo Raffino has reported on the Inka furnaces at Quillay Wayras (Raffino et al. 1996). Slag and native copper remains encrusted in gangue on the surface of the site suggest that the Inka were smelting native copper. Since the site has not been investigated and the standing furnaces identified at the site are only partially preserved, it is not known how the Inka utilized the furnaces for their smelting operations.

There is very limited information on Inka copper smelting in the frontier provinces of the south-central Andes which included northwest Argentina, Bolivia, and Chile. This thesis provides significant additional evidence on Inka extractive metallurgy as carried out at San Bartolo, a copper smelting site in northern Chile. The research reported here is the first investigation of its kind to be carried out at any archaeological site in Chile. Moreover, San Bartolo is only the second Inka smelting site anywhere in the south-central Andes to have undergone a materials processing analysis.

The five surface-collected Inka artifacts I analyzed qualitatively and quantitatively (two ores, two slags, and one furnace wall fragment) confirm that the Inka traveled 700 miles from Cuzco to exploit and process the copper ore deposits at San Bartolo. One artifact was determined to be a piece of copper ore, consisting of native copper and cuprous oxide. Another artifact was also found to be a piece of copper ore, containing veins of unaltered, primary copper sulfide mineral as well as copper oxide, copper chloride, and copper sulfate weathering products. This evidence suggests that the ores the Inka smelted consisted of a range from copper sulfides to copper oxides and including native copper.

One of the artifacts is a piece of copper smelting slag with a relatively high concentration of copper metal prills embedded in a glassy matrix. The glass exhibits pores and vesicles and contains approximately 4 wgt. % of MnO, whereas neither of the copper ores contains manganese. It is likely that MnO_2 was added to the furnace charge as a fluxing agent. Since a high concentration of copper prills was identified in the matrix, this slag never reached a temperature high enough to melt completely. The high viscosity of the slag may have been a result of adding an inadequate amount of MnO_2 flux.

A second smelting slag artifact, however, has significantly higher concentrations of MnO (about 31 wgt. %) and CaO (about 5 wgt. %). Metallographic and electron microbeam probe analyses determined that this material was once fully molten, suggesting that enough flux, in the form of MnO_2 and CaO, was added to the furnace to lower the melting point and the viscosity of the glass. As a result, the smelted copper, in the form of prills, gravitated through the slag to the furnace bottom, and this once-molten slag contains much less copper than the other slag artifact.

Manganese dioxide is an effective flux and, for example, was used as a flux in the smelting of copper ore at the site of Timna, Israel, during the Late Bronze and Early Iron Age (Rothenberg 1972). The presence of manganese in trace concentrations (0.03-0.05%, as MnO) in both pieces of San Bartolo ore indicates that the manganese did not accompany the copper ore and was mined from a separate source and added during smelting.

Thermal alteration tests with samples from the once-molten slag and examination of the cross-section of furnace wall indicate that the smelting furnaces were at least partially constructed of thick, ceramic walls that resisted temperatures as high as at least 1125°C. Smelting was carried out at temperatures that may have slightly exceeded 1125°C, and at these temperatures the slags produced were entirely molten allowing for complete separation of the

dense copper metal and the lighter slag that floated above it. Though the analysis of the once-molten slag has enabled me to determine the lowest possible smelting temperature required to operate the furnaces, I cannot determine how the metalworkers achieved the temperatures the furnaces reached without access to the remains of the smelting furnaces. Perhaps the results of this investigation will encourage the archaeologists who provided me with the San Bartolo artifacts to return to the site and to carry out excavations there that might uncover the remains of the smelting furnaces the Inka operated.

Although there is no archaeological evidence that metal smelting at San Bartolo, or anywhere in the prehistoric Andes, involved the use of bellows or any other devices for increasing the volume of air that entered the smelting furnace in order to raise the temperature, it is known that at the time of the Spanish Invasion, communities located in the south-central Andes used the *huayra* for metallic ore smelting. The *huayra,* a natural draft furnace made of stone or ceramic, was often located on the windy, steep slopes of the Andean hillsides, which provided a strong updraft that allowed Andean smelters to achieve temperatures sufficient to extract copper and silver metal from their ores. Perhaps future excavations at San Bartolo will aim to determine if San Bartolo was one such community that utilized the *huayra* in its copper smelting operations.

The piece of native copper ore is particularly interesting, because Raffino (1996) reported the presence of native copper distributed widely on the surfaces of the site at Quillay Wayras in northwest Argentina. Together, the San Bartolo and Quillay Wayras evidence suggests that the Inka deliberately mined and smelted native copper in the provinces. The sierra and coastal zones of northern Chile are widely known for their ore deposits containing native copper (Núñez 1987). The Inka were aware of the existence of these sources of native copper because the ores

were already being exploited by local communities. They chose sites where native copper was present in the ore deposit. By deliberately mining ores containing native copper, the Inka were able to extract copper of high purity.

The piece of sulfidic copper ore is also interesting, because it indicates the likelihood that the cosmelting of copper sulfide and copper oxide ores was practiced at San Bartolo. The sulfidic ore was not rejected but rather cosmelted with its associated oxide weathering products. Such an extractive process may have resulted in slags that resemble the once-molten slag containing prills of copper metal and copper sulfide prills. Unlike oxidation and direct reduction smelting, cosmelting does not require charcoal in the charge, because $CO\uparrow$ will not reduce sulfide mineral (Lechtman and Klein 1999). In cosmelting, the sulfur reduces the oxide component of the ore to metal and is eliminated as $SO_2\uparrow$. This reduction reaction is illustrated in the following example of the cosmelting of copper carbonate and enargite (copper sulfarsenide) ores:

$$\underset{\text{copper carbonate}}{8\ CuCo_3} + \underset{\text{enargite}}{Cu_3AsS_4} \xrightarrow{\text{heat}} \underset{\text{Cu-As alloy}}{Cu,\ As} + 4\ \underset{\text{gas}}{SO_2\uparrow} + 8\ \underset{\text{gas}}{CO_2\uparrow}$$

The cosmelting of copper sulfide and copper oxide ores results in products that may include smelted metal, matte (copper sulfide), and slag (Lechtman and Klein 1999). In San Bartolo, the Inka likely took advantage of this process to smelt complex ores containing native copper, copper sulfides, and copper oxides. The small amounts of matte present in the slag suggest that the proportion of sulfide in the ore was low.

Today, Chile is the world's largest producer of copper, and there is no doubt that the Inka, who ruled the Andes from Cuzco, administered copper alloy production in their far-flung

provinces, one of which included the site of San Bartolo. The combination of a cosmelting regime and the use of a highly effective fluxing agent at San Bartolo probably means that the Inka did not require vigorous reducing conditions to produce a high degree of separation between the copper metal and the slag. The results of this investigation are significant because they strongly suggest that the Inka had found a method to extract copper metal from recalcitrant sulfide ores by cosmelting these ores with oxides of copper. Thus, it is clear that Andean prehistoric extractive metallurgy was far more sophisticated than archaeologists and metallurgists have described.

Acknowledgements

I'd like to thank first and foremost Prof. Heather Lechtman, my thesis advisor who guided me throughout this research project. In addition, I'd like to thank Dr. Elizabeth Hendrix, CMRAE laboratory supervisor, for her help in preparing and examining the artifacts from this thesis. I'd also like to thank Dr. Nilanjan Chatterjee (EAPS) for his expertise on microbeam probe analysis and Dr. Harold Larson (DMSE) for allowing me to use the muffle furnace for thermal alteration tests.

References Cited

Alonso-Barba, Alvaro

1967 Arte de los Metales. Editorial Potosí: Potosí.
[1640]

Bowen, N.L. and J.F. Schairer

1932 SiO_2-FeO Phase Diagram. *American Journal of Science* 5 (24): 177-213.

Burger, Richard L. and Robert B. Gordon

1998 Early Central Andean Metalworking from Mina Perdida, Peru. *Science* 282: 1108-1111.

Castro, Victoria, Carlos Aldunate, Varinia Varela

2003 San Bartolo. Retazos de Una Historia Documentada por la Arqueología, la Historia y la Etnografía. XVI Congreso Nacional de Arqueología Chilena: 1-19.

Epstein, S.M.

1982 The Prehistoric Copper Smelting Industry at Cerro de los Cementerios, Peru: Analysis of the Product. *MASCA Journal* 2(2): 58-62.

Flint, S.

1985 Alluvial Fan and Playa Sedimentation in an Andean Arid Closed Basin: the Paciencia Group, Antofagasta Province, Chile. *Journal of the Geological Society* 142: 533-546.

González, Luis R.

2004 Bronces Sin Nombre: La Metalurgía Prehispanica en El Noroeste Argentino. Fundación Ceppa: Buenos Aires.

Graffam, Gray, Mario Rivera and Alvaro Caravic

1994 Copper Smelting in the Atacama: Ancient Metallurgy at the Ramaditas Site, Northern Chile. In *In Quest of Mineral Wealth.* Alan K. Craig and Robert C. West. *Geoscience and Man*, volume 33. Geoscience Publications: Baton Rouge, pp. 75-90.

Lechtman, Heather N.

1976 A Metallurgical Site Survey in the Peruvian Andes. *Journal of Field Archaeology* 3:1-42.

1988 Traditions and Styles in Central Andean Metalworking. In *The Beginning of the Use of Metals and Alloys*, Robert Maddin, ed. MIT Press: Cambridge, pp. 344-378.

1993 Technologies of Power: The Andean Case. In *Configurations of Power*. Cornell University Press, pp. 244-280.

2003 Middle Horizon Bronze: Centers and Outliers. In *Patterns and Process*. Lambertus van Zelst. Smithsonian Center for Materials Research and Education: Suitland, pp. 248-268.

2005 Arsenic Bronze at Pikillacta. In *Pikillacta: The Wari Empire in Cusco*, Gordon F. McEwan, ed. Iowa City: University of Iowa Press, pp. 131-146.

Lechtman, Heather N. and Andrew W. Macfarlane

2004 La metalurgía del bronce en los Andes Sur Centrales: Tiwanaku y San Pedro de Atacama. *Estudios Atacamenos* 30: 7-27.

Lechtman, Heather N. and Sabine Klein

1999 Production of Copper-Arsenic Alloys (Arsenic Bronze) by Cosmelting: Modern Experiment, Ancient Practice. *Journal of Archaeological Science* 26: 497-526.

Levin, Ernest M., Carl R. Robbins, and Howard F. McMurdie

1964 Phase Diagrams for Ceramists. The American Ceramic Society: Columbus.

Merkel, John and Izumi Shimada

1988 Arsenical Copper Smelting at Batán Grande, Peru. *IAMS (Institute for Archaeo-Metallurgical Studies)* 12: 4-7.

Moseley, Michael E.

2001 The Incas and Their Ancestors: The Archaeology of Peru. Thames and Hudson Inc.: New York.

Murra, John V.

1980 Peasant Corvee and the Revenues of the State. *Economic Organization of the Inka State*: 89-119. JAI Press Inc.

Niemeyer, Hans, Gastón Castillo, and Miguel Cervellino.

1991 Estrategía del Dominio Inca en el Valle de Copiapó. *Actas del XII Congreso Nacional de Arqueología Chilena*: 333-371.

Nuñez, Lautaro

1987 Tráfico de metales en el área centro-sur Andina: factos y expectavivas. *Cuadernos del Instituto Nacional de Antropología* 12: 73-105.

Patterson, Clair C.

1971 Native Copper, Silver, and Gold Accessible to Early Metallurgists. *American Antiquity* 36 (3): 286-321.

Raffino, Rodolfo, Rubén Iturriza, Anahí Iácona, Aylen Capparelli, Diego Gobbo, Victoria G. Montes, and Rolando Vázquez

1996 Quillay: Centro Metalurgico Inka en el Noroeste Argentino. *Tawantinsuyu* 2: 59-69.

Rostoker, W., V.C. Pigott, and J.R. Dvorak

1989 Direct Reduction to Copper Metal by Oxide-Sulfide Mineral Interaction. *Archaeomaterials* 3: 69-87.

Rothenberg, Beno

1972 Timna, Valley of the Biblical Copper Mines. Thames and Hudson: London.

Shimada, Izumi

1994 Pre-Hispanic Metallurgy and Mining in the Andes: Recent Advances and Future Tasks. In *In Quest of Mineral Wealth.* Alan K. Craig and Robert C. West. *Geoscience and Man*, volume 33. Geoscience Publications, Baton Rouge, Louisiana, pp. 38-58.

Shimada, Izumi and John F. Merkel

1991 Copper-Alloy Metallurgy in Ancient Peru. *Scientific American* July: 80-86.

Shimada, Izumi, Stephen Epstein, Alan K. Craig

1982 Batán Grande: A Prehistoric Metallurgical Center in Peru. *Science* 216: 952-959.

1983 The Metallurgical Process in Ancient North Peru. *Archaeology* Sept./Oct.: 38-45.

Van Buren, Mary and Barbara H. Mills

2005 Huayrachinas and Tocochimbos: Traditional Smelting Technology of the Southern Andes. *Latin American Antiquity* 16: 3-25.

Von Hagen, Adriana and Craig Morris.

1998. The Cities of the Ancient Andes. Thames and Hudson: London.

FIGURES

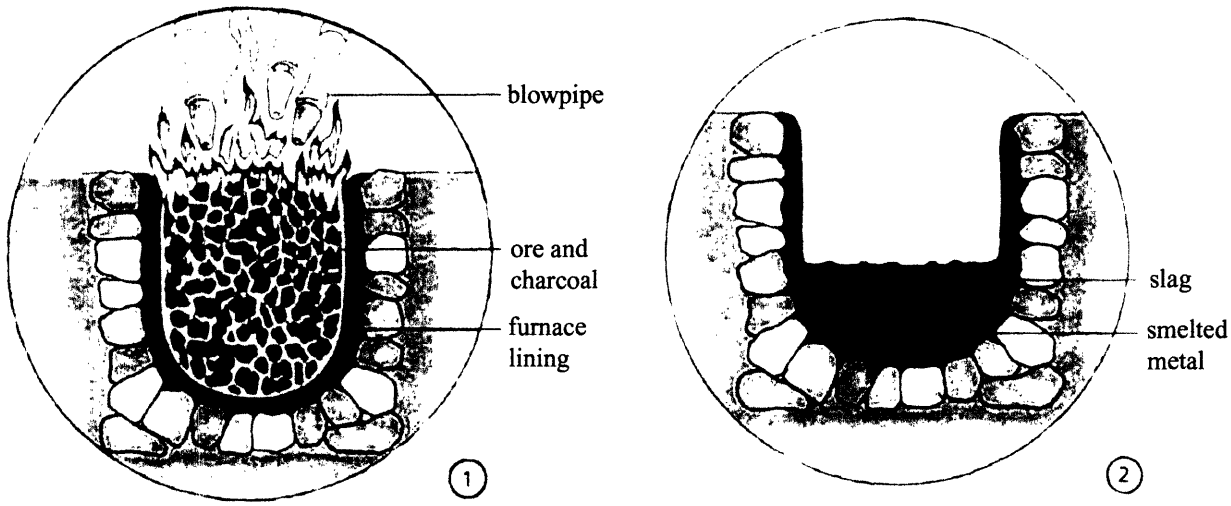

Figure 1. Simple bowl furnace of the type used in the Central Andes, before and after smelting operation (courtesy of Prof. Heather Lechtman).

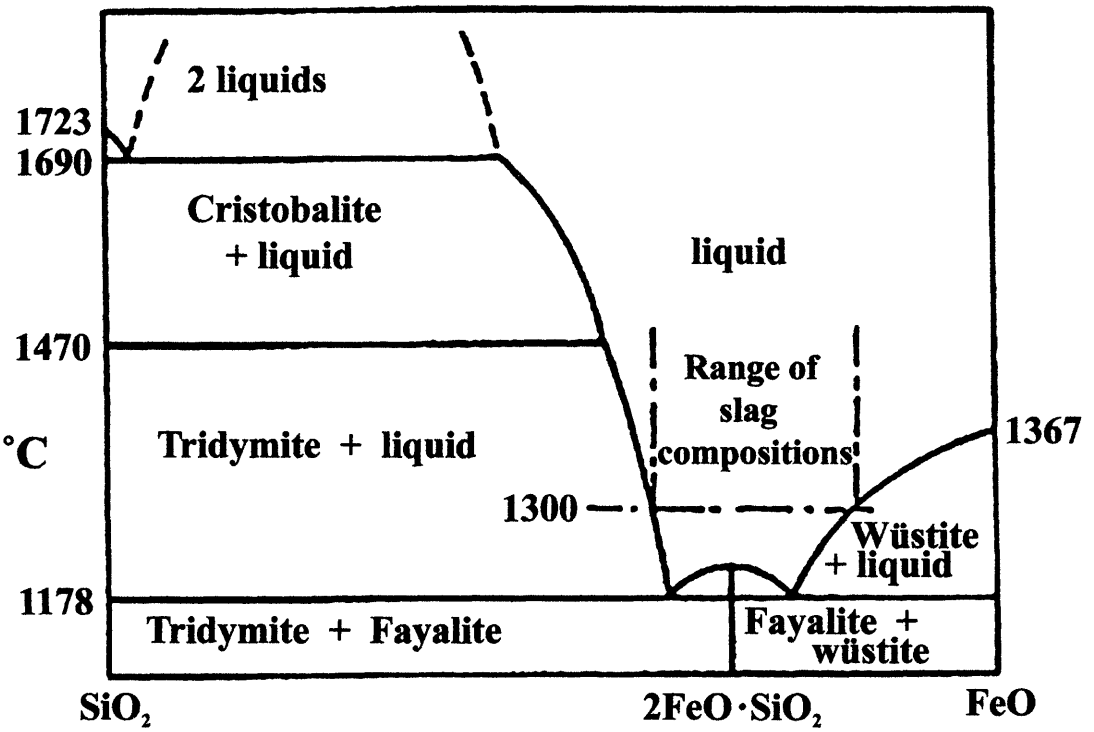

Figure 2. Equilibrium diagram of the system FeO-SiO_2 (Bowen and Schairer 1932).

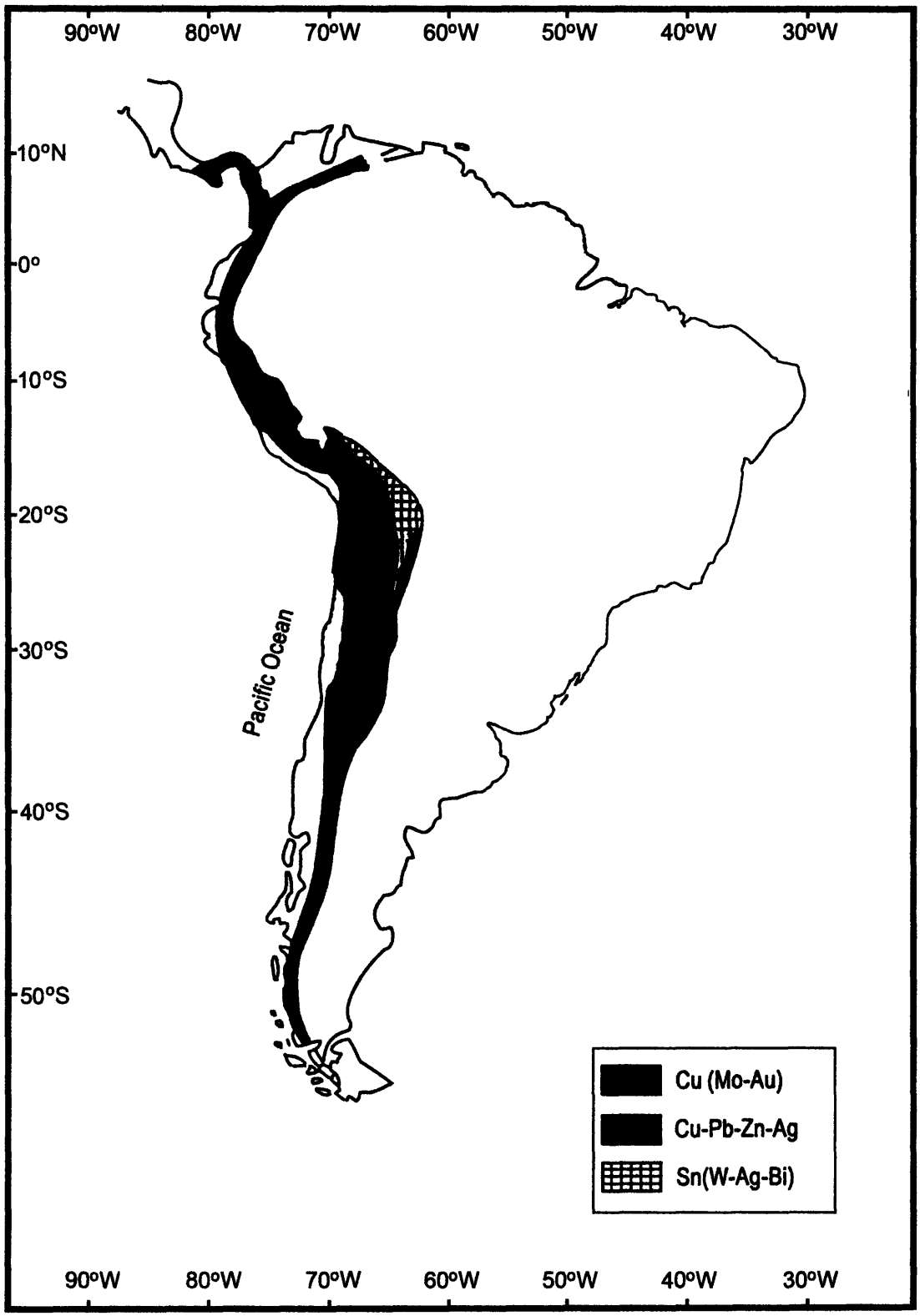

Figure 3. The copper and tin belts in Andean South America (after Jorge Oyarzún, http://www.ucm.es/info/crismine/Andes/Fig11.htm).

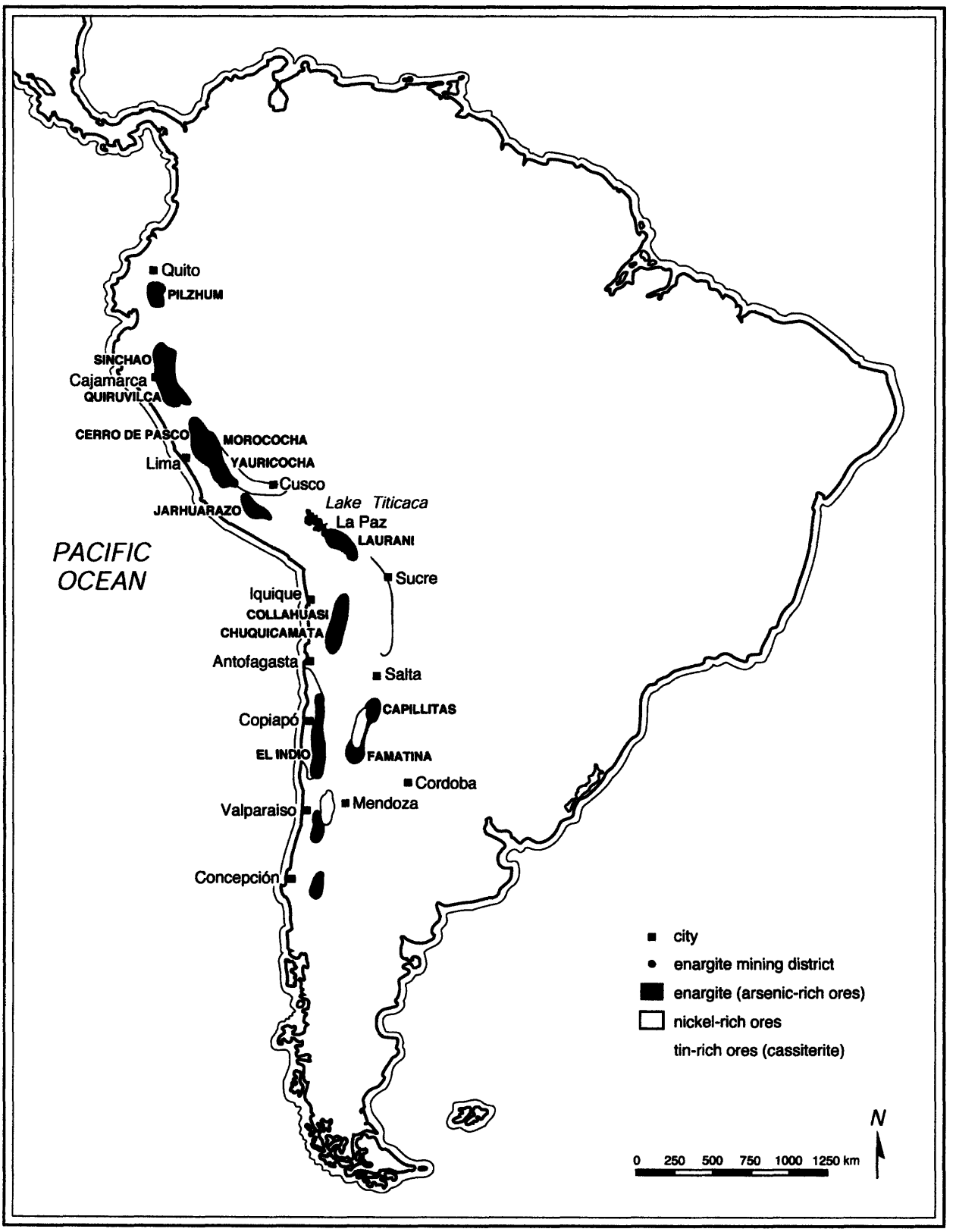

Figure 4. Enargite, nickel, and tin ore sources in the Andes (after Lechtman 2003: Fig. 3).

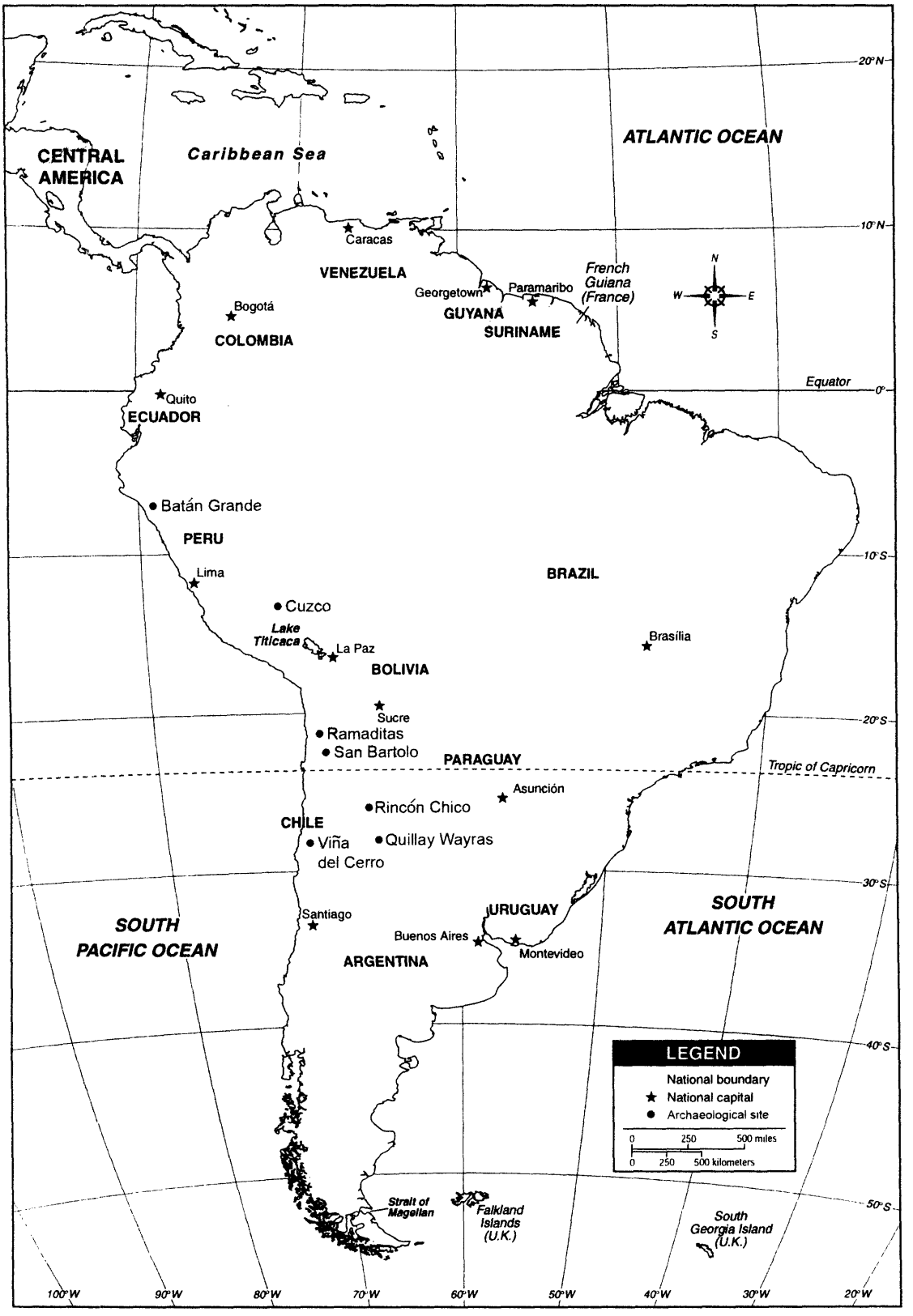

Figure 5. Archaeological sites in South America mentioned in this thesis.

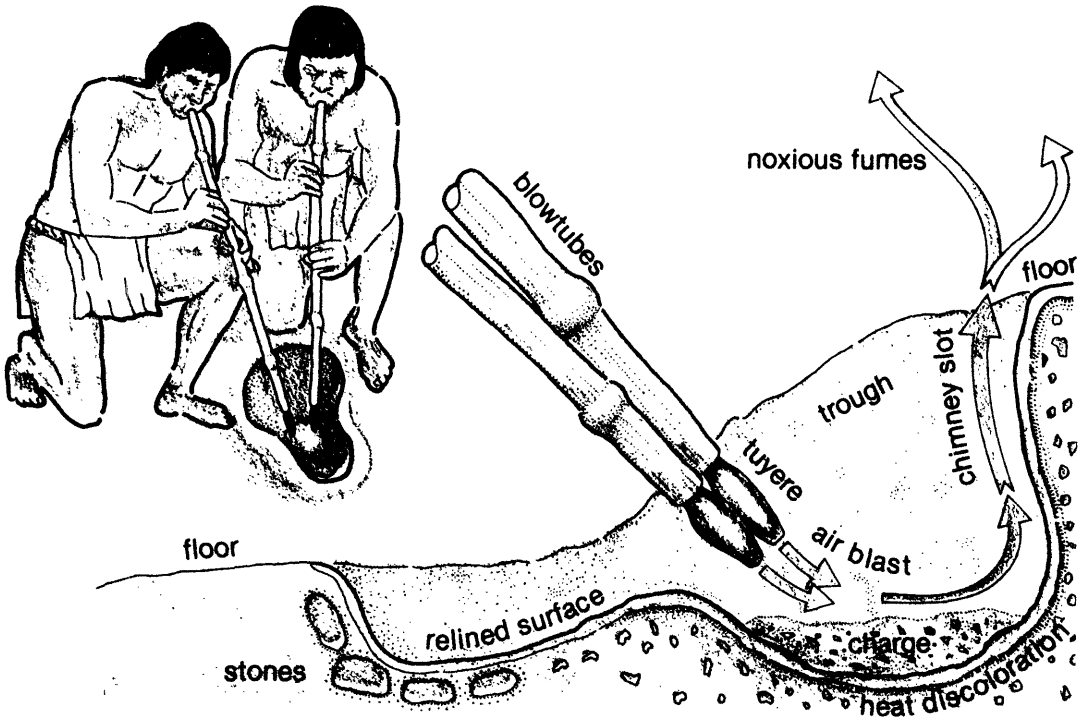

Figure 6. Artist's reconstruction of copper smelting at Batán Grande (Shimada et al. 1983: 42).

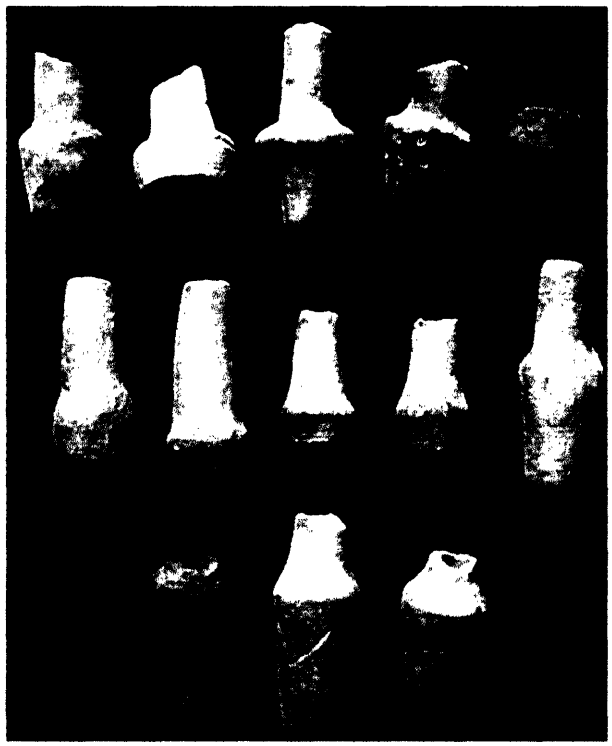

Figure 7. Ceramic blowtube tips (*toberas*) from Batán Grande (Shimada and Merkel 1991: 84).

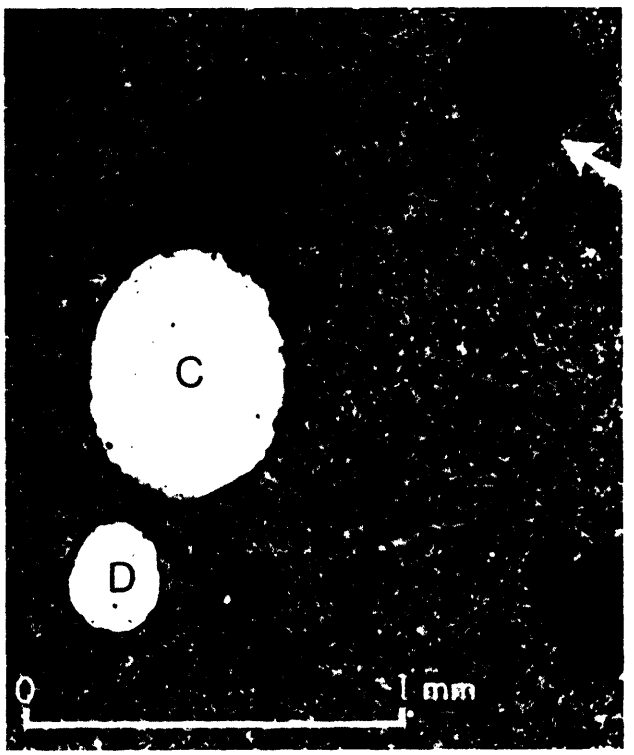

Figure 8a. Photomicrograph of slag specimen from Batán Grande showing copper prills embedded in slag (Epstein 1982: 60).

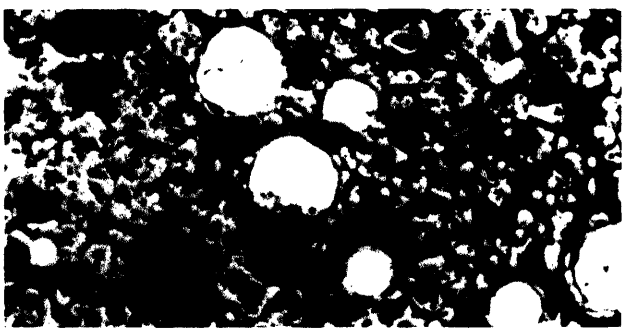

Figure 8b. Photomicrograph (80x) of slag specimen from Batán Grande showing copper prills entrapped in slag (Merkel and Shimada 1988: 6).

Figure 9. Photograph of a *huayra* furnace (Van Buren and Mills 2005: Fig. 4).

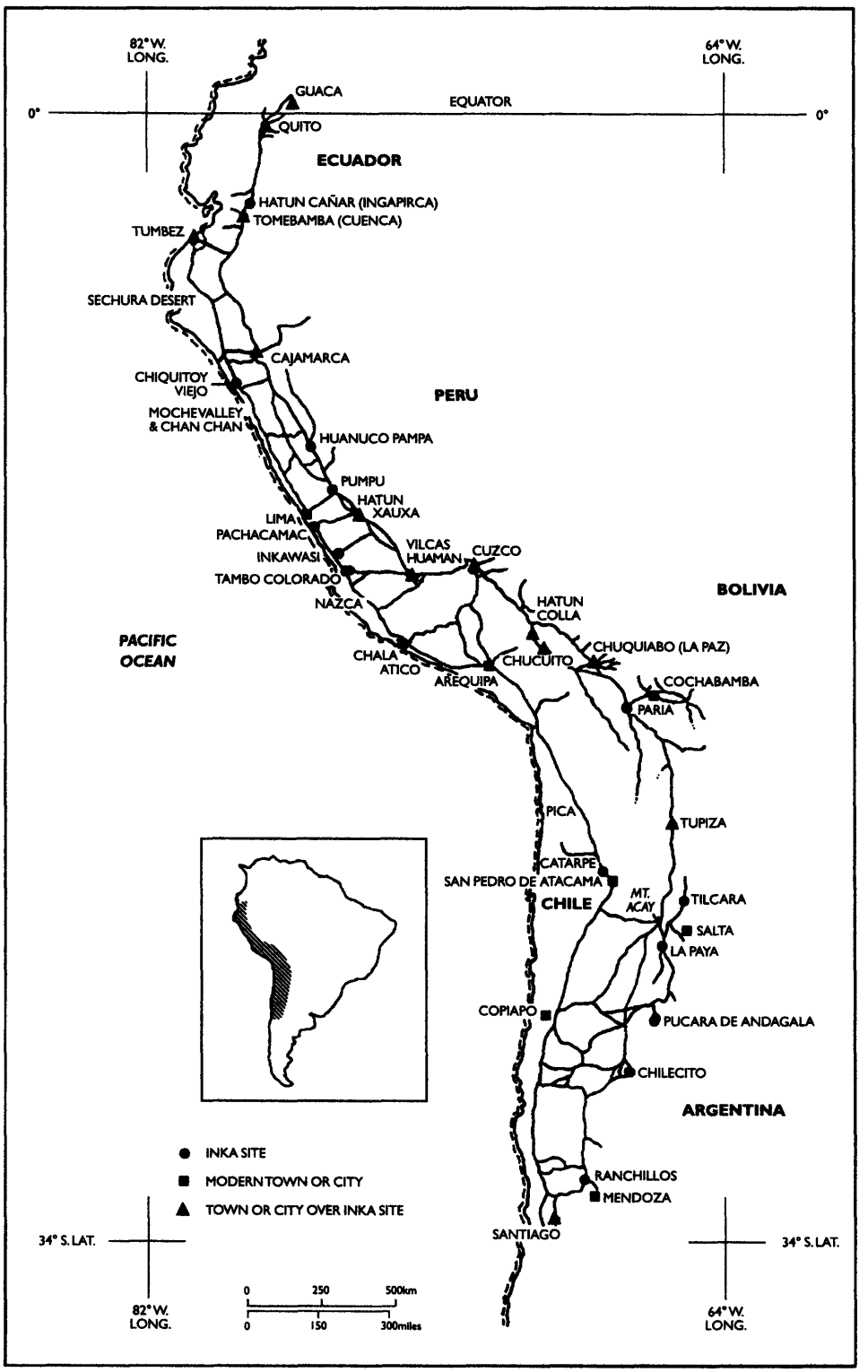

Figure 10. Map showing the Khapaq Ñan, the Inka road system, consisting of two main parallel roads, running along the Pacific coast and the Andean highlands. Many lateral roads connect these two main roads (von Hagen and Morris 1998).

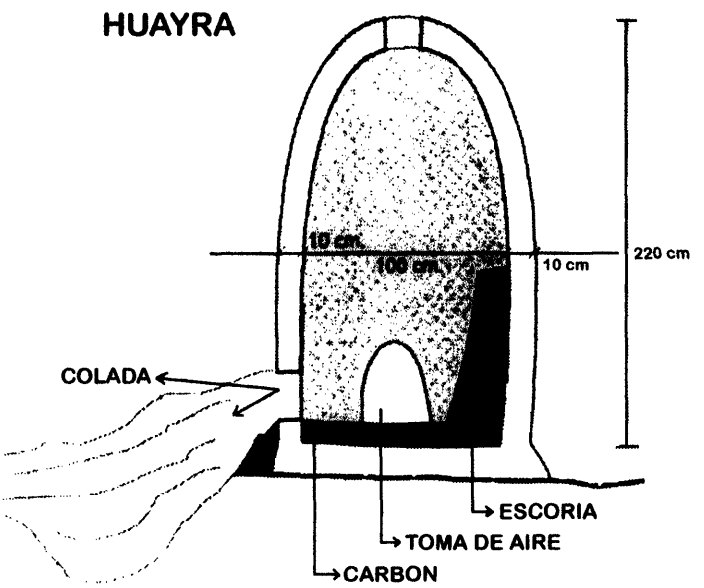

Figure 11. Artist's reconstruction of a proposed *huayra* furnace, based on remains of furnace foundations at Quillay Wayras, Argentina (Raffino et al. 1996: 63).

Figure 12. Illustration by Alvaro Alonso Barba of a traditional *huayra*, in use at Potosí, Bolivia, in the mid 16th century (Van Buren and Mills 2004:7).

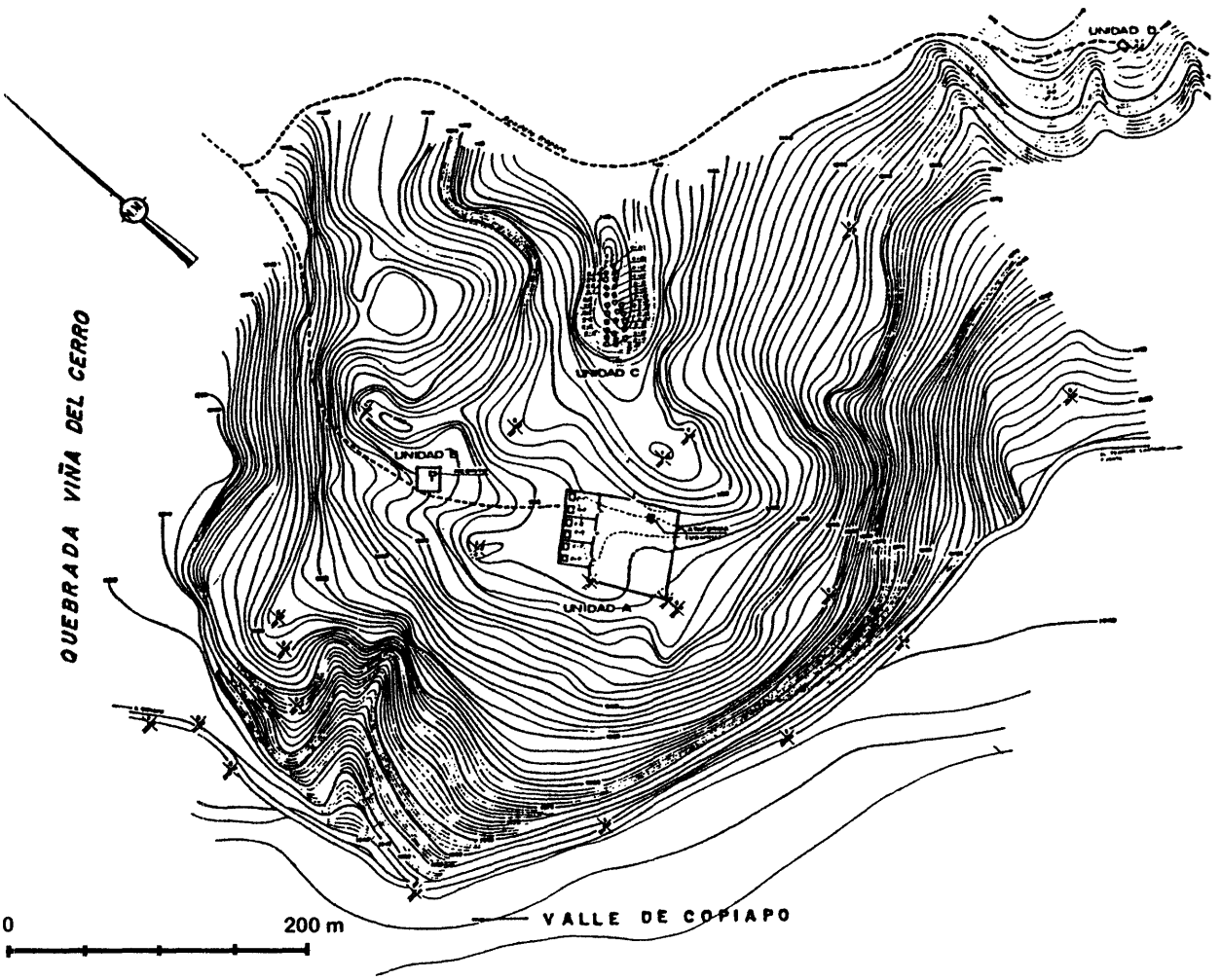

Figure 13. Map showing 26 foundations of *huayra* furnaces in Unidad C of Viña del Cerro, Copiapó Valley, Chile (Niemeyer et al. 1991: 342).

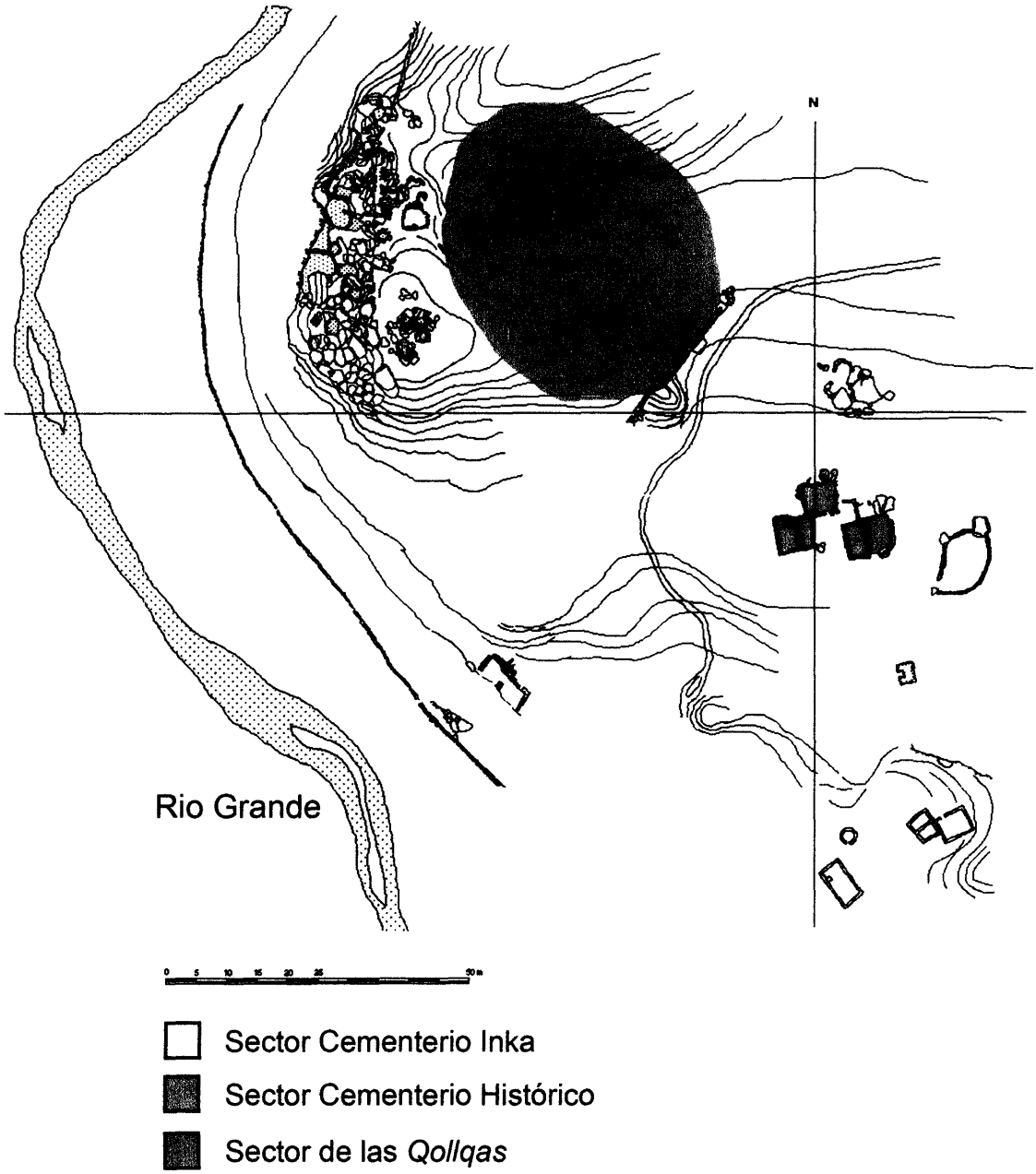

Figure 14. Site map of El Establecimiento in San Bartolo. Pieces of slag and the portion of furnace wall were collected from Sector Cementerio Histórico, and pieces of ore were collected from Sector de las *Qollqas* (after Castro et al. 2003).

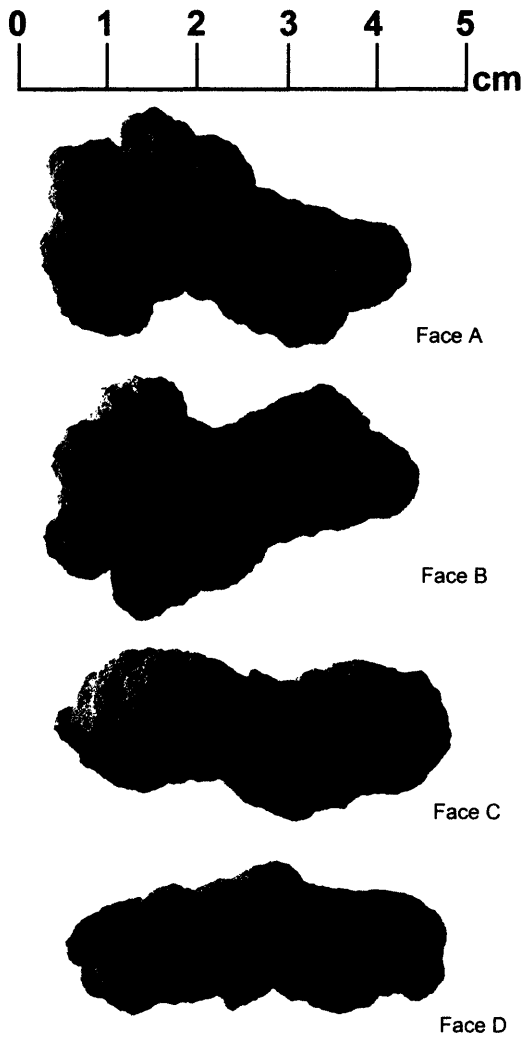

Figure 15. MIT 5313. Four views of the object, showing bulbous and knobby components with cavities in between the contiguous globular parts.

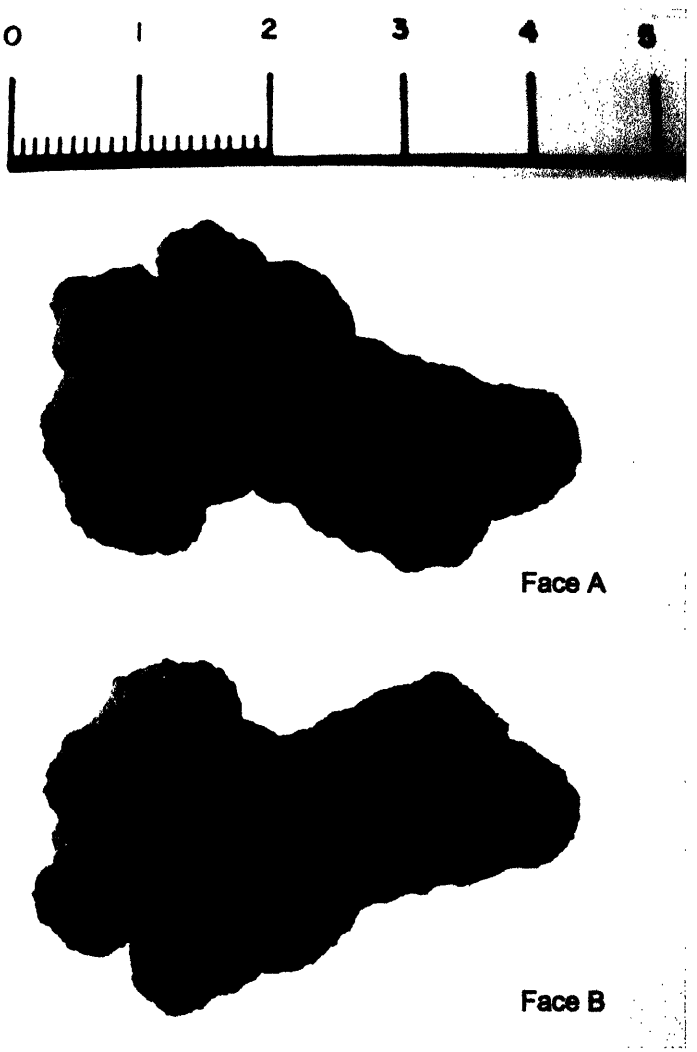

Figure 16. MIT 5313. Two views, showing the pale green color of the object.

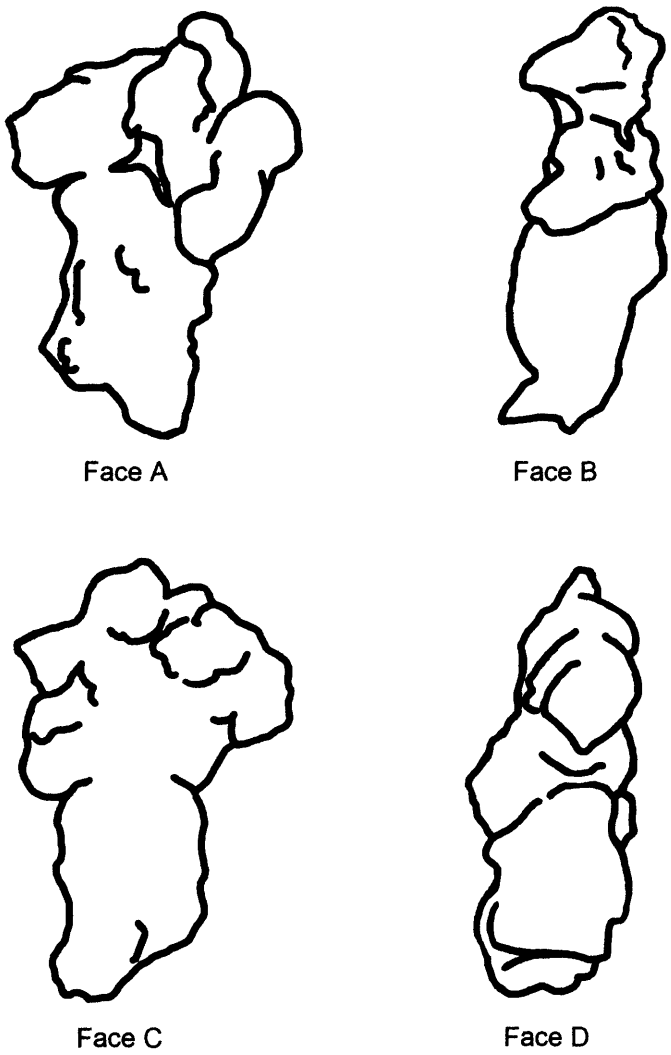

Figure 17. MIT 5313. Line drawing showing four views.

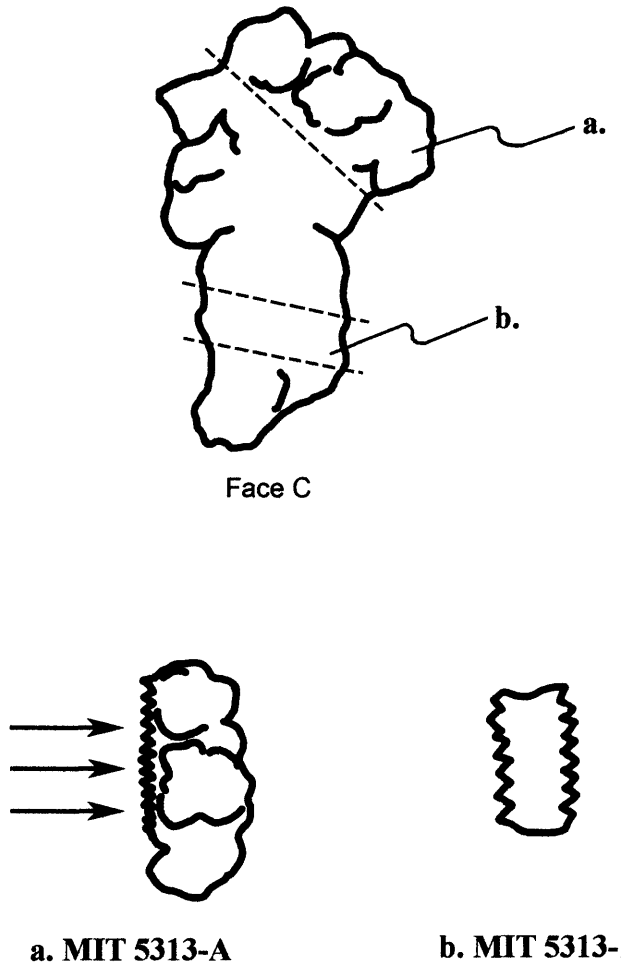

Figure 18. MIT 5313. Line drawing showing locations and orientations of samples removed.

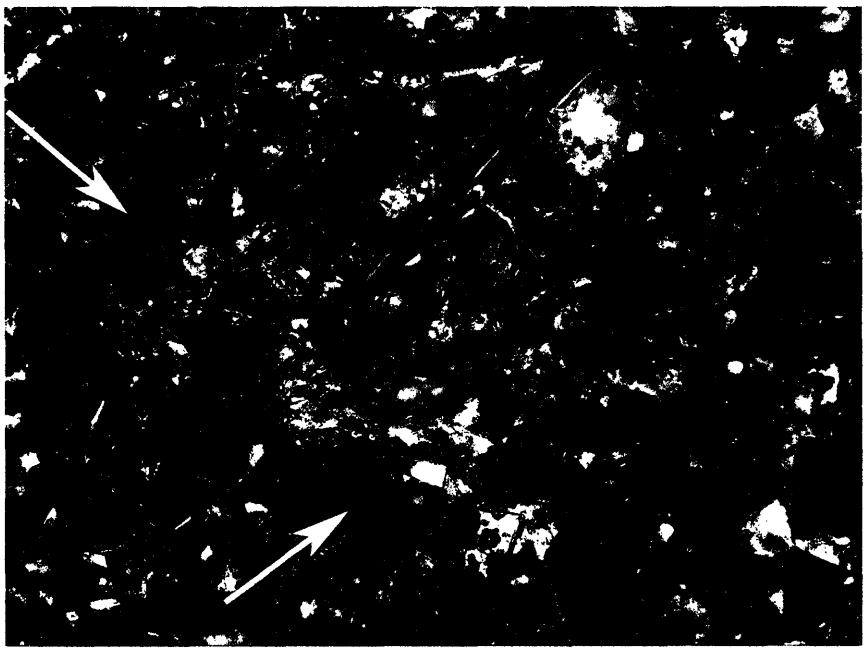

Figure 19. MIT 5313-A. 200x, etched with K_2CrO_7. Cross-polarized light; arrows point to red cuprous oxide grains.

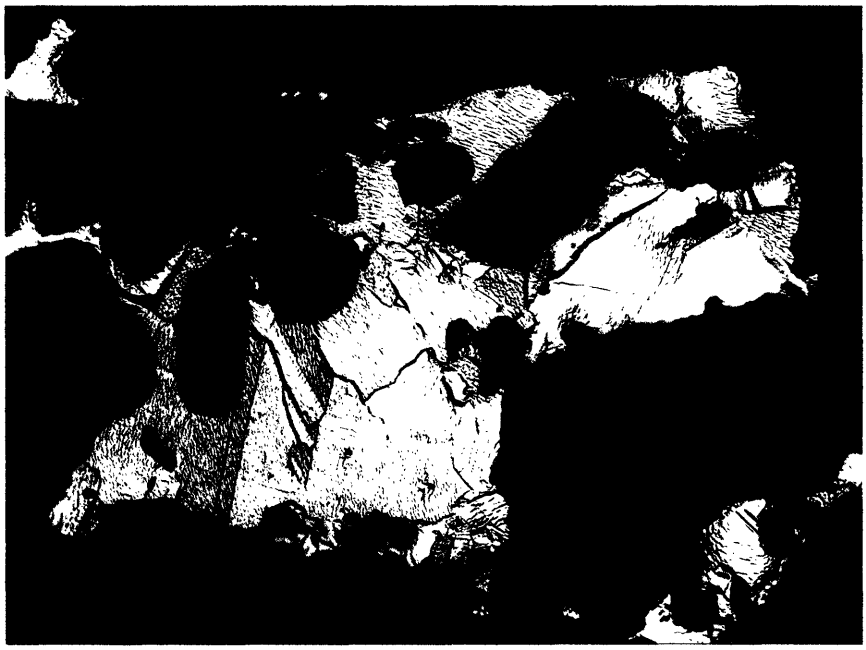

Figure 20. MIT 5313-A. 500x, etched with K_2CrO_7. Copper grains displaying annealing twins.

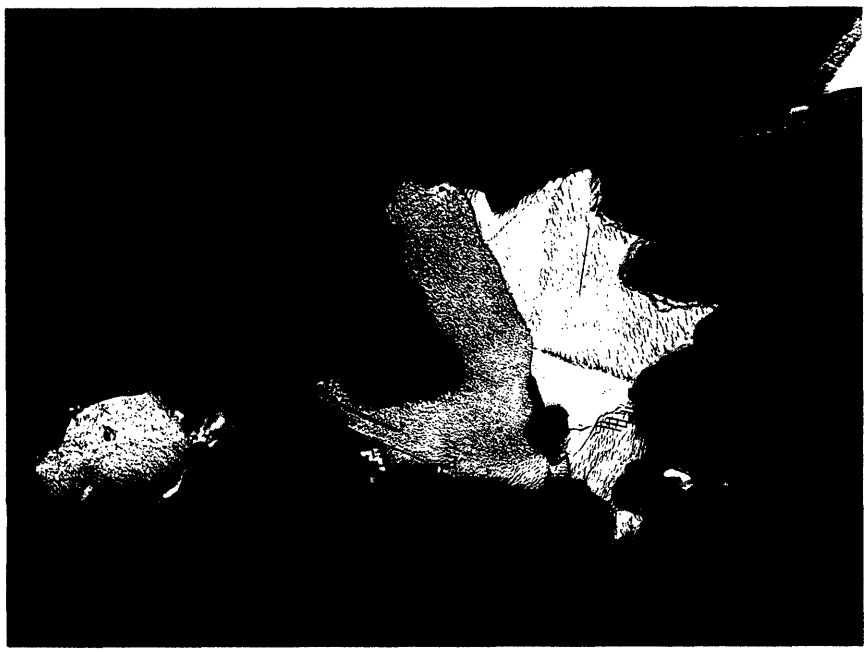

Figure 21. MIT 5313-A. 500x, etched with K_2CrO_7. Copper grain exhibiting slip planes.

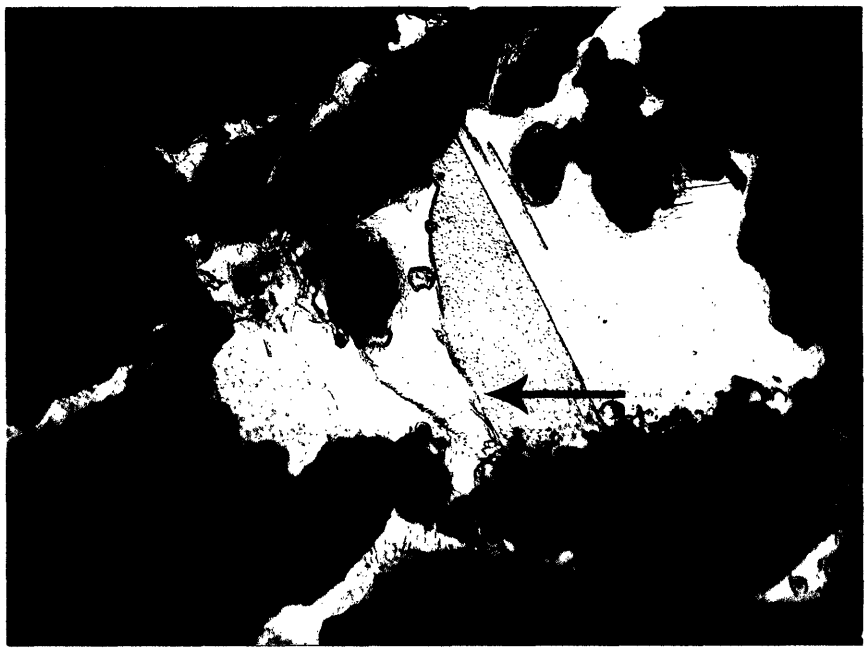

Figure 22. MIT 5313-A. 500x, etched with K_2CrO_7. Copper grain exhibiting a double-grain boundary, as indicated by the arrow.

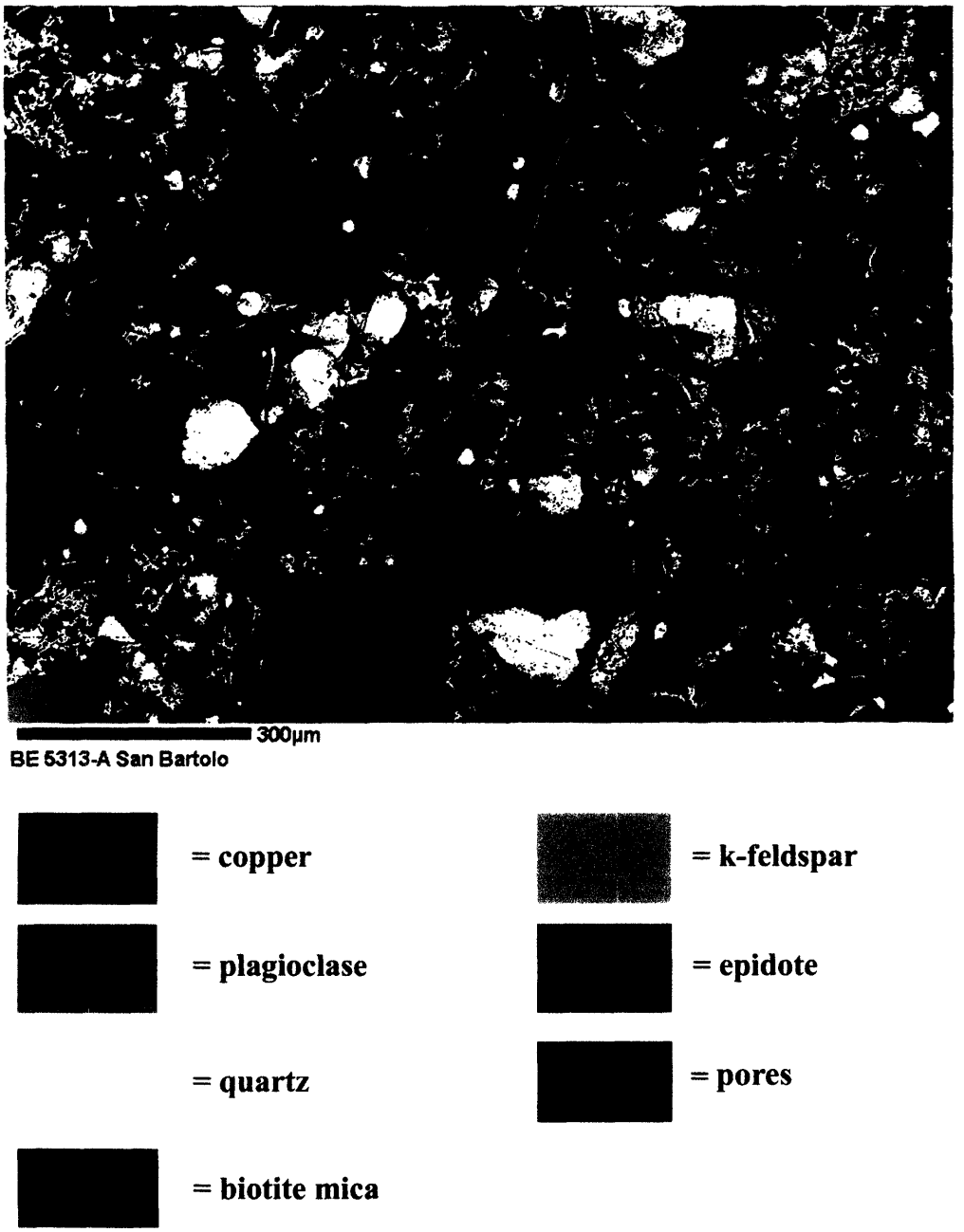

Figure 23. MIT 5313-A. Color image analysis with an electron micro-analyzer identifying an assemblage of granitic grains, copper, and pores.

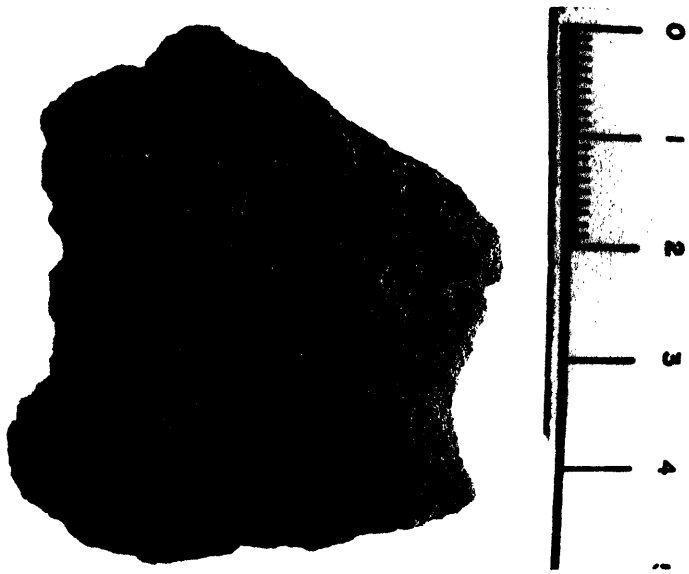

Face A

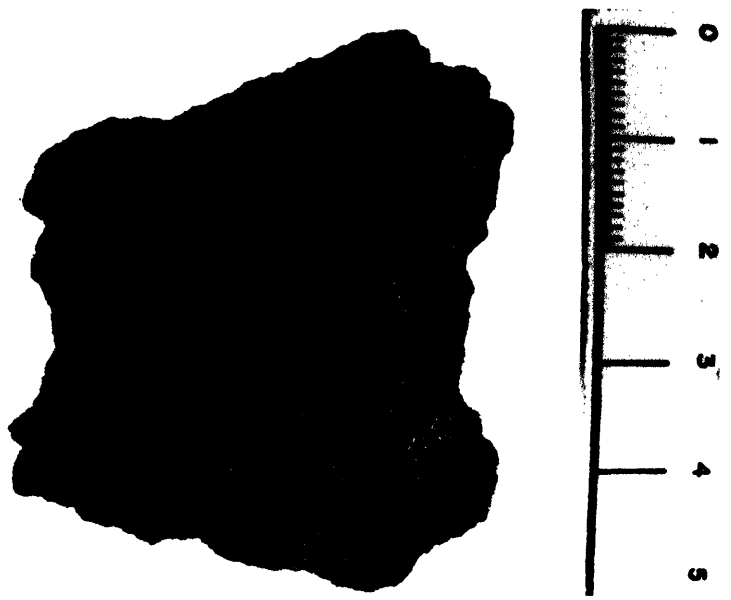

Face B

Figure 24. MIT 5319. Two views of the object, which is sub-rounded, trapezoidal, and generally flat, except for a few bumps and bulges on Face A.

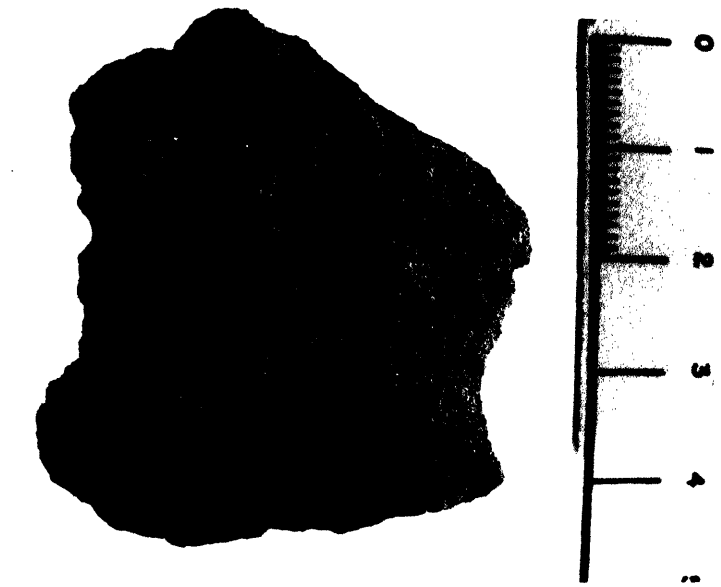

Face A

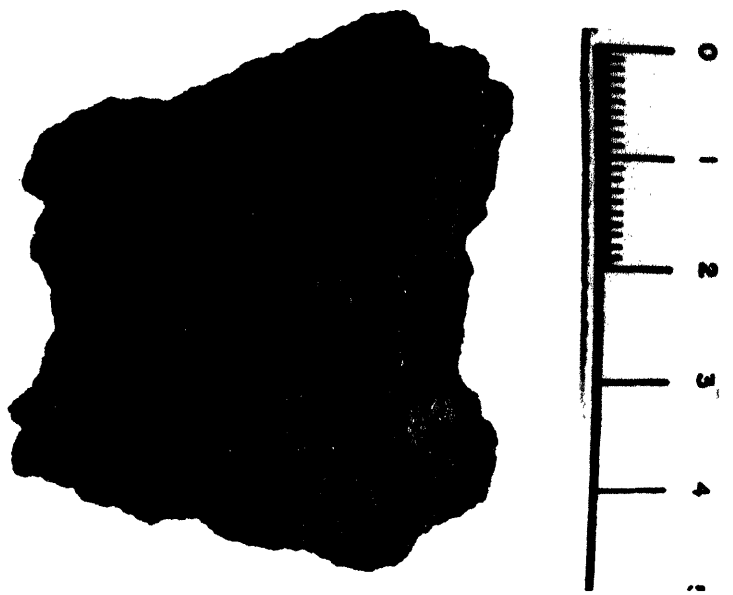

Face B

Figure 25. MIT 5319. Two views, showing the green color of the object.

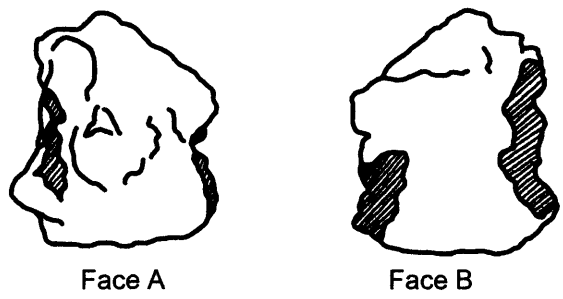

Figure 26. MIT 5319. Line drawing showing sandy accretions that were removed.

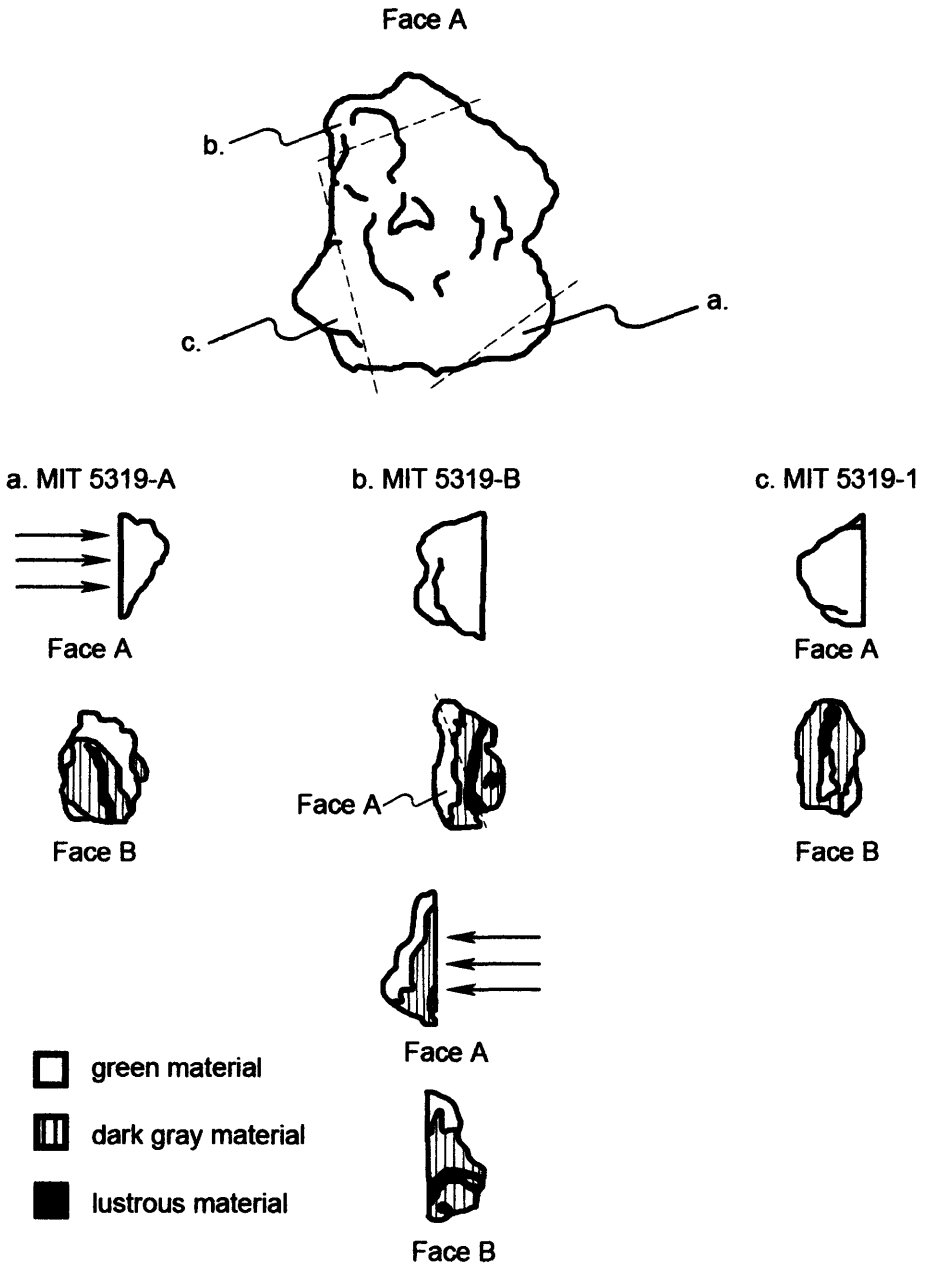

Figure 27. MIT 5319. Line drawing showing locations and orientations of samples removed for electron microanalysis.

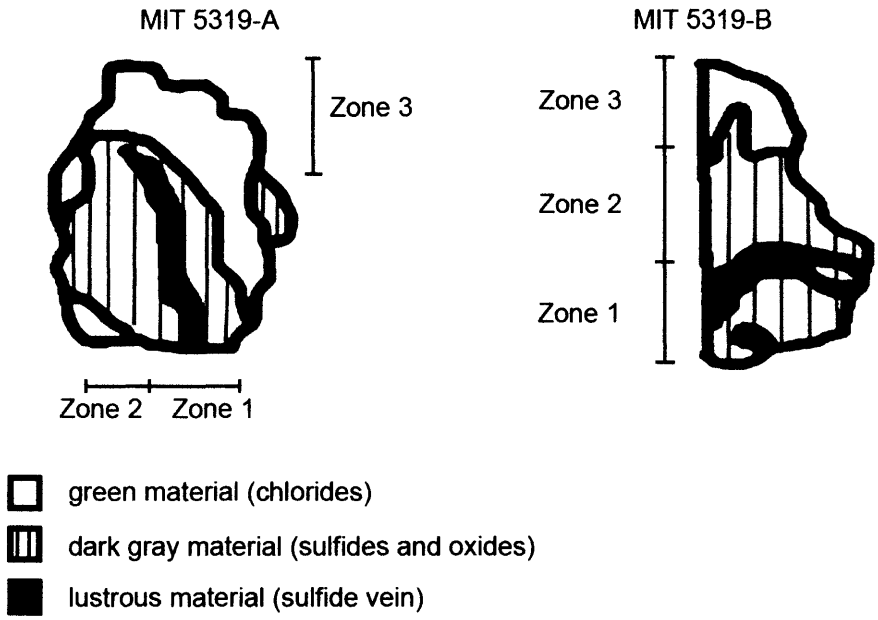

Figure 28. MIT 5319-A and MIT 5319-B. Line drawing of the two specimens, showing the samples divided into zones.
Zone 1: lustrous veins of primary copper sulfide containing some cuprous oxide weathering product, intergrowth of copper sulfide and copper sulfate, and lead sulfide.
Zone 2: intergrowth of copper sulfide and barium-strontium sulfate.
Zone 3: chloride weathering product of the primary copper sulfide vein.

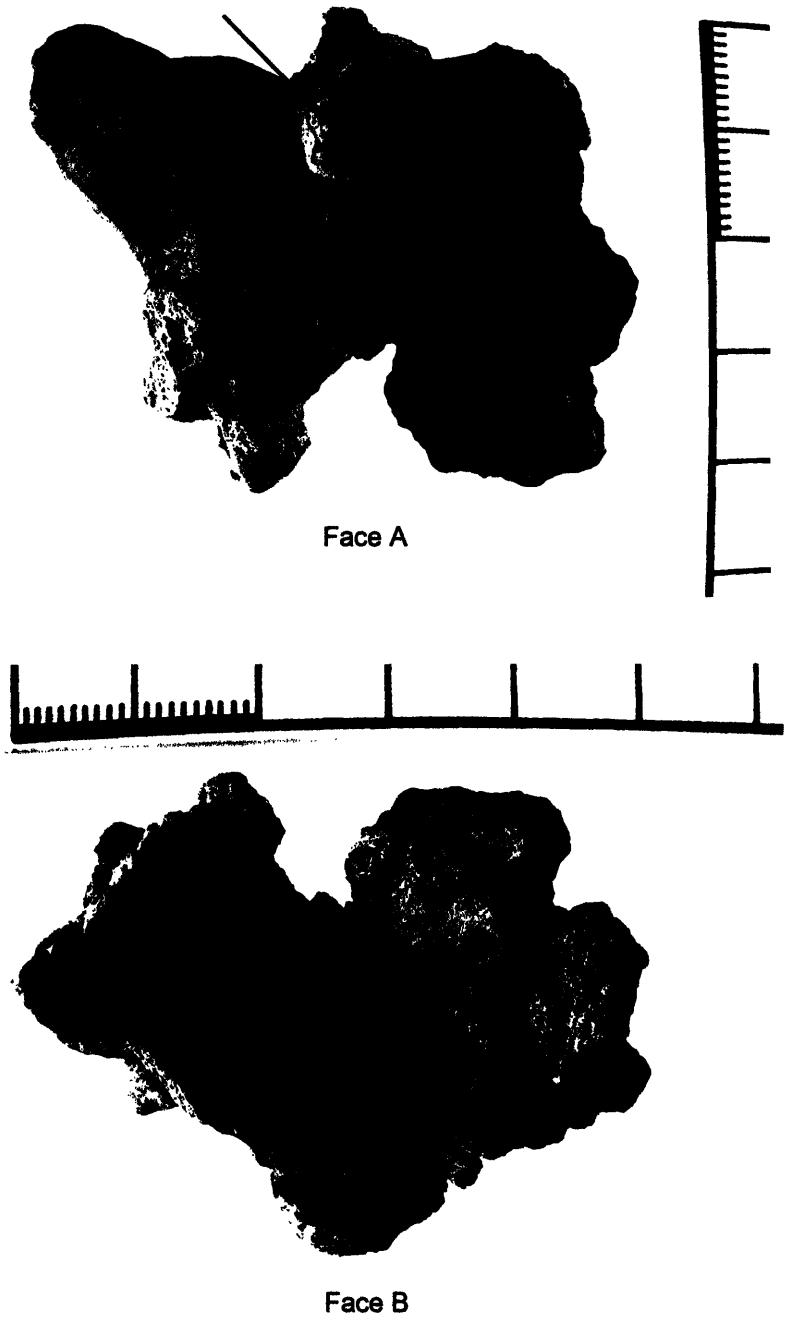

Figure 29. MIT 5318. Two views of the object, showing rounded surfaces, chipped surfaces, and vesicles; arrow points to corroded copper prill.

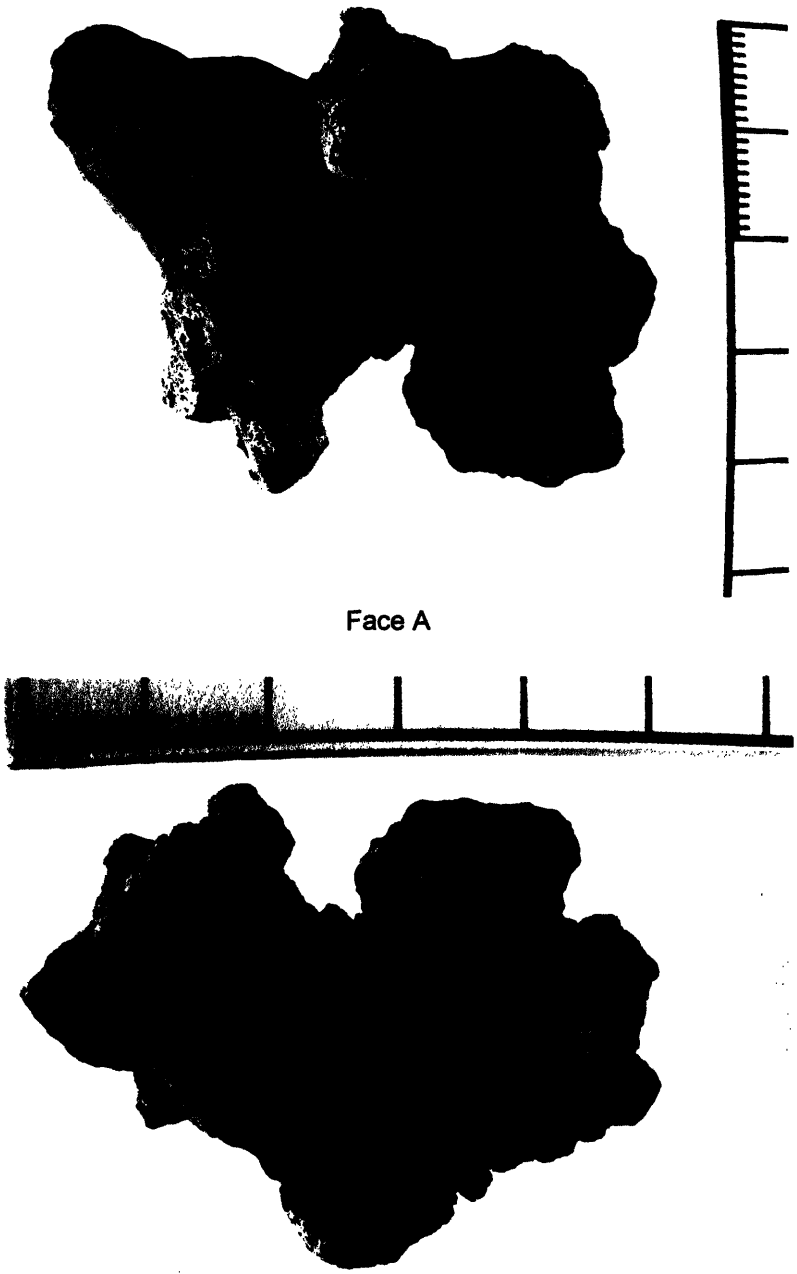

Figure 30. MIT 5318. Two views showing green, corroded copper prills and red oxide material.

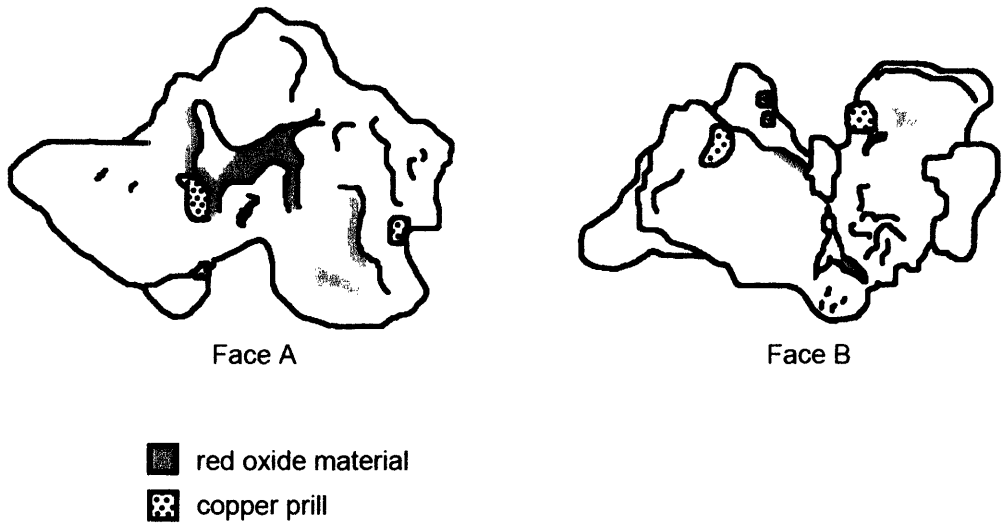

Figure 31. MIT 5318. Line drawing showing red oxide material and relatively large, exposed copper prills.

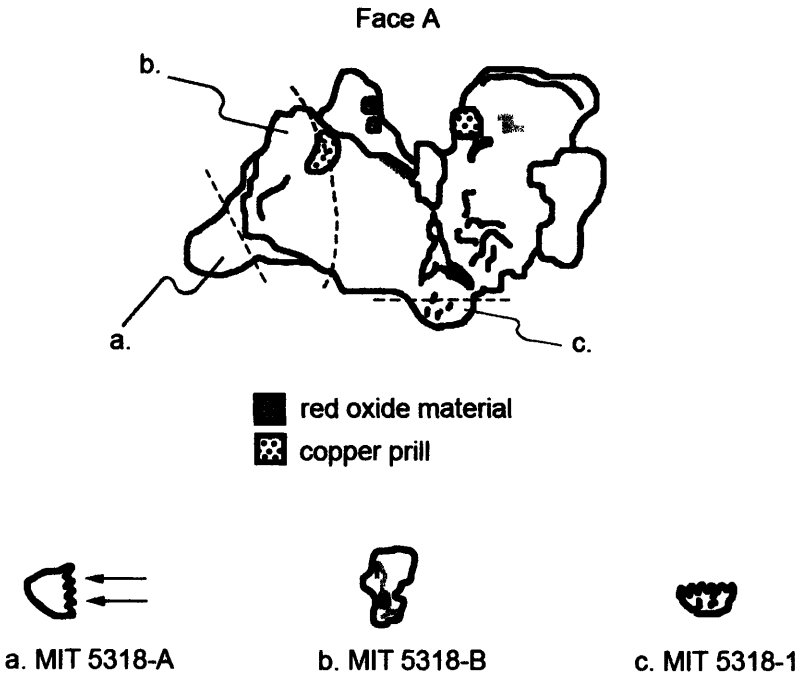

Figure 32. MIT 5318. Line drawing showing location and orientation of samples removed.

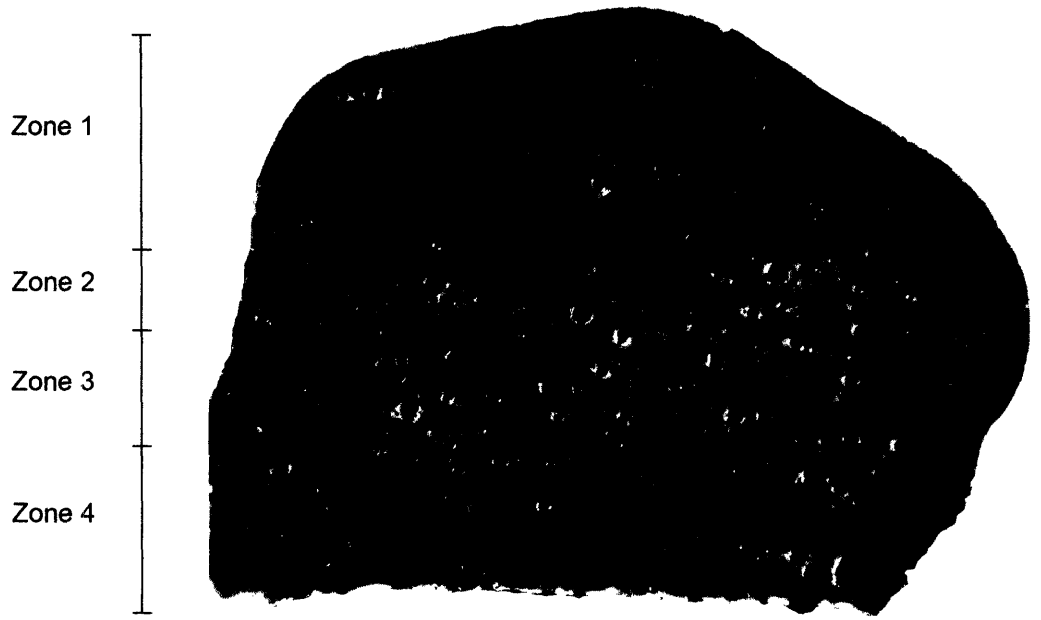

Figure 33. MIT 5318-A. Polished cross-section; sample exhibits four zones. Going from Zone 1 to Zone 4, pore size decreases, but quantity and size of copper prills increase.

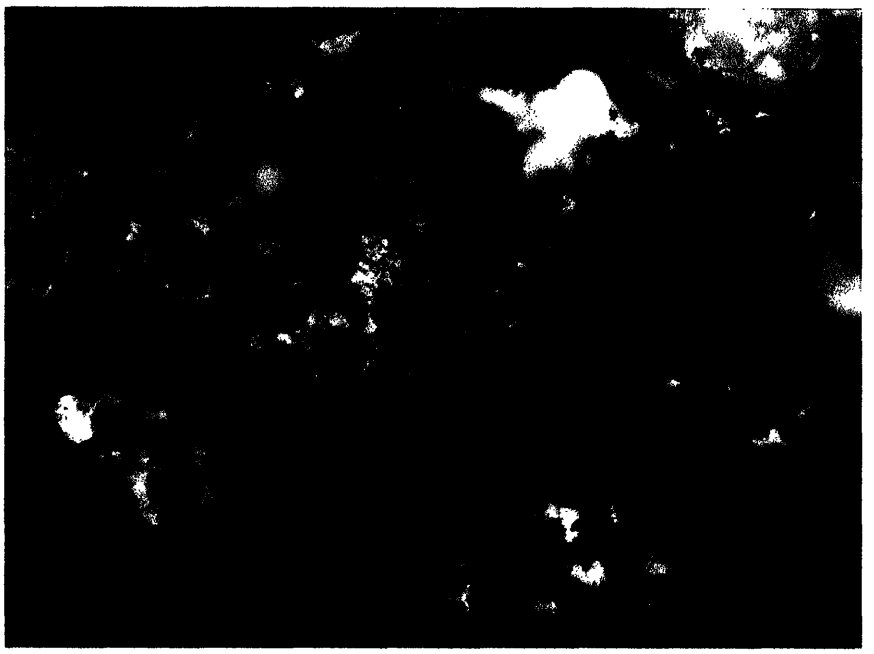

Figure 34. MIT 5318-A. 200x, metallographic microscope, cross-polarized light. Zone 1 (see Fig. 33). Inclusion of cuprous oxide, located on edge of large pore, appears red.

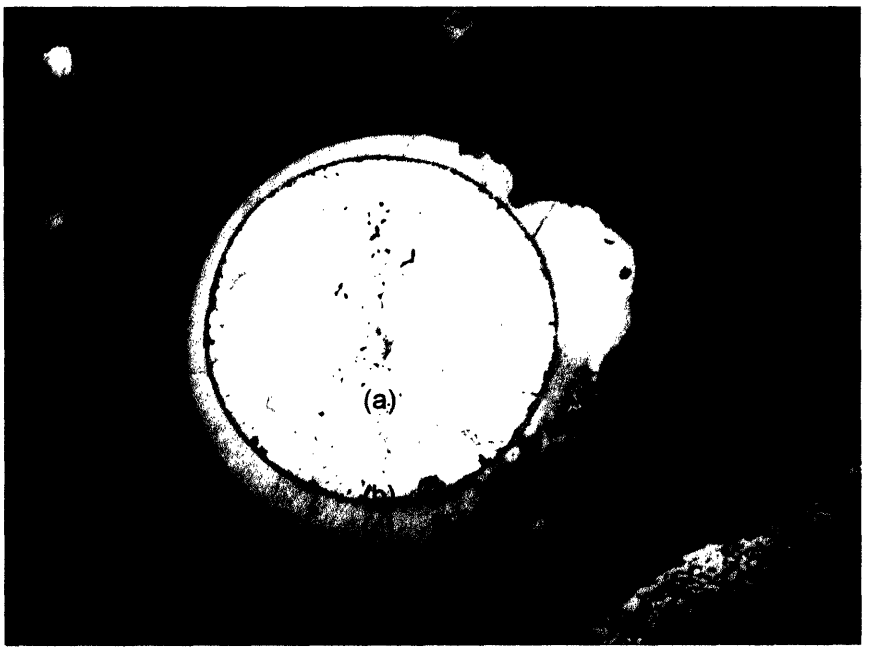

Figure 35. MIT 5318-A. 50x, as-polished. Photomicrograph of a copper prill and the phases surrounding it: (a) copper, (b) thin cuprous oxide "rind," (c) copper sulfide matte, and (d) glassy matrix.

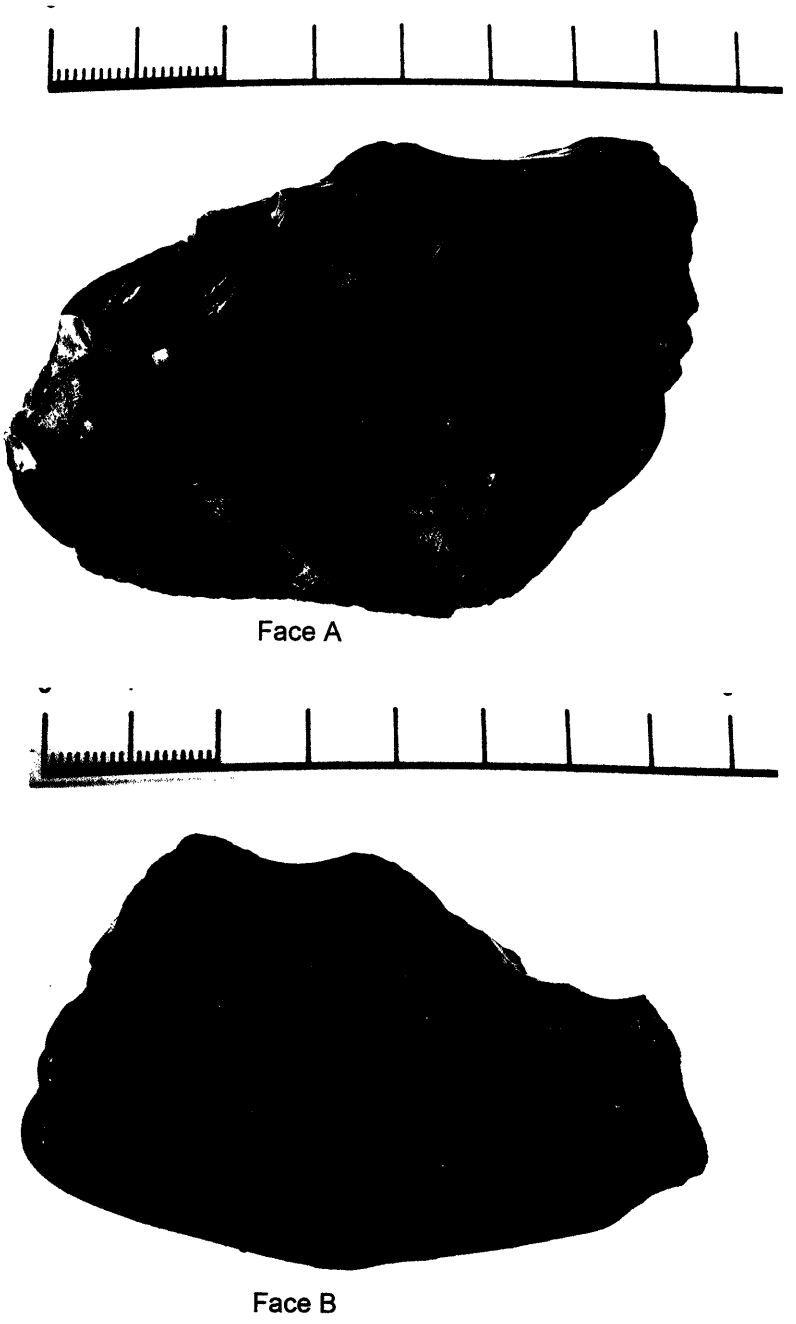

Figure 36. MIT 5316. Two views, showing the burnt sienna and dark brown colors of the object.

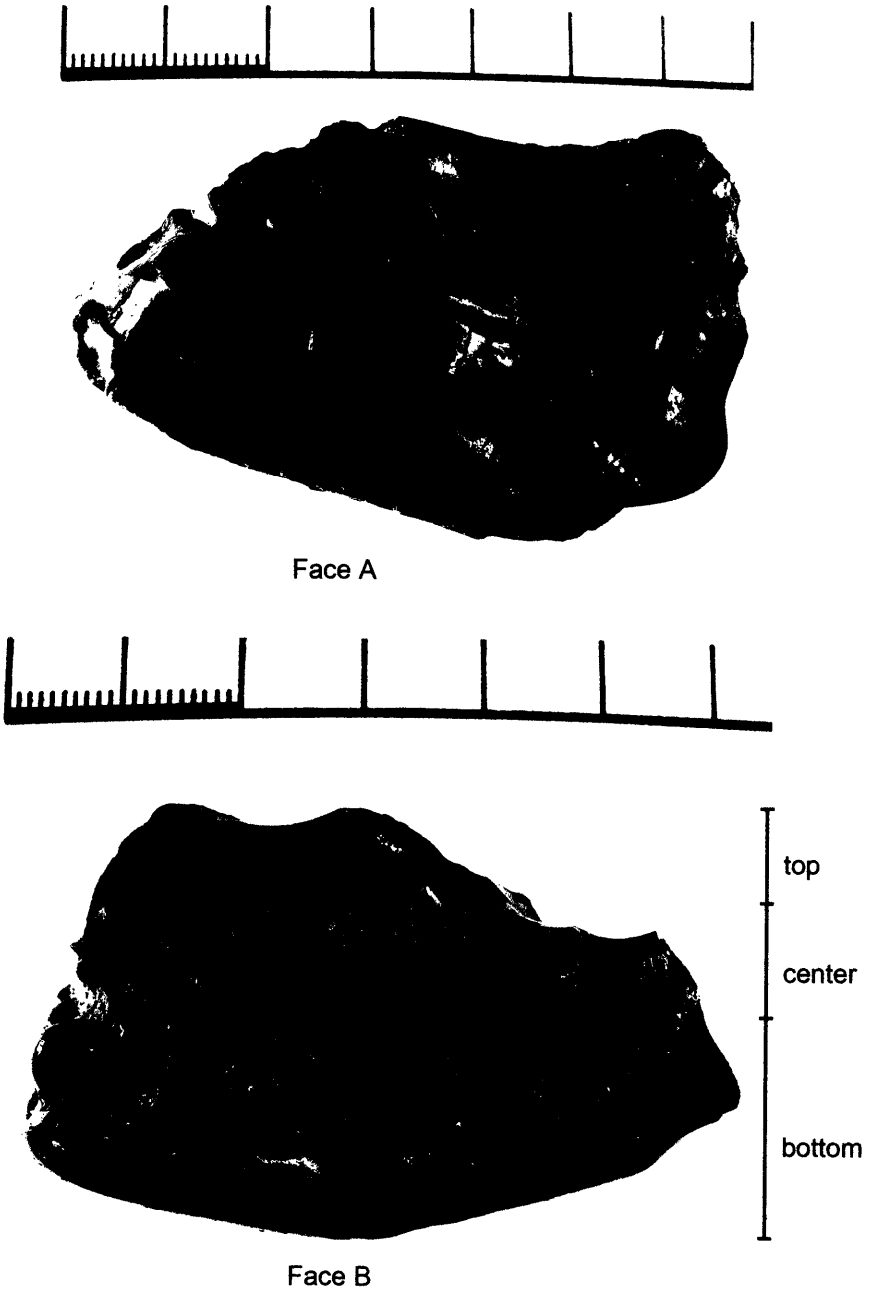

Figure 37. MIT 5316. Two views of the object, showing conchoidal features at the top, fused rocky material in the center, and rounded features at the bottom.

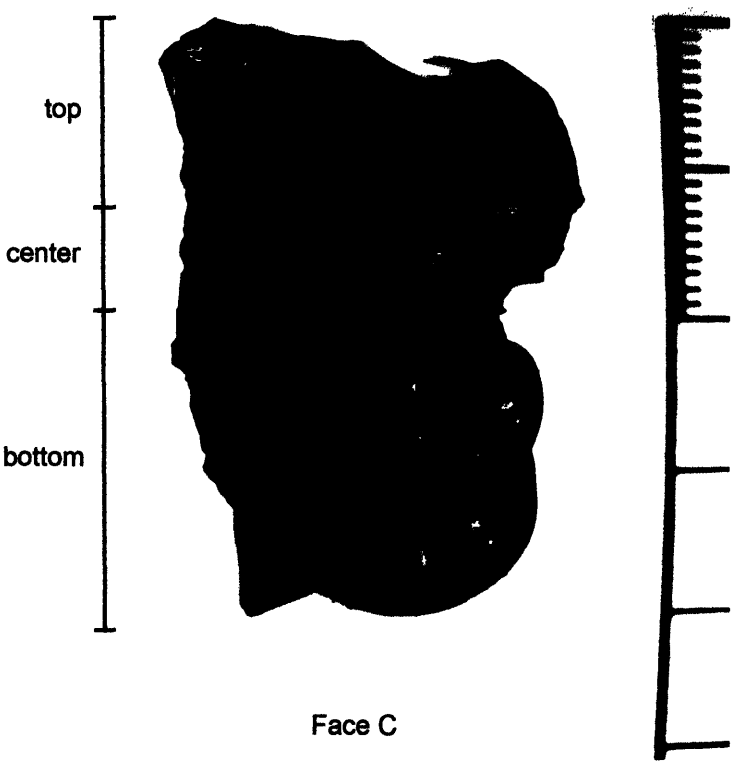

Figure 38. MIT 5316. Side view of object, showing conchoidal features on top, fused rocky material in the center, and rounded features on the bottom.

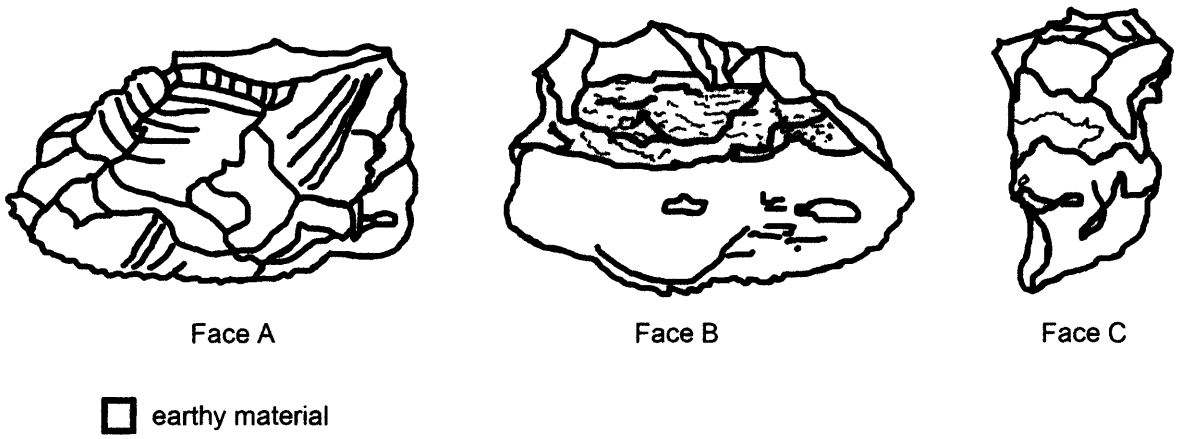

Figure 39. MIT 5316. Line drawing showing three views of the object and the location of the band of earthy material.

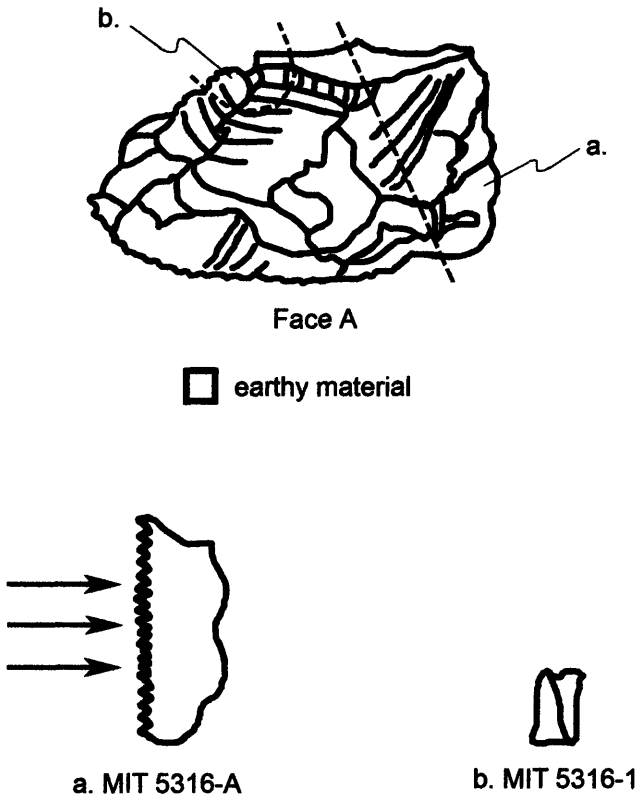

Figure 40. MIT 5316. Line drawing showing location and orientation of samples removed.

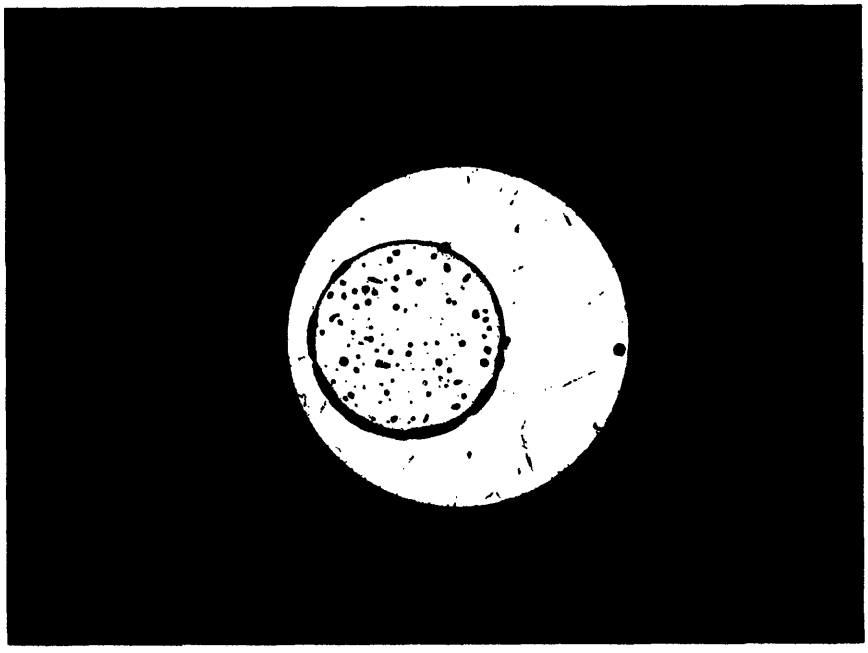

Figure 41. MIT 5316-A. 100x, as-polished. Bright orange, copper prill surrounded by a thin rind of cuprous oxide, which is in turn surrounded by a region of bright blue copper sulfide matte. The prill formed within a glassy matrix.

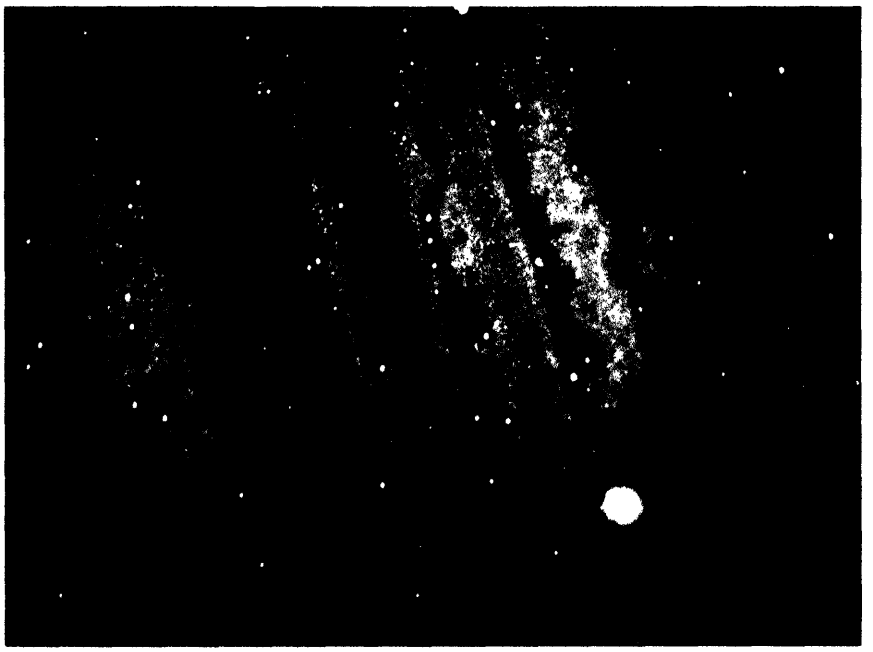

Figure 42. MIT 5316-A. 500x, as-polished, plane-polarized light. At this magnification, copper sulfide prills appear as tiny white specks scattered in a glassy matrix. The matrix is characterized by alternating bands of red and dark blue color.

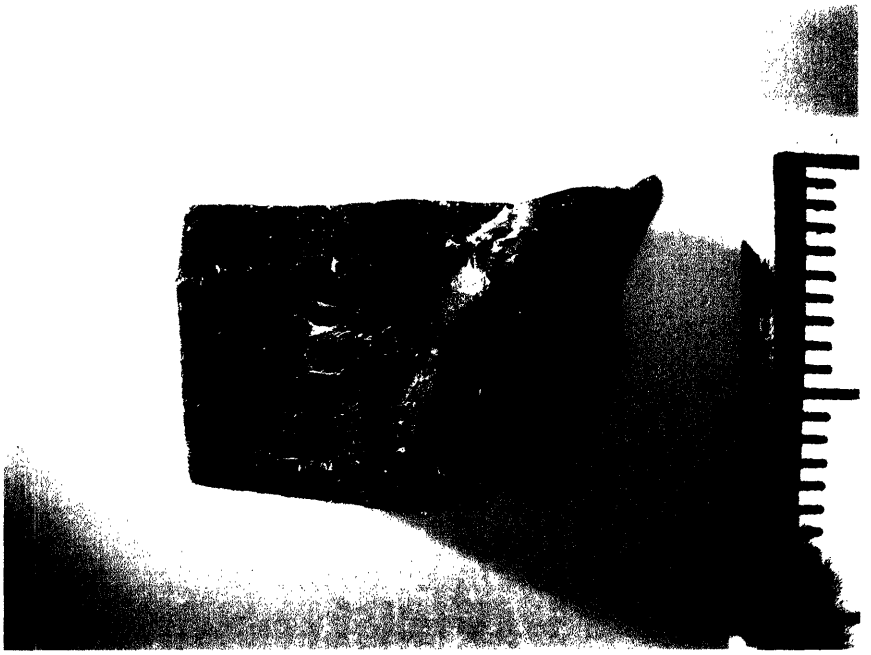

Top View

Side View

Figure 43. MIT 5316-B4. Thermal alteration test: standard sample, not subjected to heat, exhibiting sharp and angular edges.

Top View

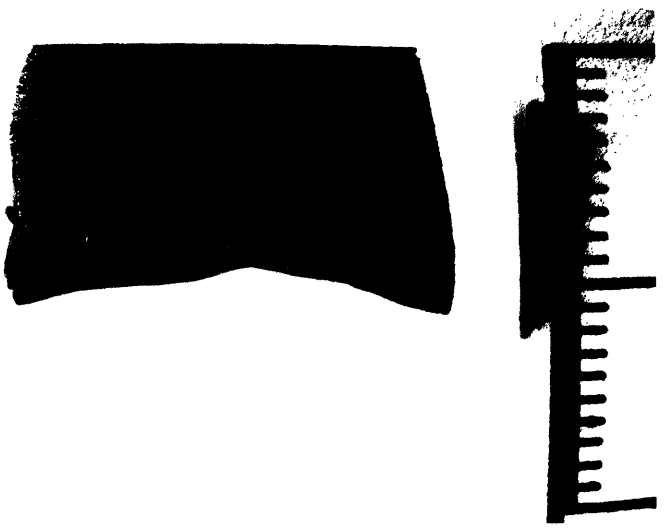

Side View

Figure 44. MIT 5316-C3. Thermal alteration test: sample held at 800 degrees C for 10 minutes, resulting in loss of luster on the surfaces but no gross morphological changes.

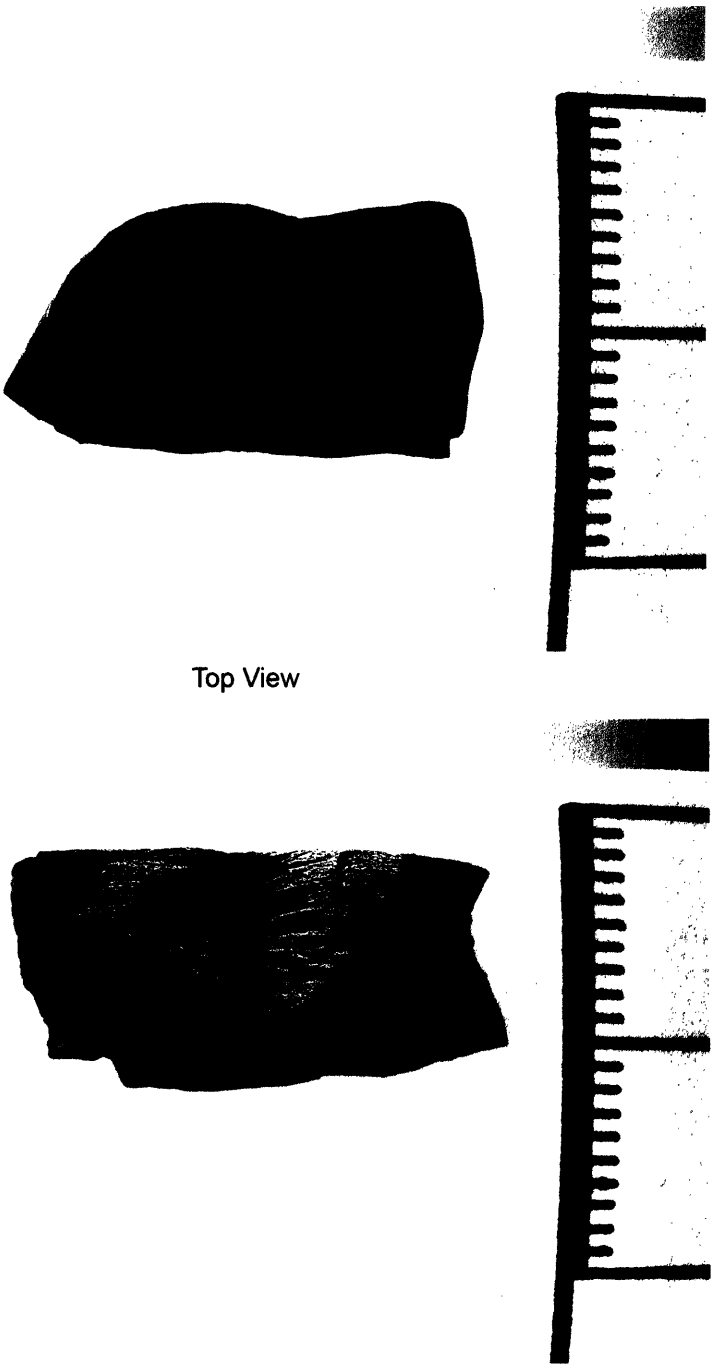

Figure 45. MIT 5316-B1. Thermal alteration test: sample held at 900 degrees C for 10 minutes, resulting in dramatic wrinkling on the surfaces of the sample.

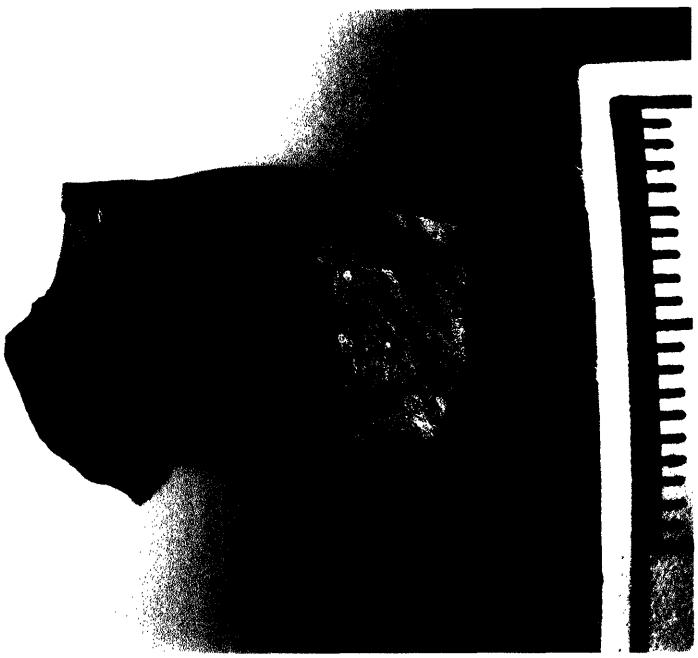

Top View

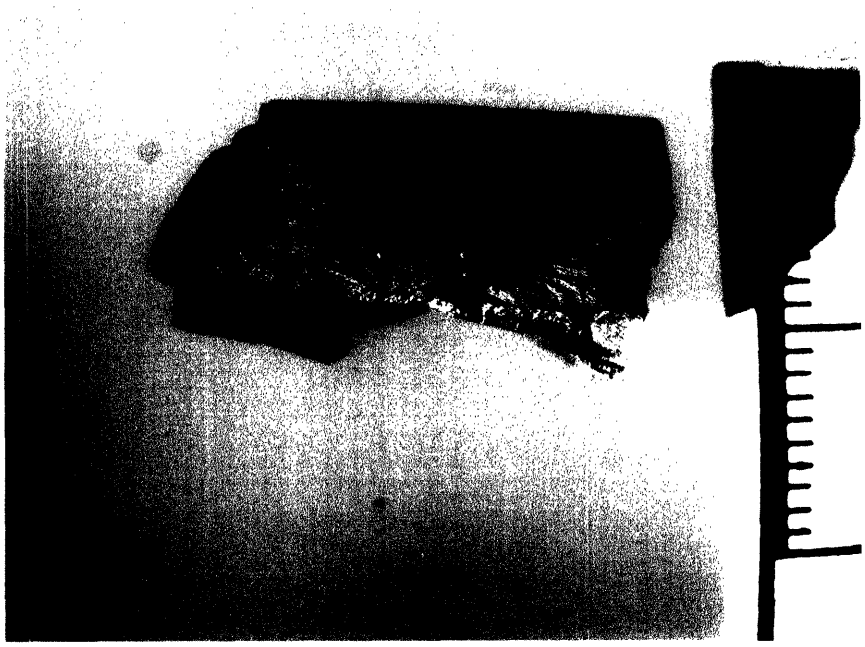

Side View

Figure 46. MIT 5316-D3. Thermal alteration test: sample held at 1000 degrees C for 10 minutes, resulting in continued wrinkling on the surfaces of the sample.

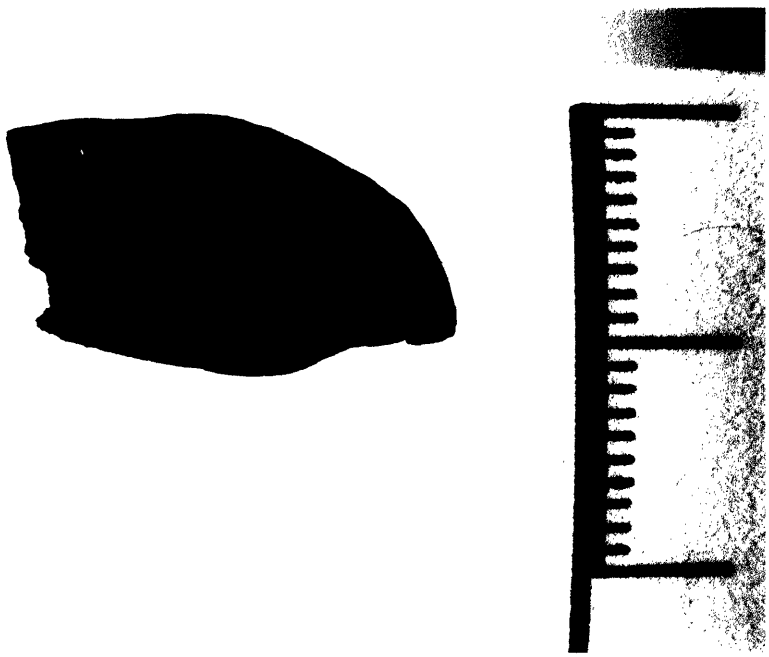

Figure 47a. MIT 5316-C1. Thermal alteration test: sample held at 1050 degrees C for 10 minutes, at which point surface sweating occurred. Sample displays continued wrinkling.

Figure 47b. MIT 5316-B3. Thermal alteration test: sample held at 1075 degrees C for 10 minutes, at which point the sample slumped. As a result, the sample buckled in on itself, and its edges became rounded.

Figure 48a. MIT 5316-E1. Thermal alteration test: sample held at 1100 degrees C for 5 minutes, at which point the sample slumped completely.

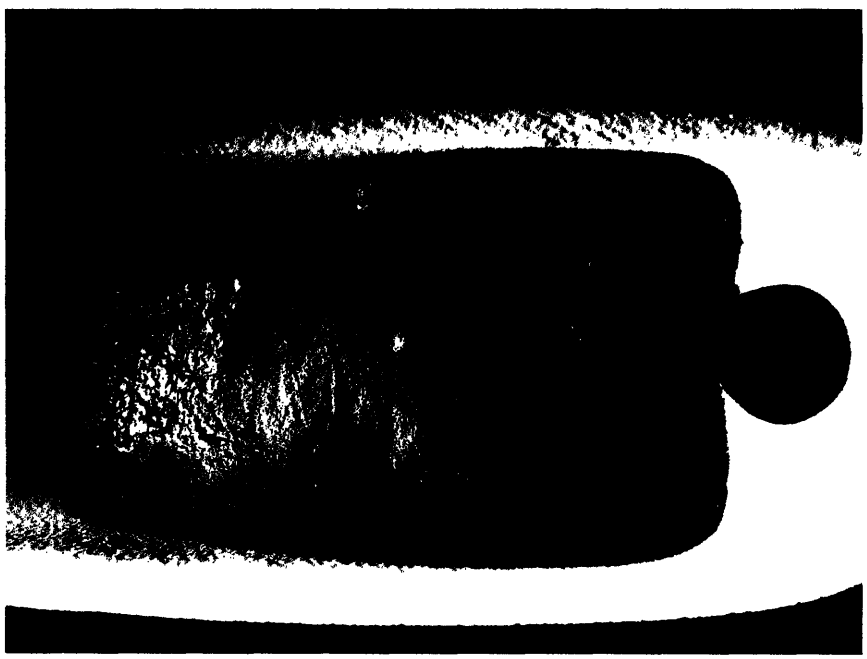

Figure 48b. MIT 5316-D2. Thermal alteration test: sample held at 1125 degrees C for 10 minutes, at which point the sample melted.

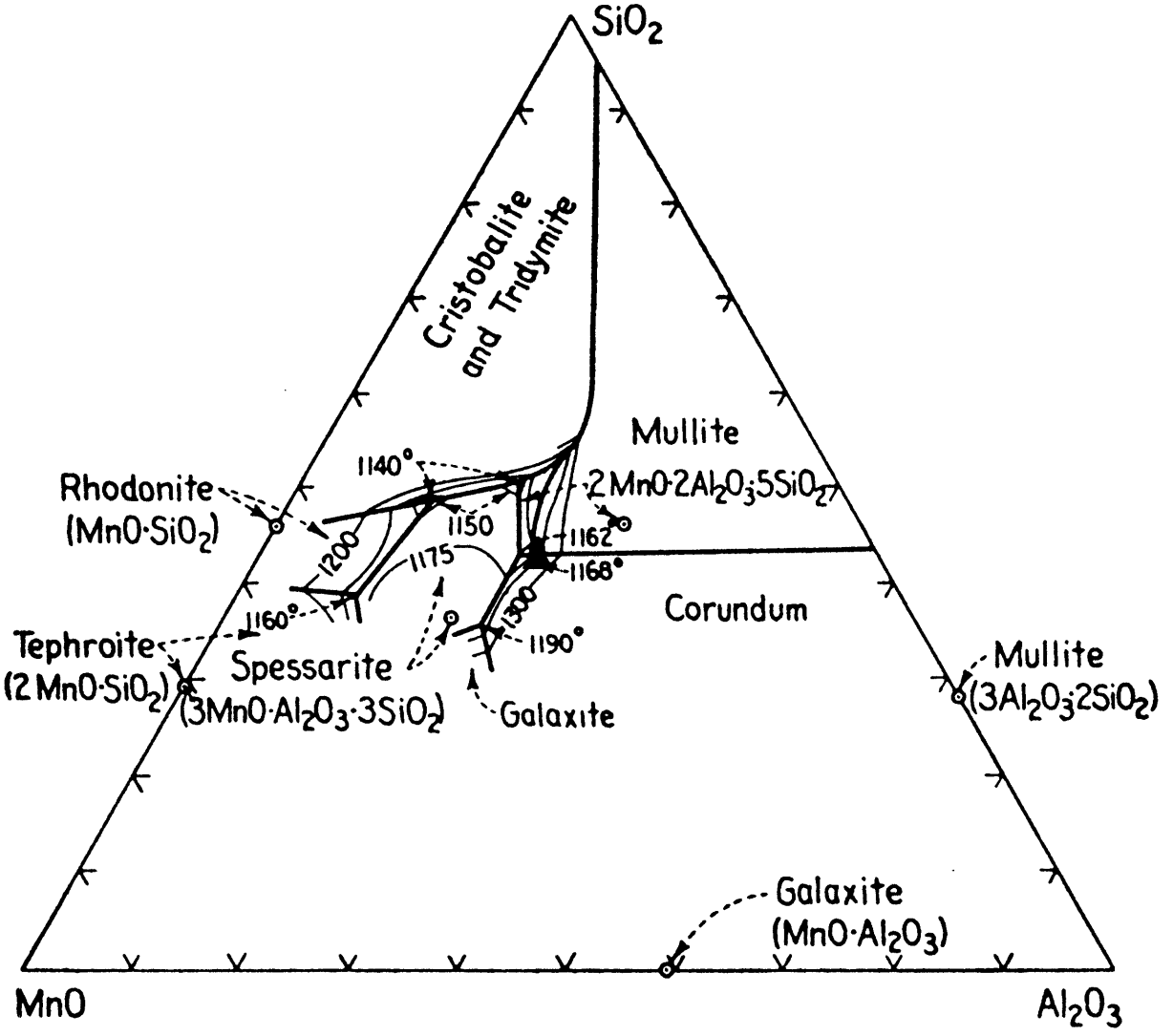

Figure 49. Ternary phase diagram of system MnO-Al_2O_3-SiO_2 (Snow 1943). The composition of the once-molten slag (MIT 5316; see Table 2) is plotted in red. The concentrations of Fe_2O_3, MgO, CaO, Na_2O, K_2O, TiO_2, and P_2O_5 were added to the concentration of Al_2O_3. Using this bulk value for the component oxides, the melting point of the slag is 1168 degrees C.

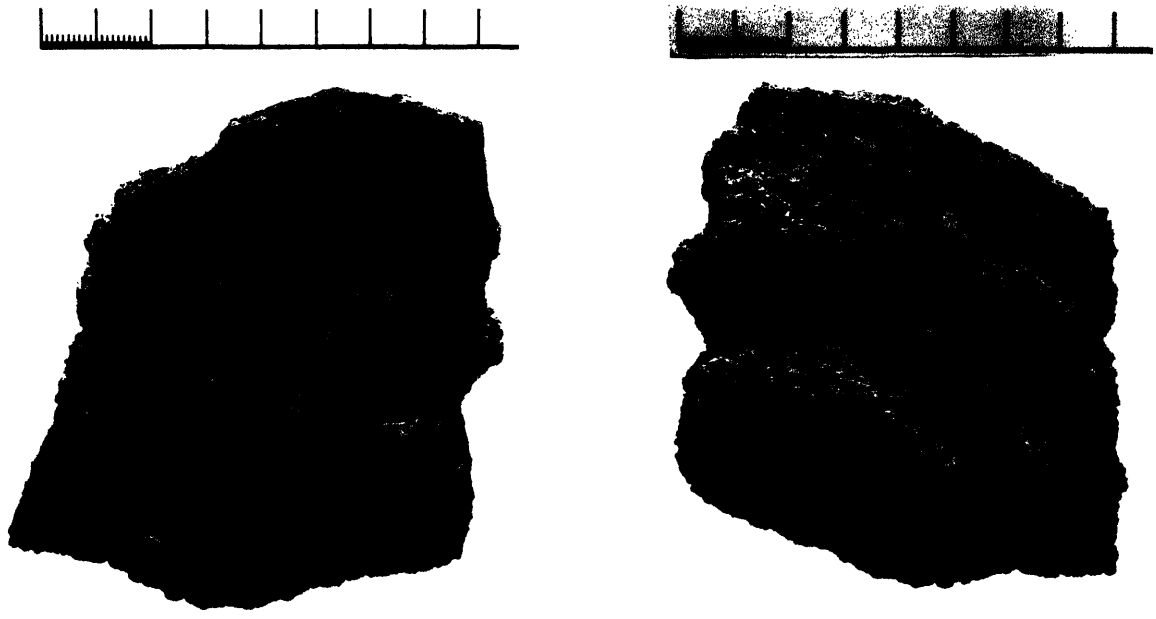

Figure 50. MIT 5320. Two views of the object. Face A displays the slag-coated interior of the furnace wall, and Face B displays the ceramic exterior of the furnace wall.

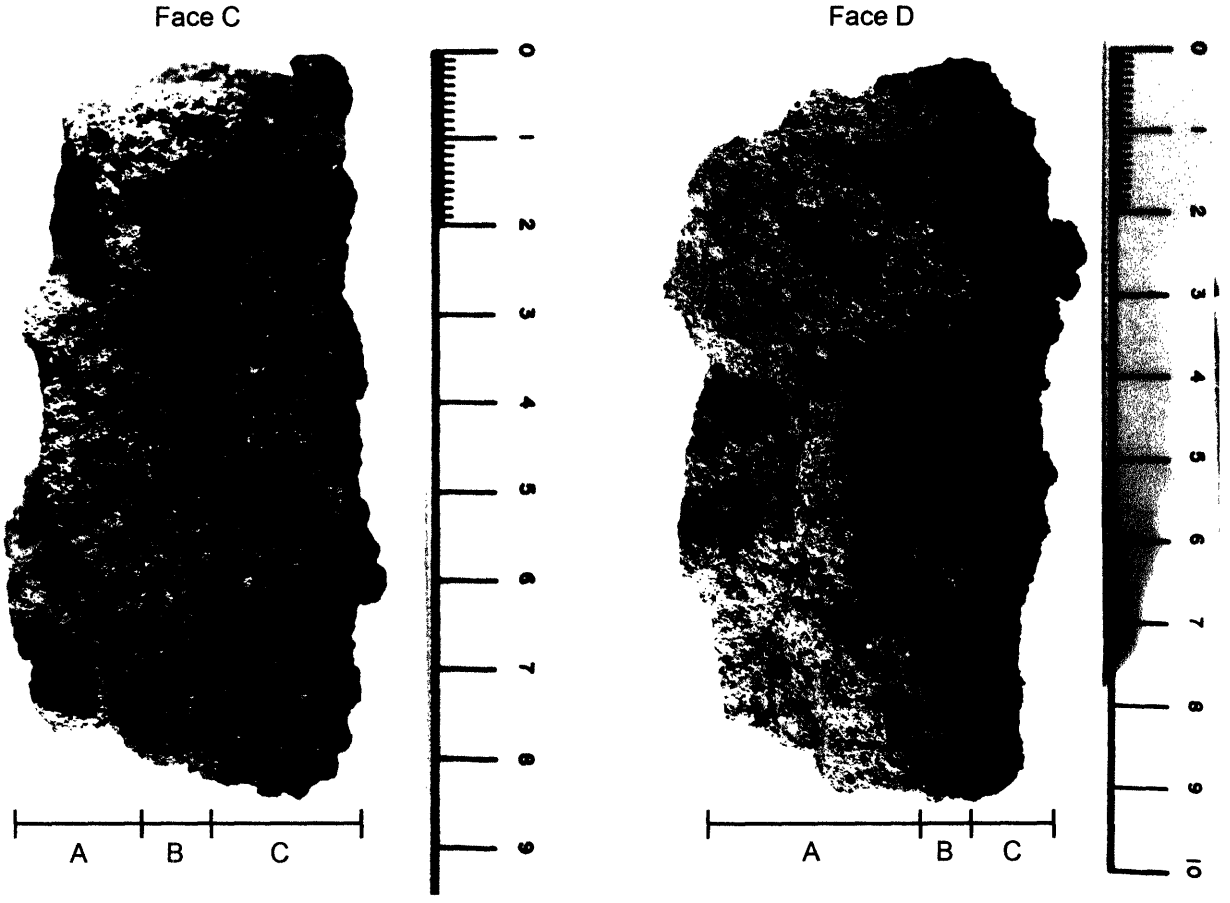

Figure 51. MIT 5320. Two side views of the object, exhibiting three zones. Zone A is a largely unaltered ceramic zone that corresponds with the exterior of the furnace wall, zone B is a partially heat-altered intermediate zone, and zone C is a highly heat altered zone that corresponds with the interior of the furnace wall.

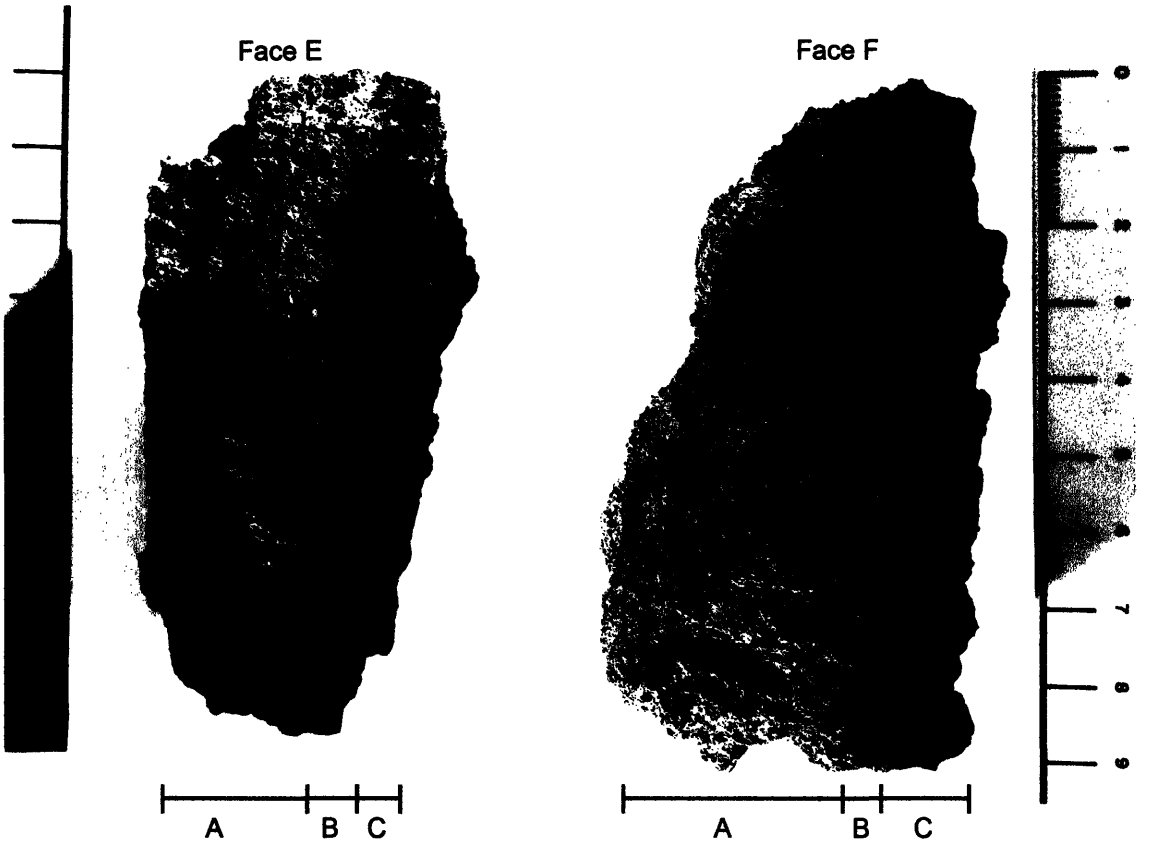

Figure 52. MIT 5320. A top view of the object on the left, and a bottom view of the object on the right. Both views exhibit three zones. Zone A is a largely unaltered ceramic zone that corresponds with the exterior of the furnace wall, zone B is a partially heat-altered intermediate zone, and zone C is a highly heat altered zone that corresponds with the interior of the furnace wall.

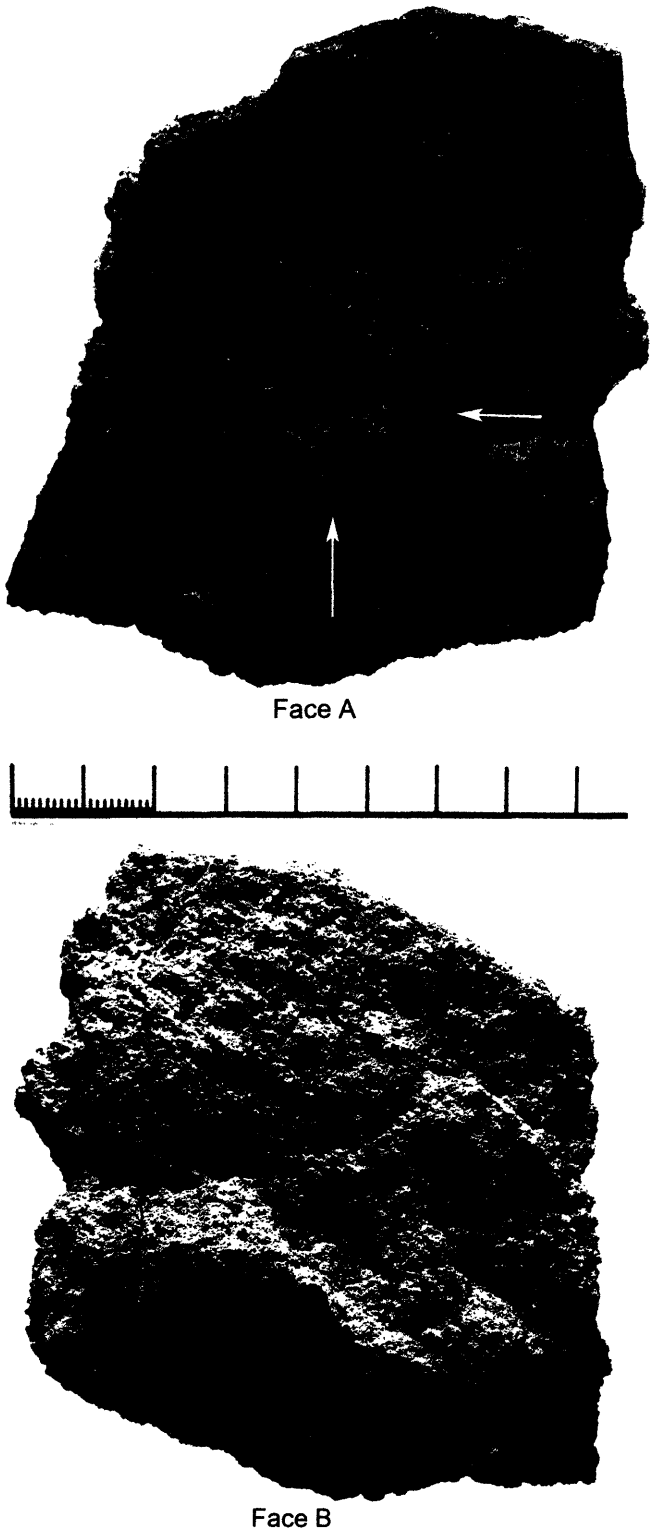

Figure 53. MIT 5320. Face A, the black interior of the furnace wall with white arrows pointing at copper prills. Face B, the earth-colored exterior of the furnace wall.

Figure 54. MIT 5320. Top view, showing the black, highly heat-altered interior (zone C) and the exterior (zone A) of the furnace wall.

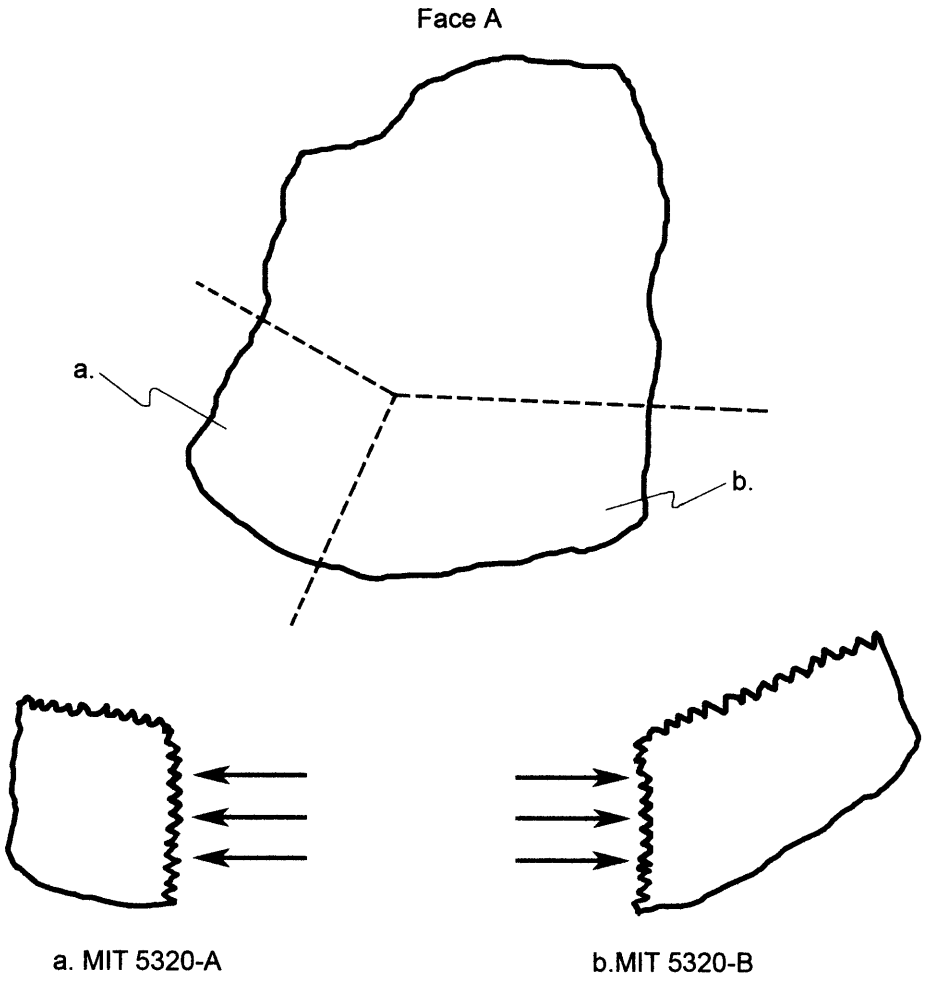

Figure 55. MIT 5320. Line drawing showing locations and orientations of samples removed.

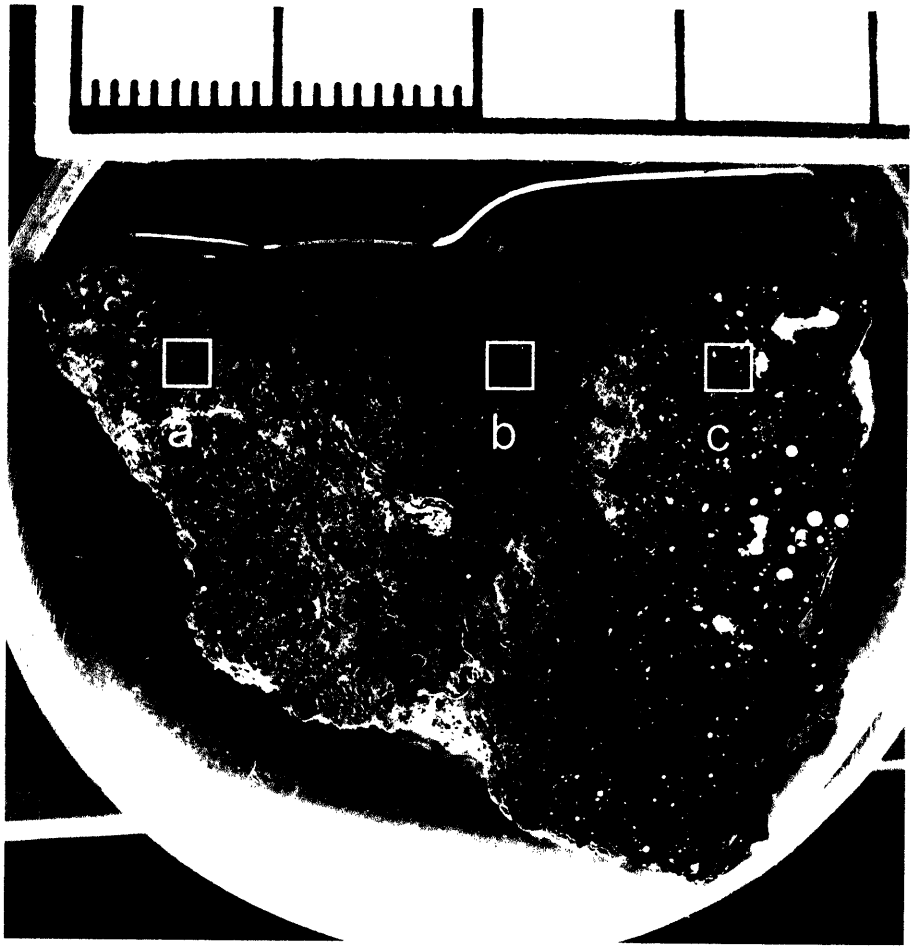

Figure 56. MIT 5320-B. As-polished. Furnace wall showing progression of heat alteration, where zone C appears most affected and zone A appears to be least affected by heat.

Figure 56a. 50x, as-polished. Unaltered zone.

Figure 56b. 50x, as-polished. Intermediate zone.

Figure 56c. 50x, as-polished. Strongly heat-altered zone.

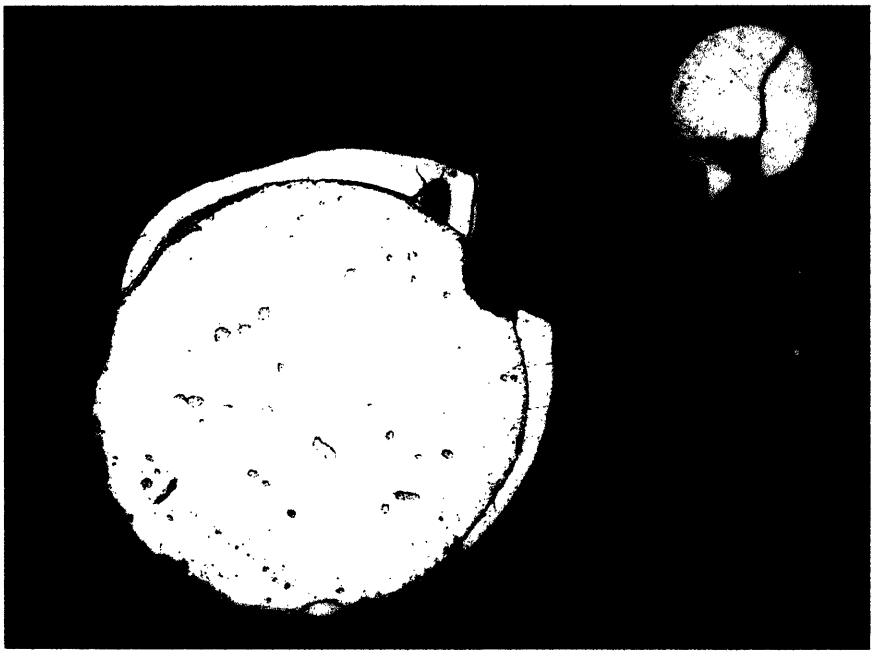

Figure 57. MIT 5320-A. 200x, as-polished. Interior of the furnace wall, zone C. Copper prill surrounded by a copper oxide rind, which is in turn surrounded by a copper sulfide matte. In the upper right corner, a prill of copper sulfide matte.

TABLES

Table 1. Metal assay results for two pieces of ore and two pieces of slag.

Metallic Cu Analysis-ICP **Activation Laboratories Ltd. Work Order: A05-2238 Report: A05-2238D**

	Code Sample	+100 mesh Cu %	-100 mesh Cu %	Cu %	+100 mesh W g	-100 mesh W g	Total W g
ORE	MIT 5313	52.17	68.43	58.16	0.254	0.148	0.402
ORE	MIT 5319	23.92	25.79	24.19	0.500	0.084	0.584
SLAG	MIT 5318	9.94	89.33	27.74	0.128	0.037	0.165
SLAG	MIT 5316	1.098	2.252	1.36	0.505	0.151	0.656

Table 2. ICP-OES results for two pieces of ore and two pieces of slag.

Fusion ICP

Activation Laboratories Ltd. Work Order No. A05-2238 Report No. A05-2238B

SAMPLE	SiO2 %	Al2O3 %	Fe2O3 (T) %	MnO %	MgO %	CaO %	Na2O %	K2O %	TiO2 %	P2O5 %	LOI %	TOTAL %	Ba ppm	Sr ppm	Y ppm	Sc ppm	Zr ppm	Be ppm	V ppm	
MIT 5313	23.79	5.36	0.73	0.031	0.43	1.50	1.78	1.04	0.147	0.04	*	34.84	904	1932	4	12	38	-1	-5	
MIT 5316	42.43	9.09	1.45	31.214	1.14	5.05	2.40	1.53	0.389	0.09	-1.79	92.99	6726	47520	10	6	124	2	127	
MIT 5318	49.31	10.34	1.50	4.098	1.02	3.57	3.21	2.38	0.405	0.10	*	75.93	9094	64353	11	8	165	-1	60	
MIT 5319	31.13	6.54	0.74	0.052	0.58	2.25	2.27	1.40	0.192	0.06	15.81	61.02	5097	13805	5	7	66	-1	16	
METHOD BLANK	-0.01	-0.01	-0.01	-0.001	-0.01	-0.01	-0.01	-0.01	-0.001	-0.01			-1	-1	-1	-1	-1	-1	-5	
SY3 CERT	59.62	11.75	6.49	0.32	2.67	8.26	4.12	4.23	0.15	0.54	1.16		450	302	718	6.8	320	20	50	syenite
SY-3/B	59.55	11.71	6.47	0.320	2.56	8.25	4.12	4.22	0.152	0.54			452	304	717	8	321	21	50	
NIST 694 CERT	11.20	1.80	0.79	0.01	0.33	43.60	0.86	0.51	0.11	30.20									1736	western phosphate rock
NIST 694/C	11.16	1.88	0.73	0.011	0.32	43.48	0.88	0.56	0.110	28.54			117	932	155	3	93	5	1544	
W-2 CERT	52.44	15.35	10.74	0.163	6.37	10.87	2.14	0.627	1.06	0.131	0.60		182	194	24	35	94	1.3	262	diabase
W-2/C	52.31	15.20	10.73	0.161	6.31	10.85	2.22	0.65	1.059	0.13			176	192	23	35	84	-1	263	
DNC-1 CERT	47.04	18.30	9.93	0.149	10.05	11.27	1.87	0.229	0.48	0.085	0.60		114	145	18	31	41	1	148	dolerite
DNC-1/C	47.06	18.14	9.82	0.140	10.02	11.13	1.90	0.16	0.476	0.08			105	139	18	31	29	-1	139	
BIR-1 CERT	47.77	15.35	11.26	0.171	9.68	13.24	1.75	0.027	0.96	0.05			7.7	108	16	44	22	0.58	313	basalt
BIR-1/C	47.64	15.32	11.26	0.168	9.65	13.22	1.81	0.03	0.955	0.03			8	106	16	44	12	-1	322	
GBW 07113 CERT	72.78	12.96	3.21	0.140	0.16	0.59	2.57	5.43	0.30	0.05			506	43	42.5	5.2	403	4.09	3.8	granite
GBW 07113/C	72.76	12.72	3.15	0.138	0.14	0.58	2.49	5.40	0.279	0.05			498	39	47	5	391	4	34	
NBS 1633b CERT	49.24	28.43	11.13	0.020	0.799	2.11	0.271	2.26	1.32	0.53			709	1041		41			296	fly ash
NBS 1633b/C	49.13	28.33	11.04	0.017	0.77	2.12	0.27	2.33	1.291	0.53			709	1022	93	41	221	14	290	
STM-1 CERT	59.64	18.39	5.22	0.22	0.101	1.09	8.94	4.28	0.135	0.158			560	700	46	0.61	1210	9.6	(8.7	syenite
STM-1/C	59.51	18.20	5.24	0.218	0.08	1.12	8.85	4.26	0.130	0.15			599	700	46	-1	1209	9	-5	
IF-G CERT	41.20	0.15	55.85	0.042	1.89	1.55	0.032	0.012	0.014	0.063			1.5	3	9	0.38	2.4	4.7	4	iron form sample
IF-G/C	41.15	0.15	55.51	0.035	1.88	1.53	0.05	-0.01	-0.001	0.06			5	5	11	-1	11	4	-5	
FK-N CERT	65.02	18.61	0.09	0.005	0.01	0.11	2.58	12.81	0.02	0.02			200	39	0.3	0.05	13	1	3	K-feldspar
FK-N/C	65.05	18.34	0.13	0.002	-0.01	0.10	2.45	12.75	-0.001	0.02			209	37	-1	-1	-1	-1	-5	

Note: Certificate data underlined are recommended values; other values are proposed except those preceded by a "(" which are information values.
Note: The Fe2O3 for the standards is Total Fe2O3 and has not been adjusted for the FeO.
Note: * Insufficient sample for LOI determination and analysis verification.

Table 3. INAA results for two pieces of ore and two pieces of slag

INAA

Activation Laboratories Ltd. Work Order A05-2238 Report A05-2238

	Sample ID	Au	As	Br	Co	Cr	Cs	Hf	Ir	Mo	Rb	Sb	Se	Ta	Th	U	W	La	Ce	Nd	Sm	Eu	Tb	Yb	Lu	Mass
		ppb	ppm	ppm	ppm	ppm	ppm	ppm	ppb	ppm	ppm	ppm	ppm	ppm	ppm	ppm	ppm	ppm	ppm	ppm	ppm	ppm	ppm	ppm	ppm	g
ORE	MIT 5313	-2	15.4	-0.5	4	-5	10	-1	-5	-1	42	0.4	-3	-0.5	1.0	3.0	-1	5.4	14	-5	0.8	-0.2	-0.5	0.8	-0.05	1.030
ORE	MIT 5319	-2	154	-0.5	7	-5	10	-1	-5	4000	50	1.4	-3	-0.5	3.2	-0.5	-1	7.0	9	-5	1.4	-0.2	-0.5	0.5	0.10	0.9189
SLAG	MIT 5318	-2	34.6	-0.5	10	34	6	7	-5	11200	-15	0.9	-3	-0.5	8.1	-0.5	-1	17.4	39	39	3.8	-0.2	3.9	1.3	0.18	0.2217
SLAG	MIT 5316	-2	9.8	-0.5	7	54	3	6	-5	1280	60	1.1	-3	-0.5	6.5	2.2	10	15.0	33	16	2.8	0.8	-0.5	1.2	0.14	0.9600
	BLANK	-2	-0.5	0.8	1	-5	-1	-1	-5	-1	-15	-0.1	-3	-0.5	-0.2	-0.5	-1	-0.5	-3	-5	-0.1	-0.2	-0.5	-0.2	-0.05	1.000
	DMMAS-10	572	210	2.8	67	154	-1	2	-5	1	44	14.8	-3	-0.5	1.6	-0.5	25	11.3	22	-5	4.3	1.1	-0.5	3.4	0.62	0.8302
Dmmas-10	Accepted	540	2237	1.9	67	149		1			5	15.7			0.6		15	12.4	21		3.8	0.8		3.2	0.51	

Table 4. Electron beam microprobe identification of various colored features observed with the petrographic microscope.

	Petrographic Examination		**Electron microprobe EDS/WDS analysis**
	Color/phase in plane-polarized light	Color/phase in cross-polarized light	
Zone 1	gray grains	green, brown, white, and gray grains	SiO_2 grains with CuCl
Zone 2	gray grains	dark gray grains	SiO_2 grains (no CuCl)
	pale green matrix	red and yellow crystals in dark gray matrix	Cu_2S and (Ba, Sr)SO_4 intergrowth
Zone 3	pale gray grains	gray, green, and brown grains	Cu_2S
	dark gray grains	gray matrix	Cu_2S and Cu_2SO_4 intergrowth
	light blue crystals	dark green, pale green, red, and yellow crystals	PbS

Table 5. Results of heating samples of glassy slag from MIT 5316.

Sample	Mass (g)	Temperature (°C)	Observations
5316-B2	5.7	750	morphology unchanged
5316-C3	4.7	800	very subtle rounding of edges
5316-C2	5.3	850	slight rounding of edges
5316-B1	4.3	900	edges are rounded and bottom face conforms to the shape of the boat
5316-E2	4.6	950	all faces touching the boat have conformed to the shape of the boat
5316-D3	5.1	1000	slight slumping
5316-C1	3	1050	surface sweating, still slumped
5316-B3	5.5	1075	surface sweating, still slumped
5316-E1	3.8	1100	completely slumped, i.e. viscous
5316-D2	5.5	1125	completely melted, i.e. fluid
5316-D1	2.9	1150	completely melted, i.e. fluid

APPENDIX A

MIT 5313

EDS Spectra

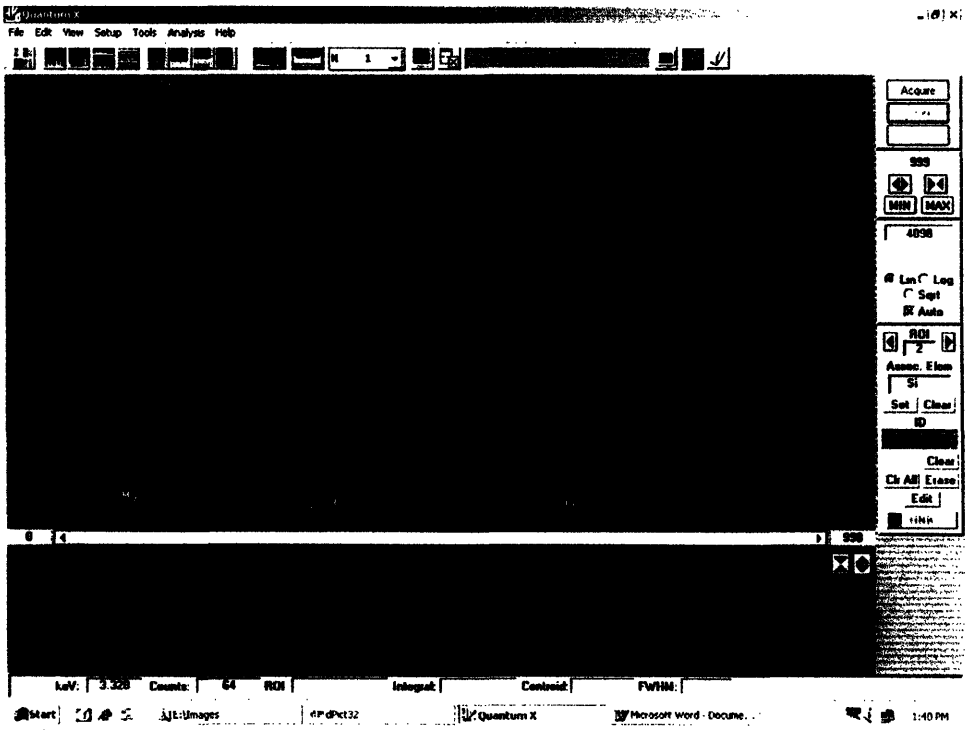

Grain 1 Quartz

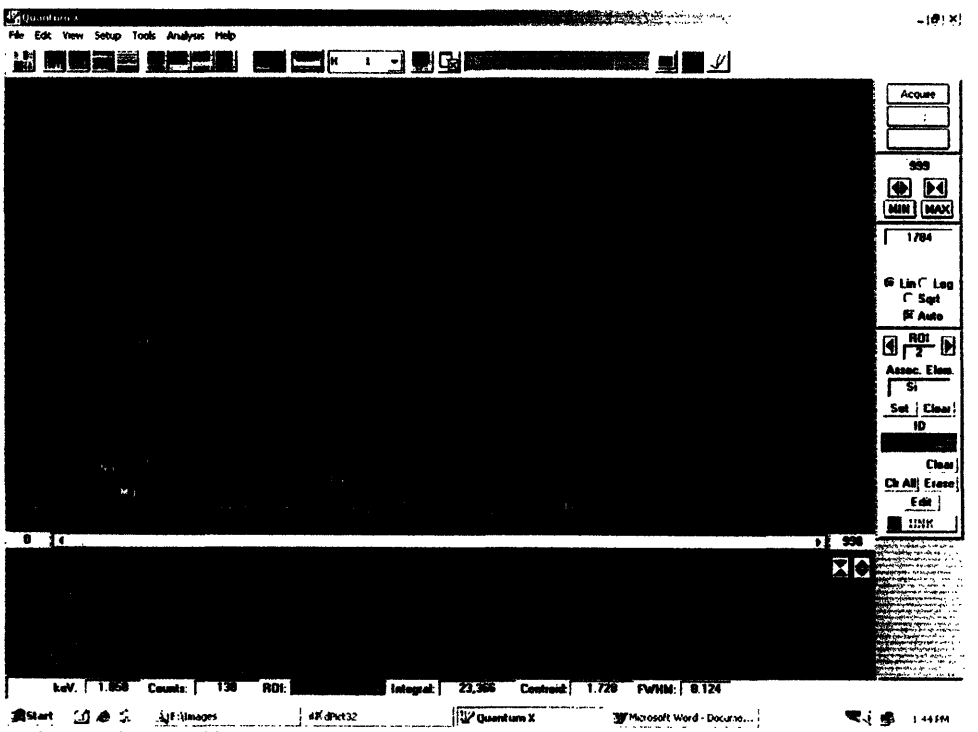

Grain 2 Plagioclase feldspar

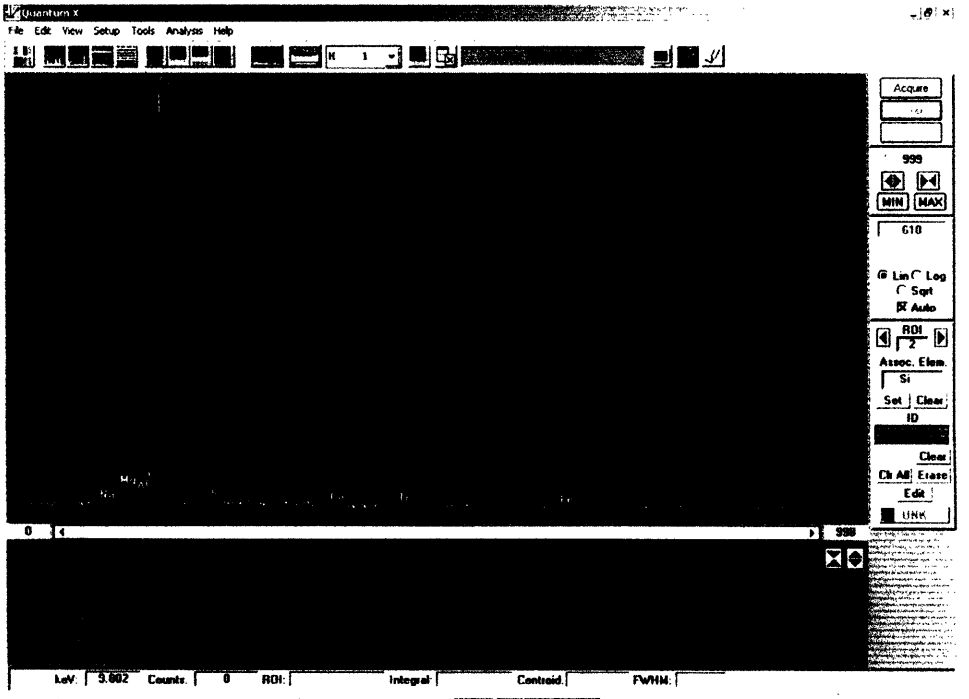

Grain 3 Quartz

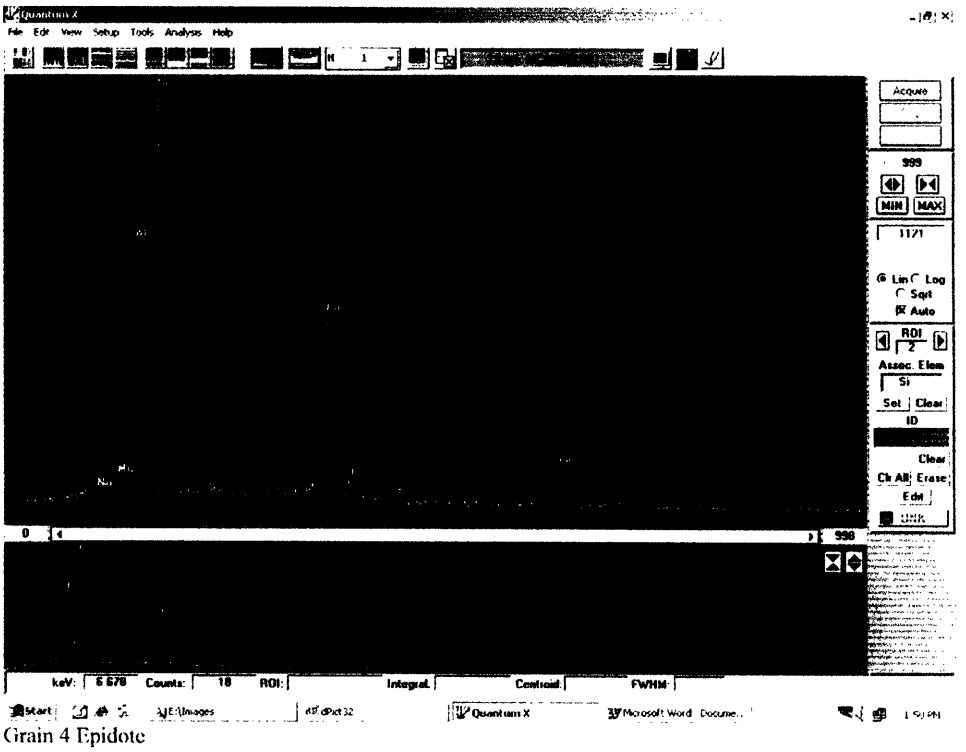

Grain 4 Epidote

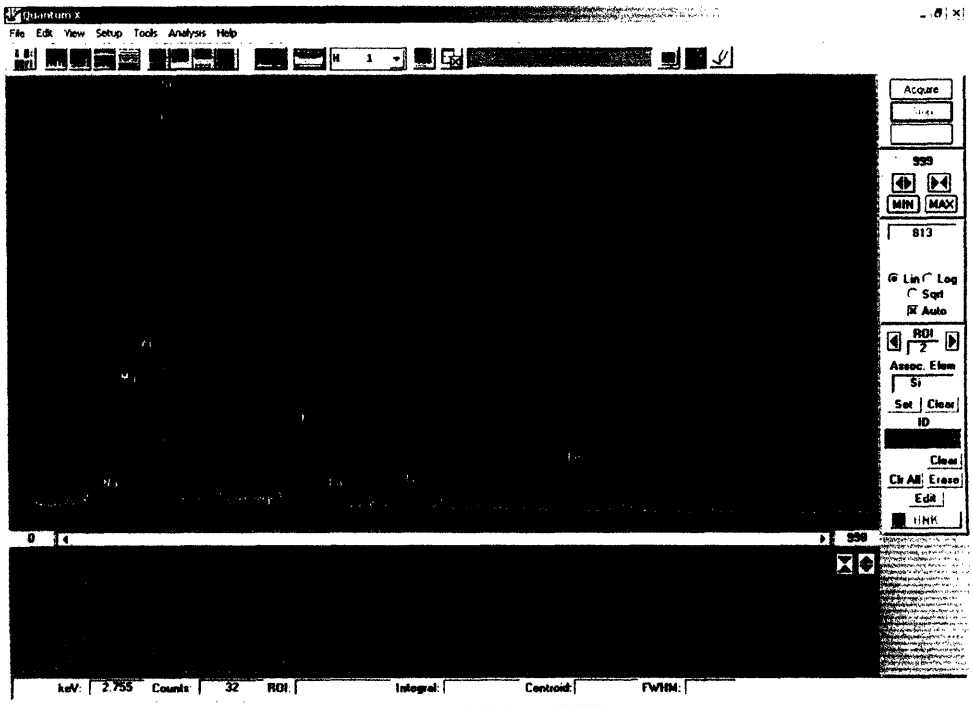

Grain 5 Biotite mica

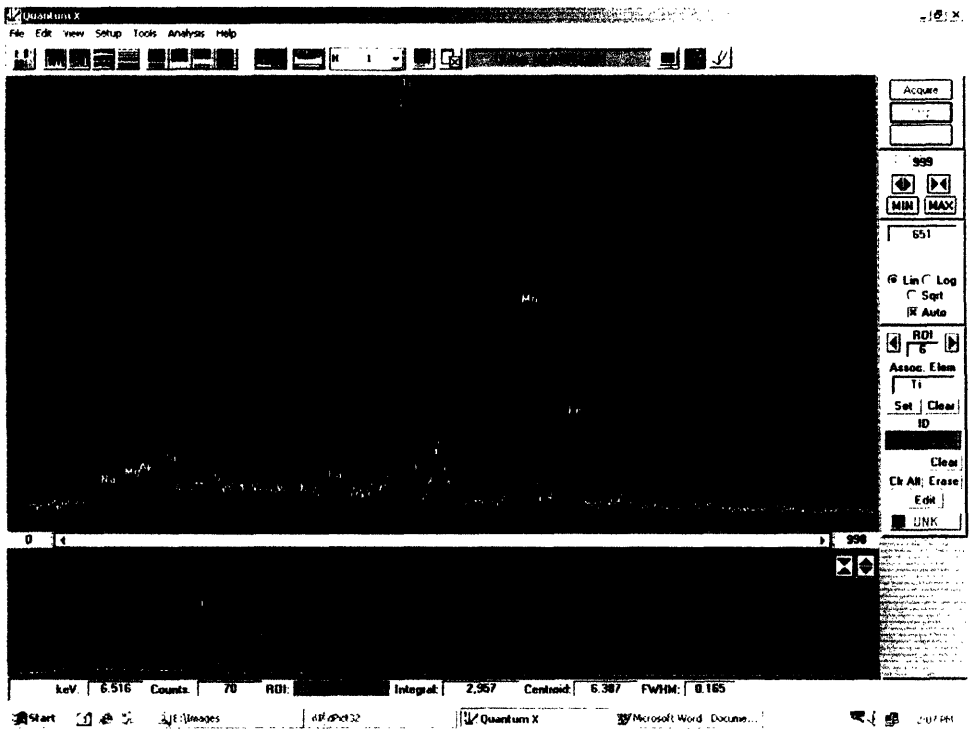

Grain 6 Mn-Ti oxide

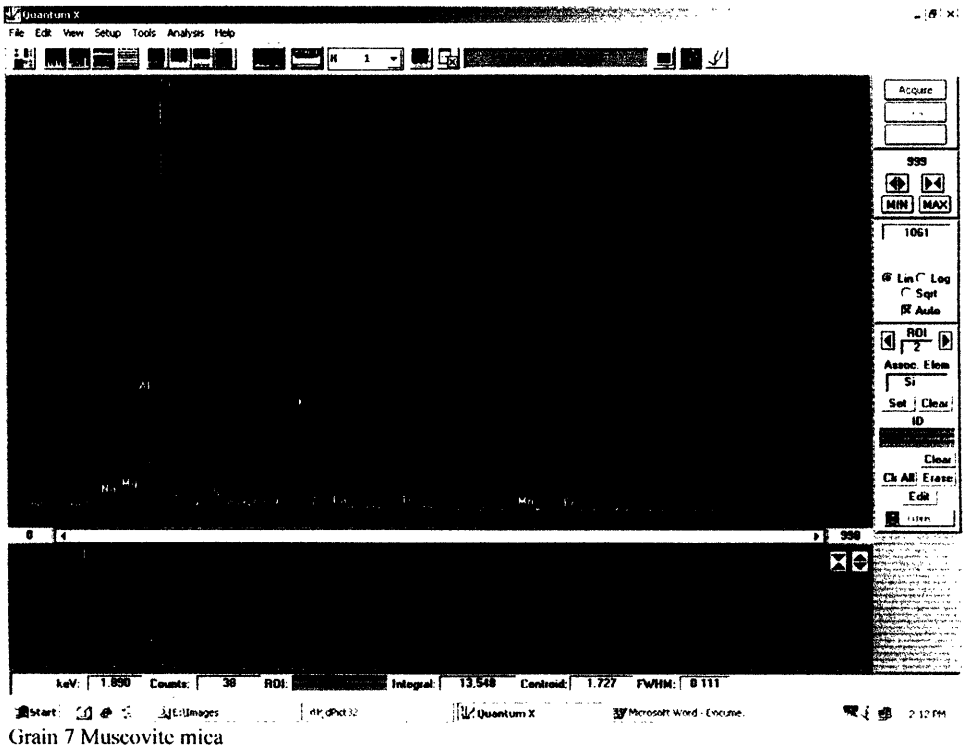

Grain 7 Muscovite mica

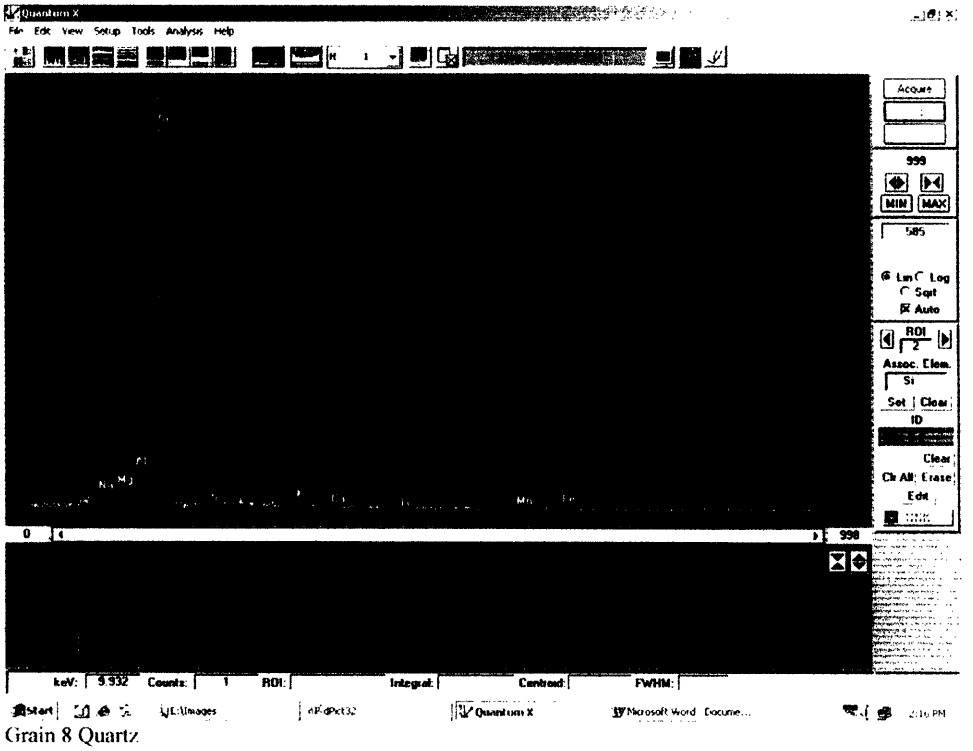

Grain 8 Quartz

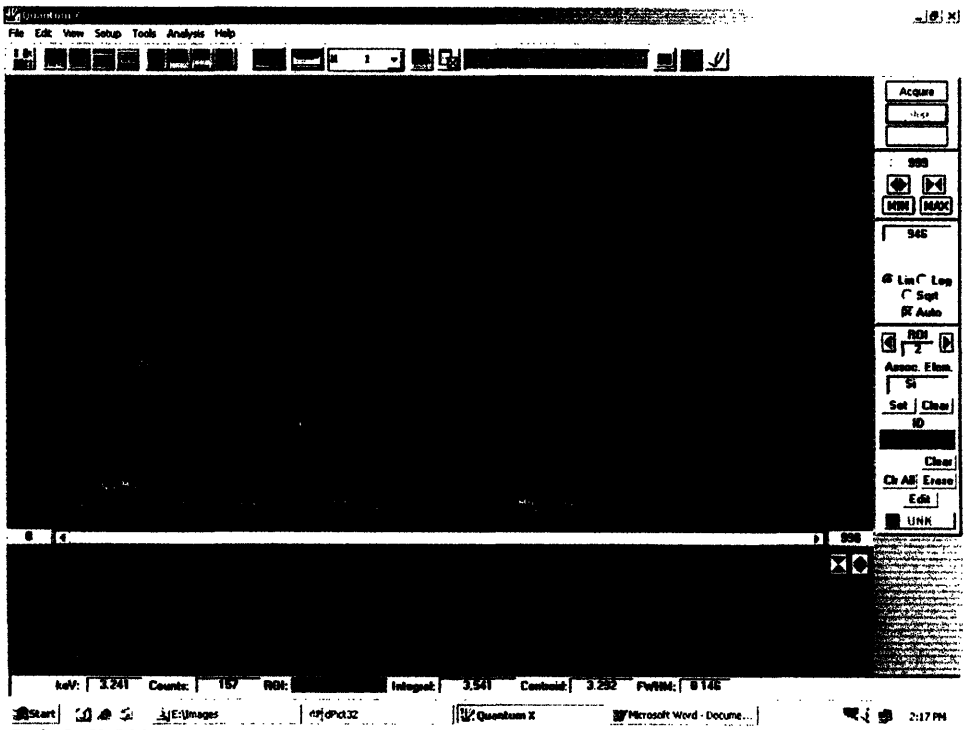

Grain 9a K-feldspar

Grain 9b Quartz

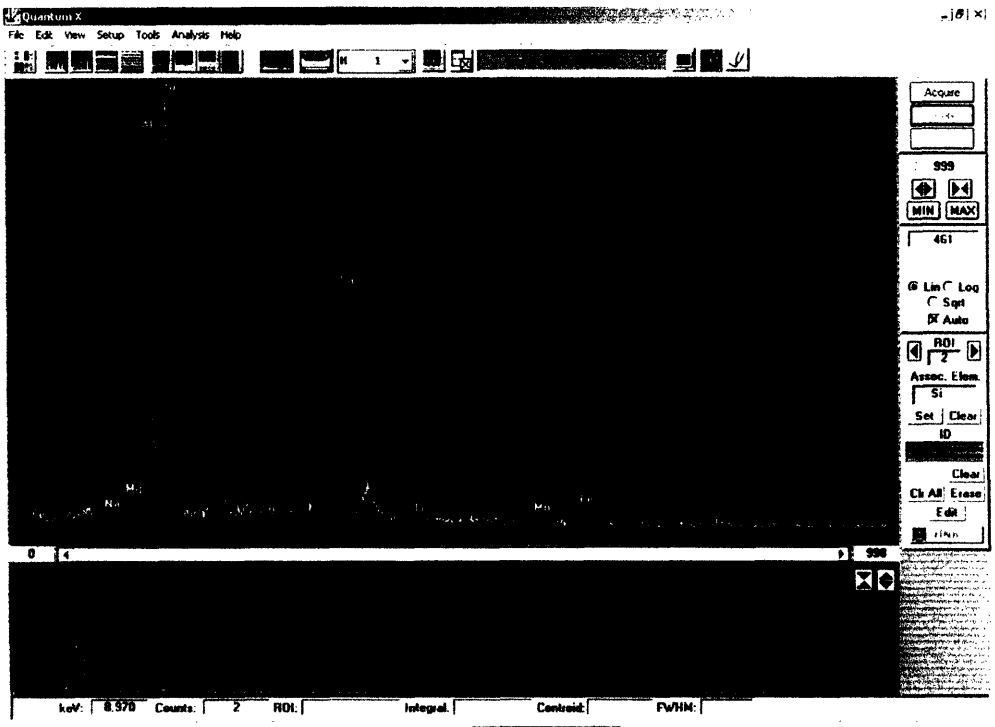

Grain 10a Epidote

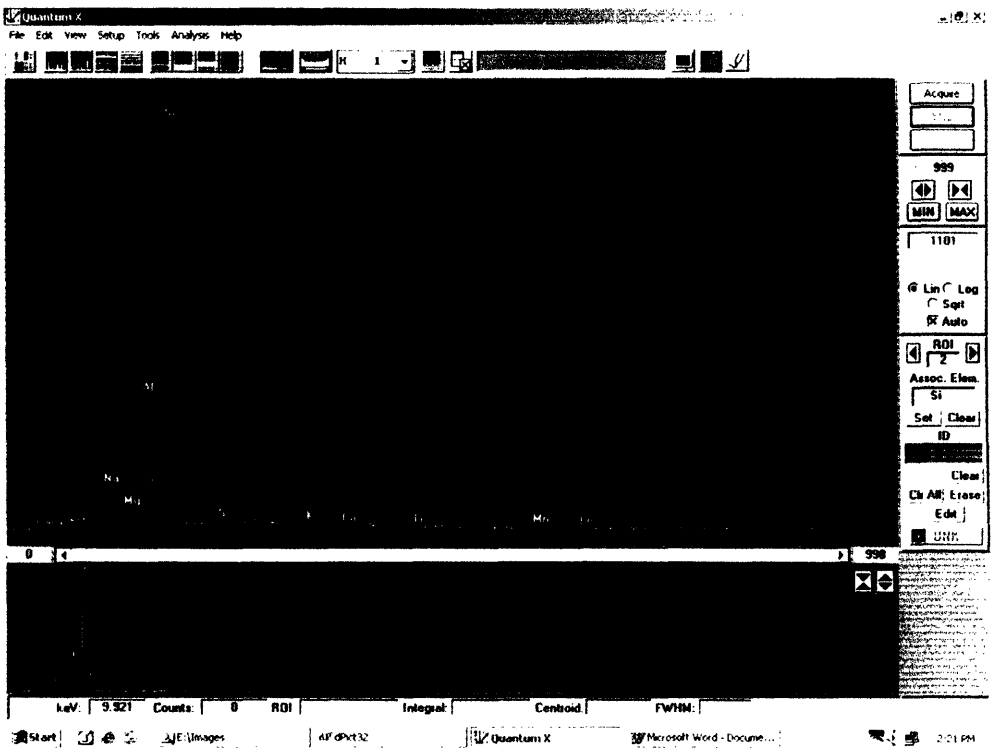

Grain 10b Albite (plagioclase feldspar)

MIT 5319

EDS Spectra

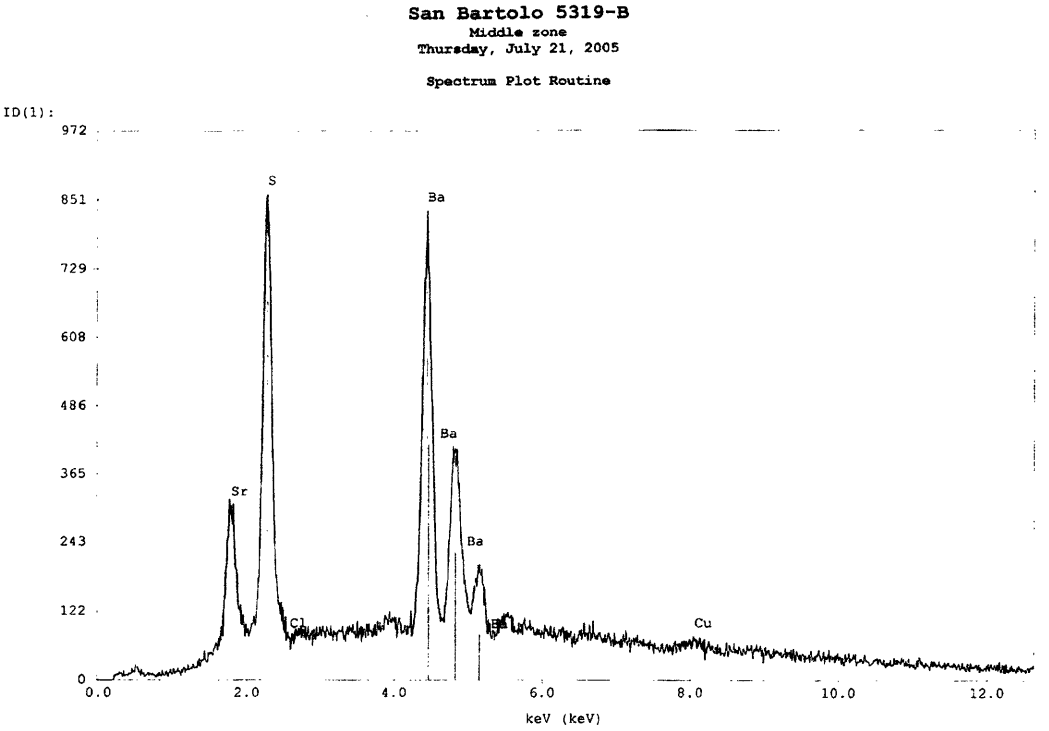

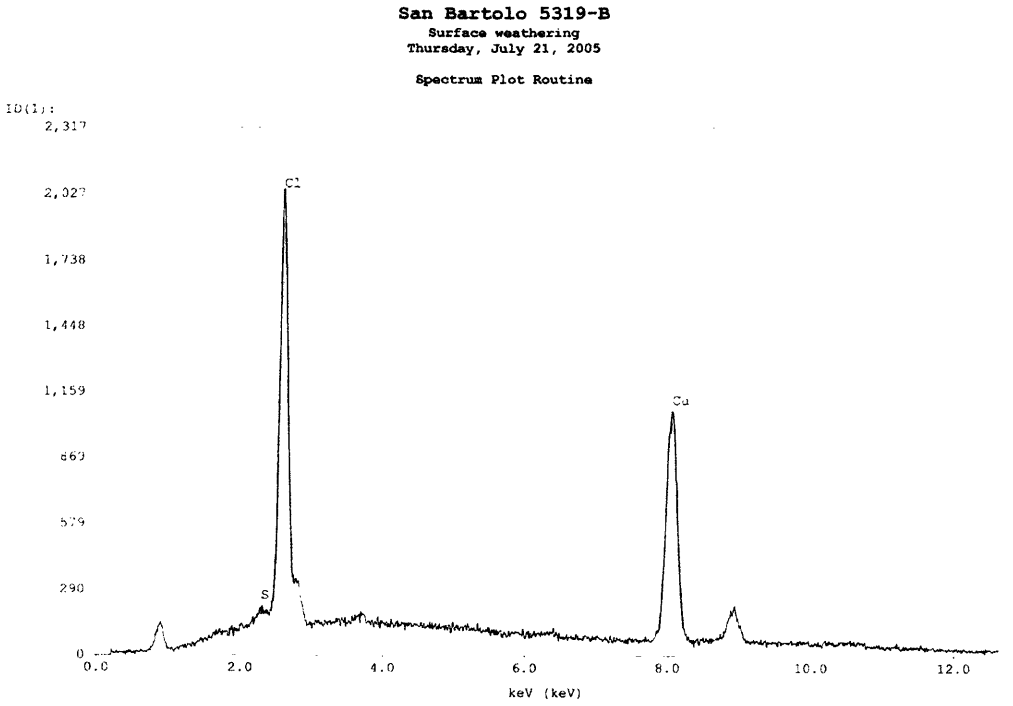

MIT 5318

EDS Spectra

San Bartolo MIT 5318-A
Zone 1: center of Cu-Fe sulfide
Tuesday, March 29, 2005

Spectrum Plot Routine

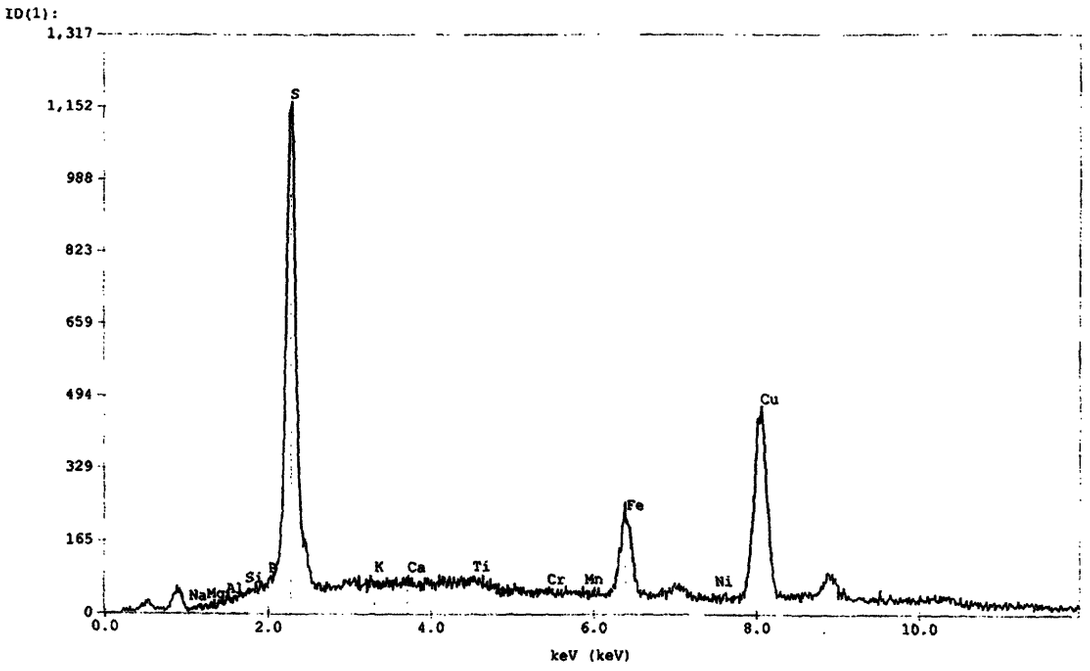

San Bartolo MIT 5318-A
Zone 1: large crystal in the slag matrix
Tuesday, March 29, 2005

Spectrum Plot Routine

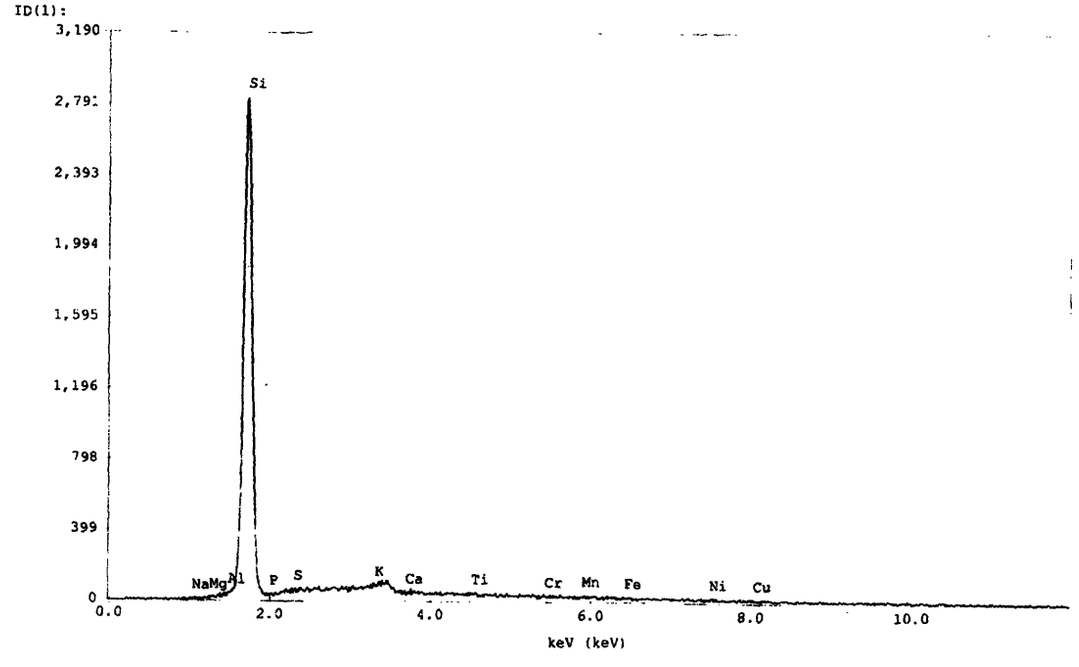

San Bartolo MIT 5318-A
Zone 1: non-crystalline slag matrix
Tuesday, March 29, 2005

Spectrum Plot Routine

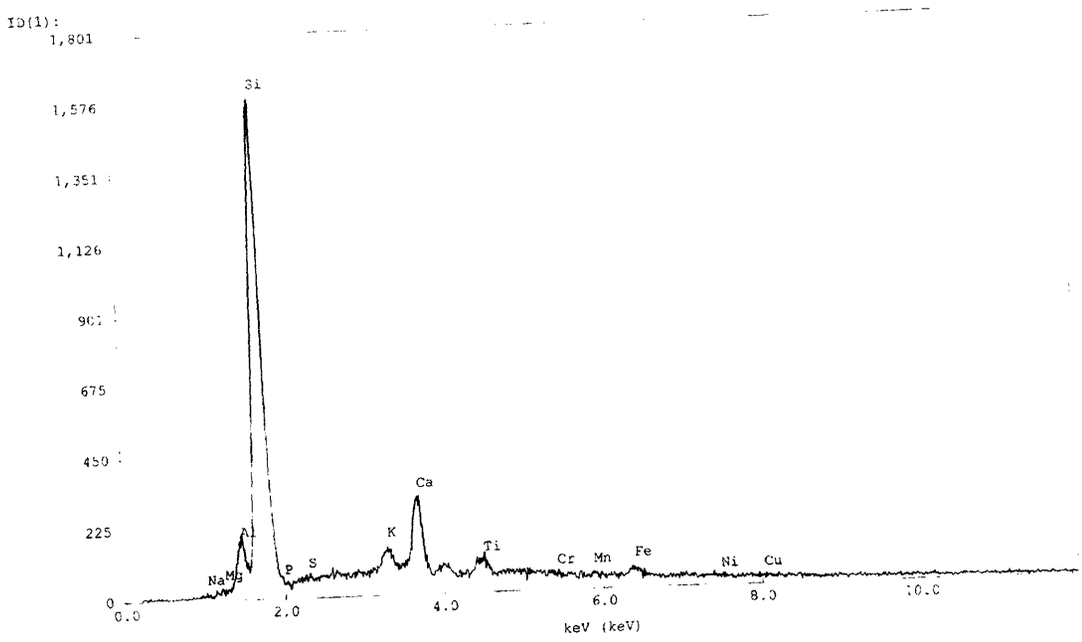

MIT 5316

EDS Spectra

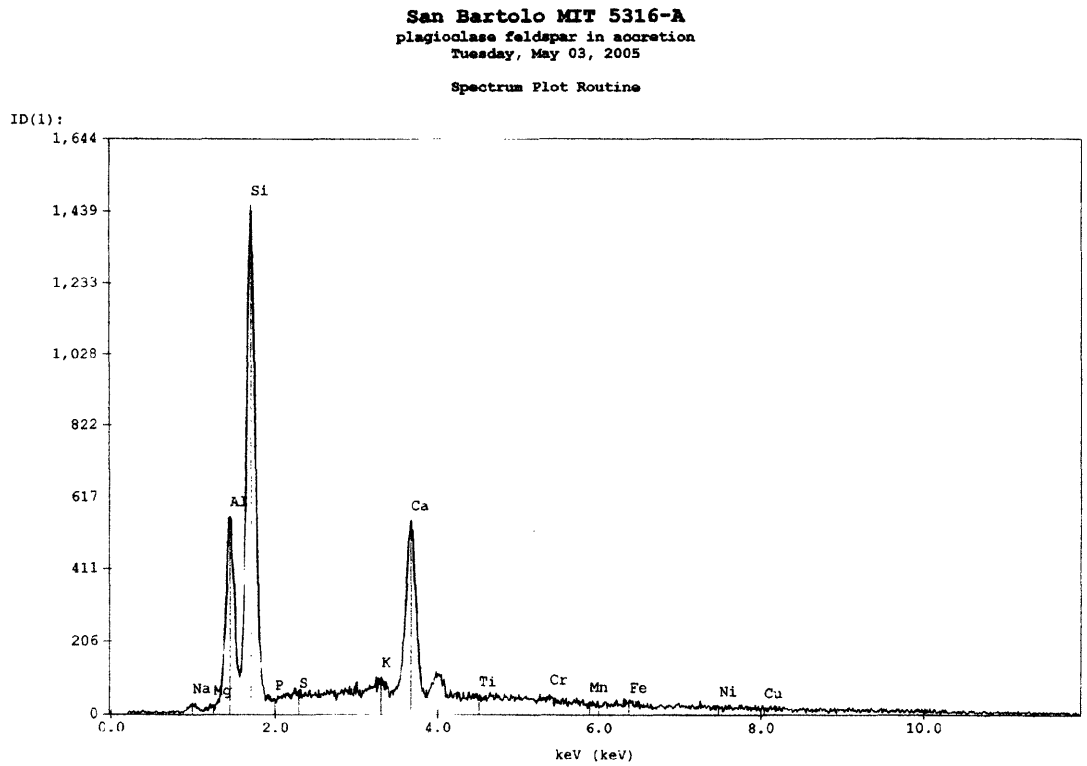

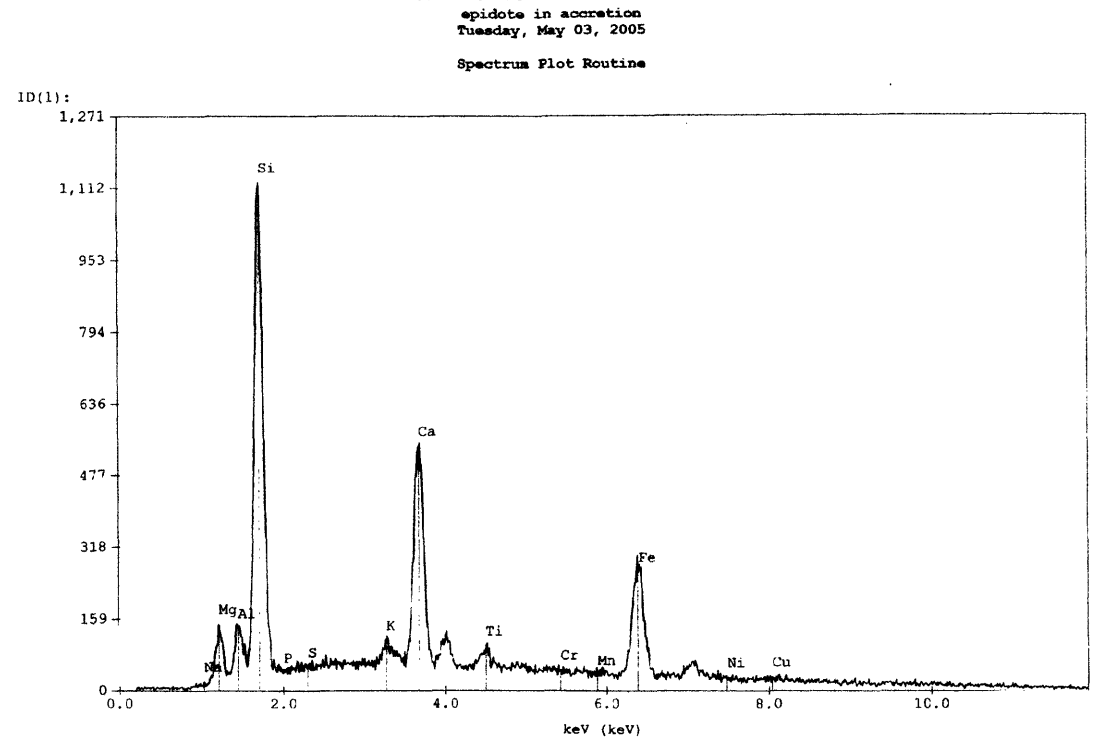

San Bartolo MIT 5316-A
dark band matrix
Tuesday, May 03, 2005

Spectrum Plot Routine

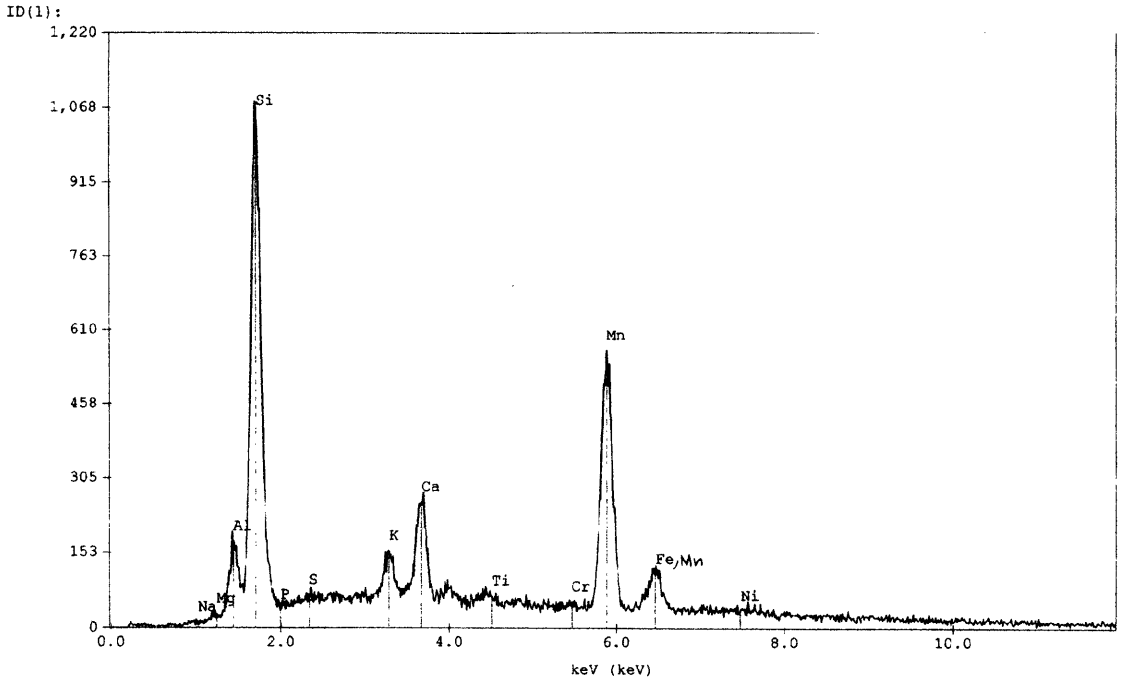

San Bartolo MIT 5316-A
light band matrix
Tuesday, May 03, 2005

Spectrum Plot Routine

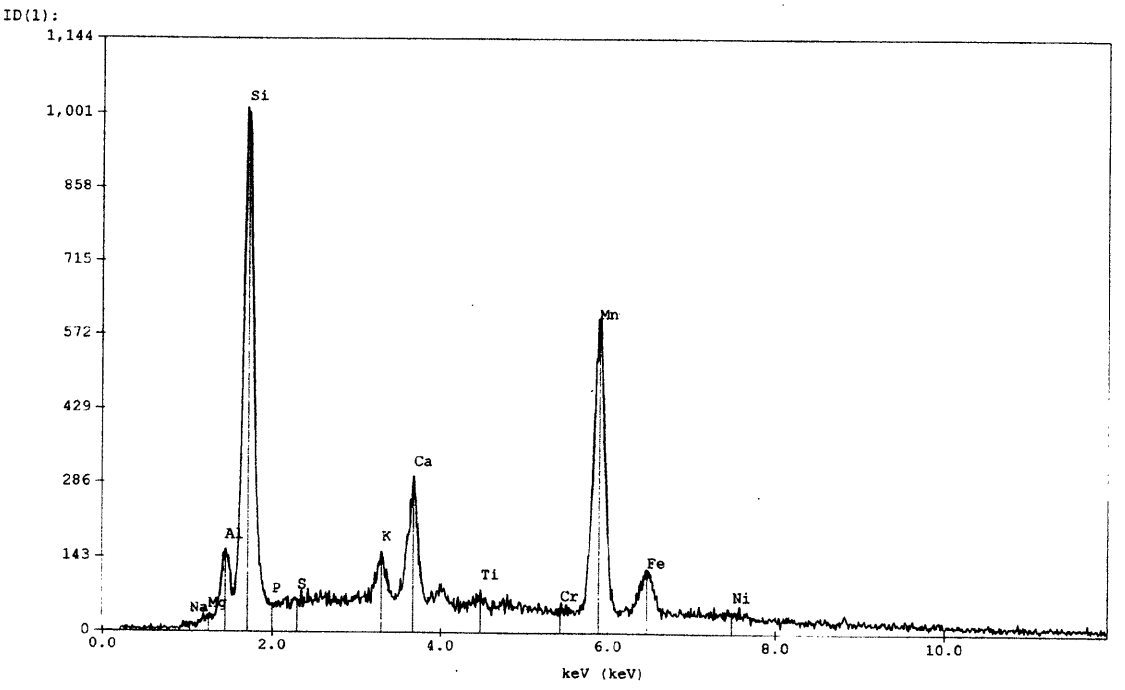

San Bartolo MIT 5316-A
Cu_2S ~~Cu~~-prill in light band matrix
Tuesday, May 03, 2005

Spectrum Plot Routine

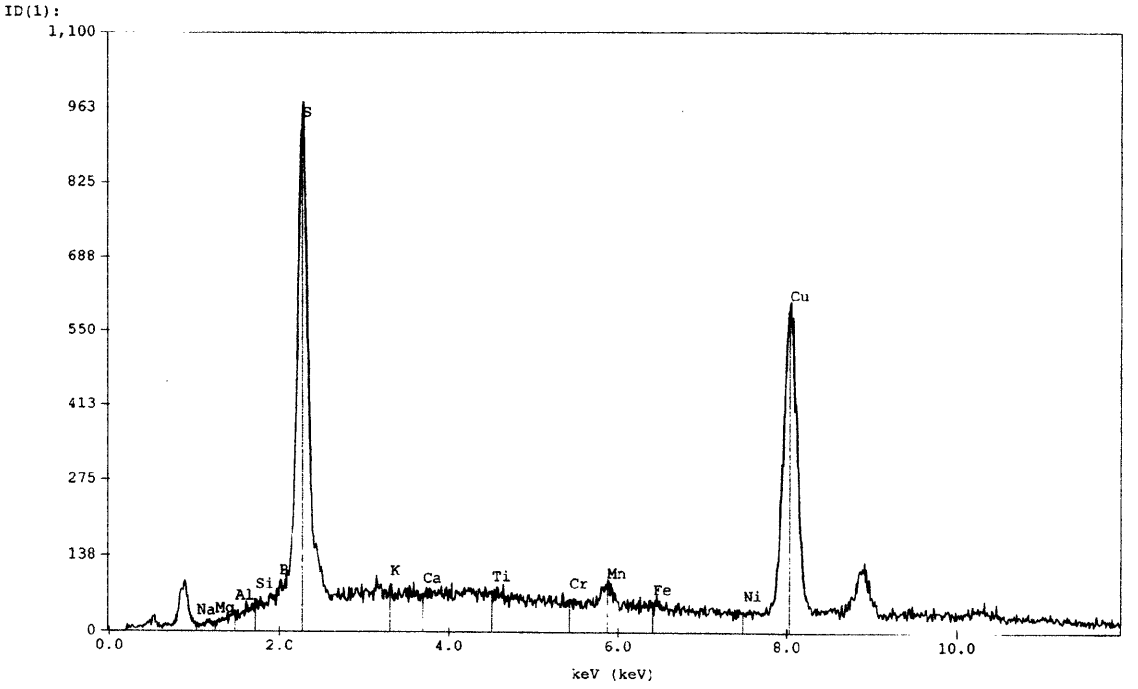

San Bartolo MIT 5316-A
center of large prill
Tuesday, May 03, 2005

Spectrum Plot Routine

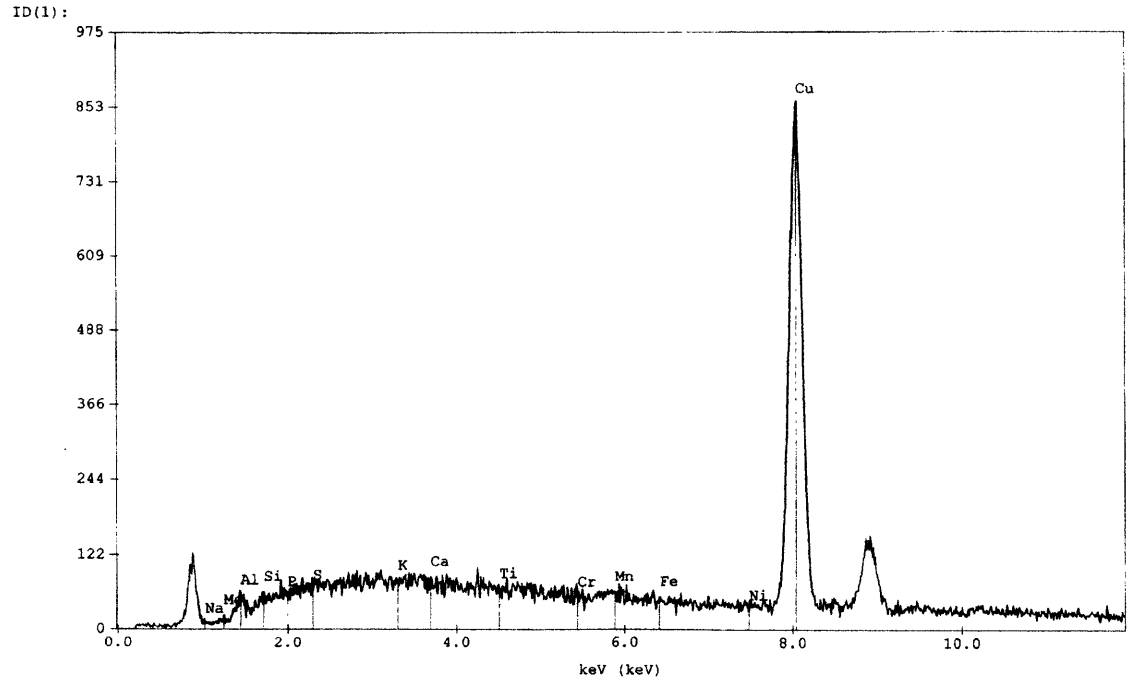

San Bartolo MIT 5316-A
edge of large prill
Tuesday, May 03, 2005

Spectrum Plot Routine

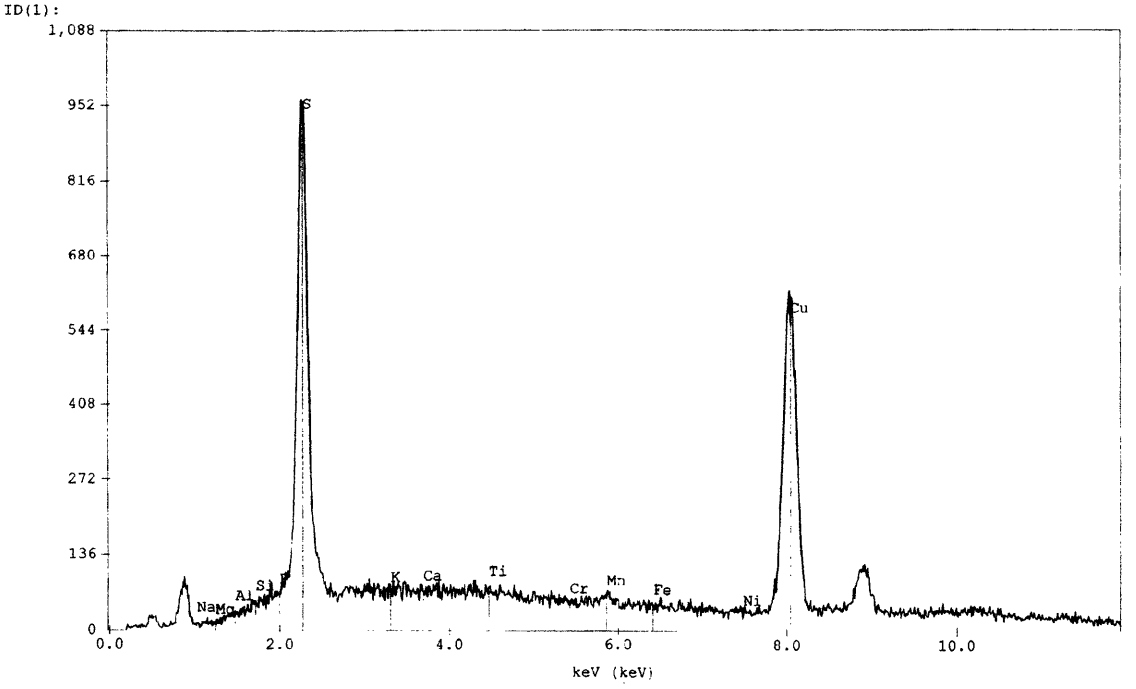

San Bartolo MIT 5316-A
ilmenite in accretion
Tuesday, May 03, 2005

Spectrum Plot Routine

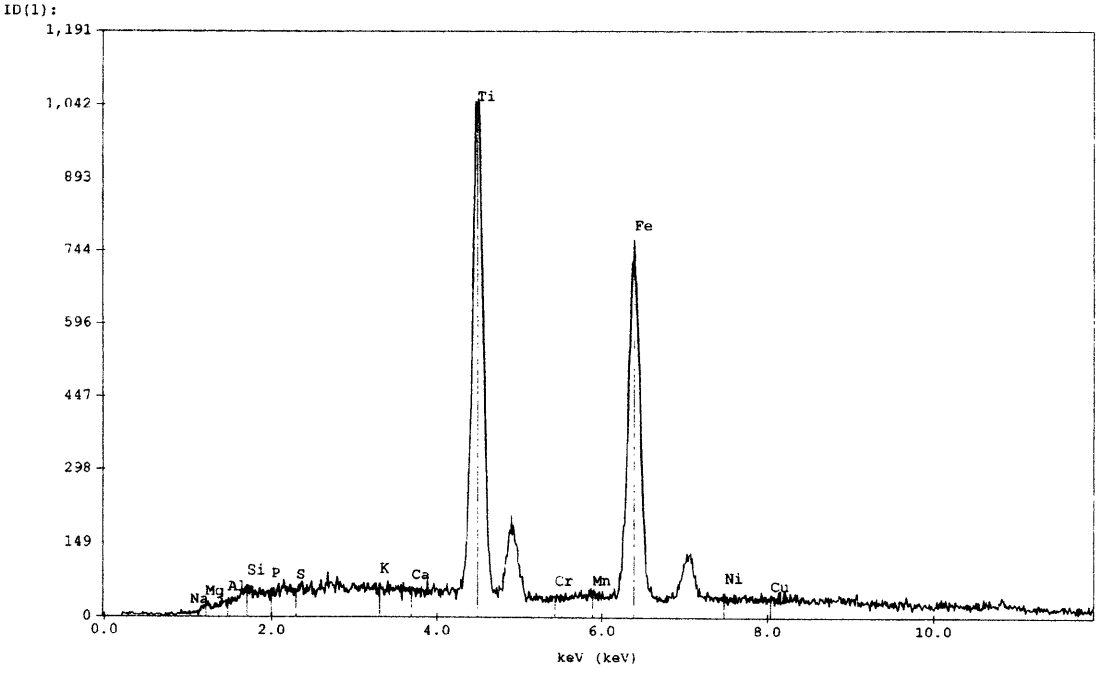

MIT 5320

EDS Spectra

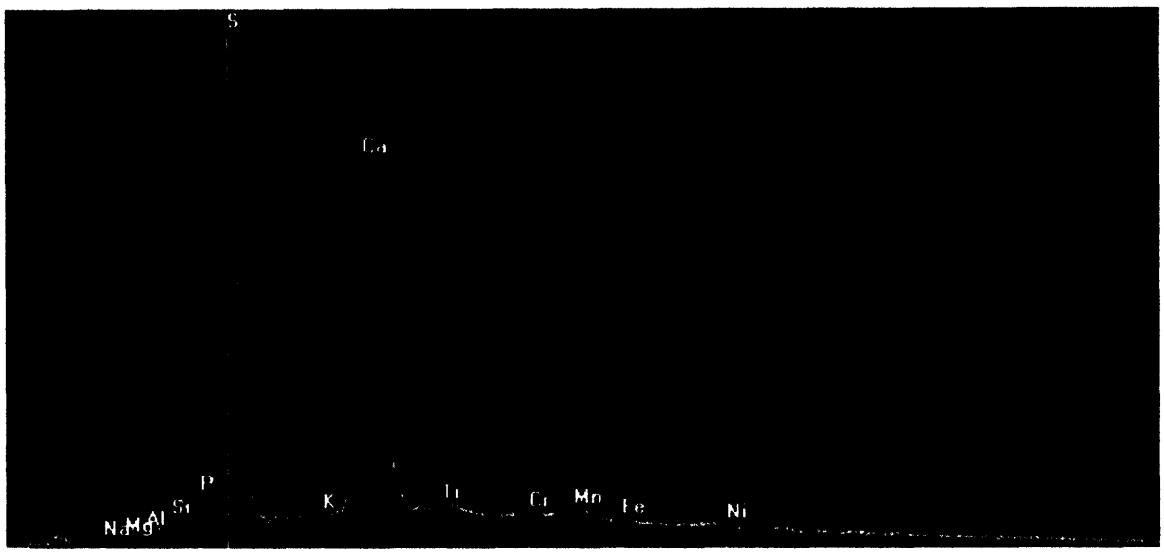

San Bartolo MIT5320-A EDS 1

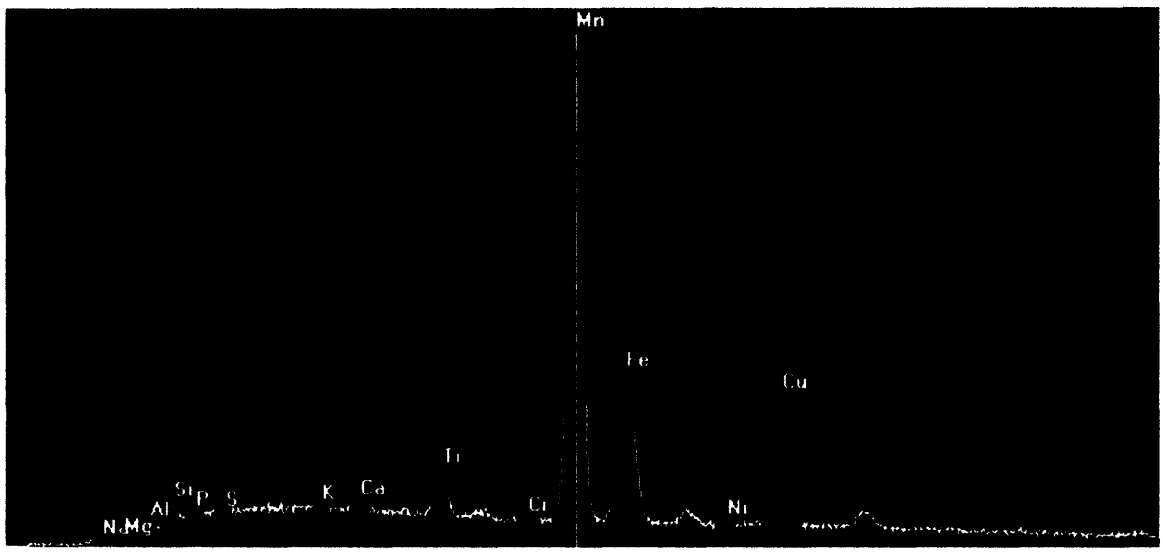

San Bartolo MIT5320-A EDS 2

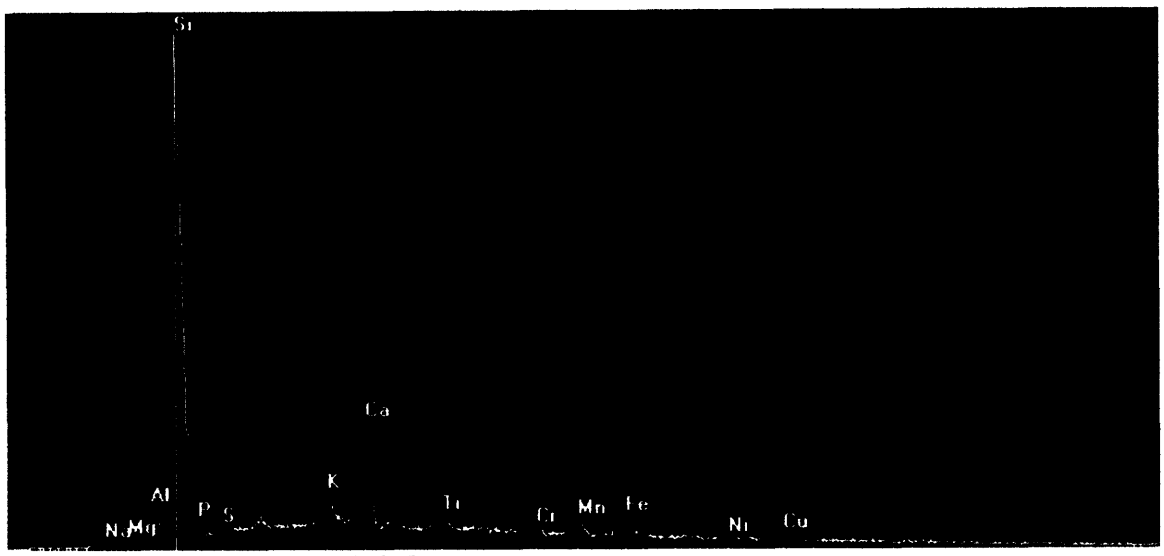

San Bartolo MIT5320-A EDS 5

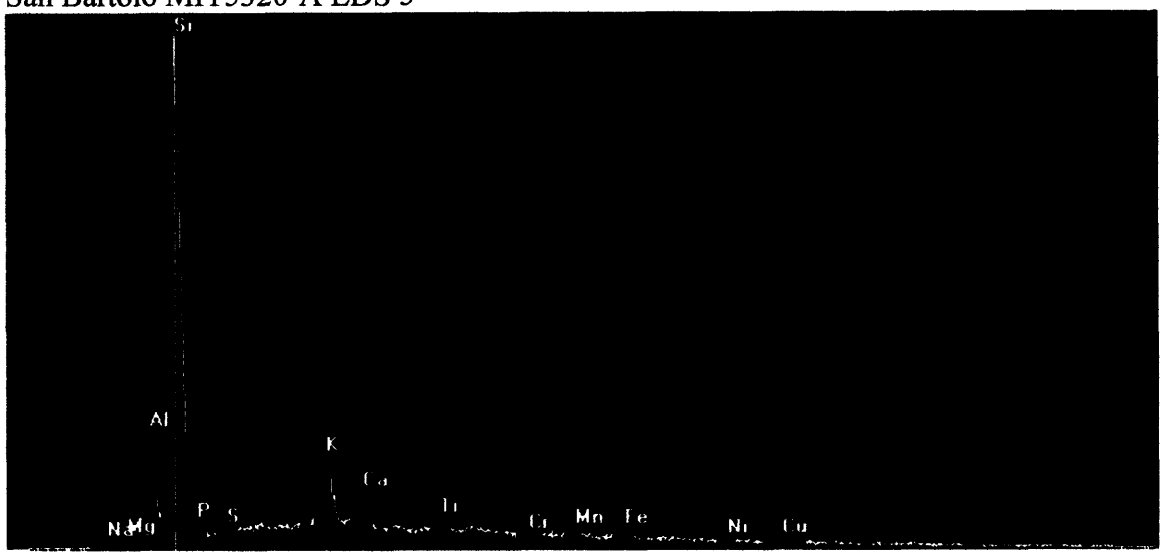

San Bartolo MIT5320-A EDS 6

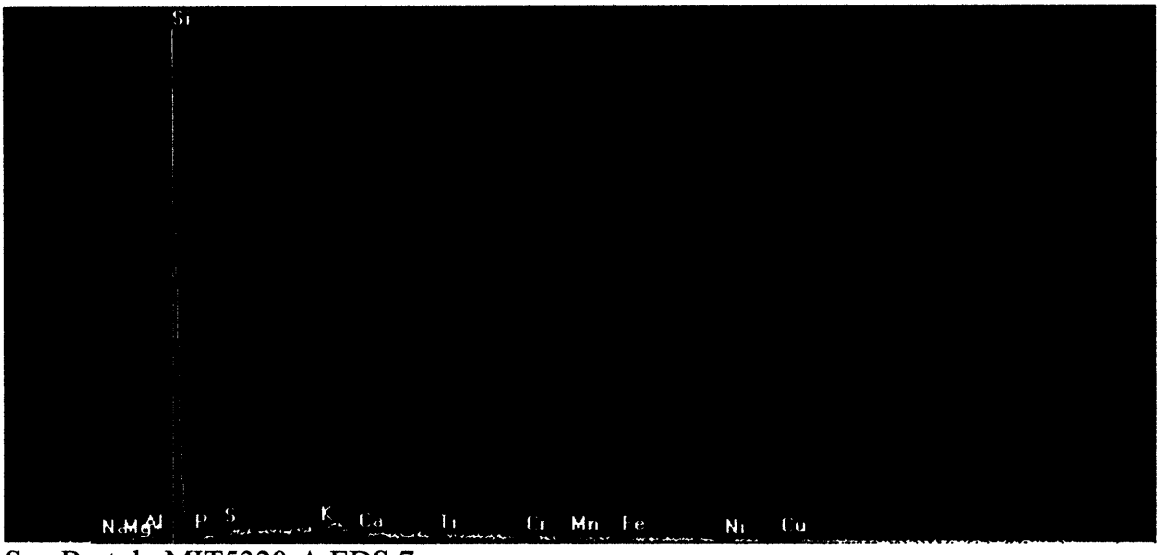

San Bartolo MIT5320-A EDS 7

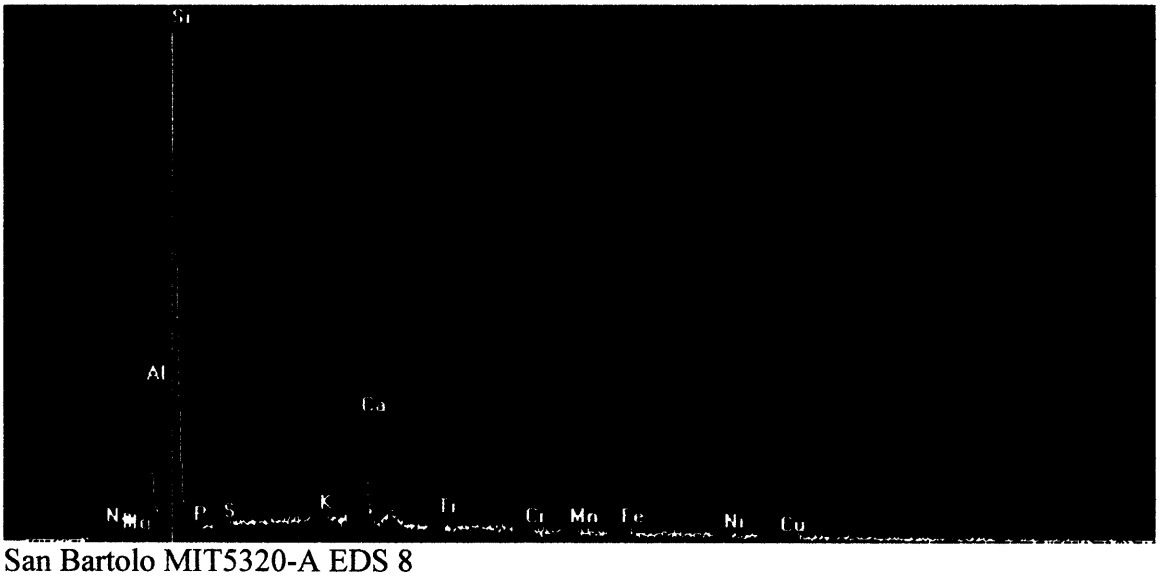

San Bartolo MIT5320-A EDS 8

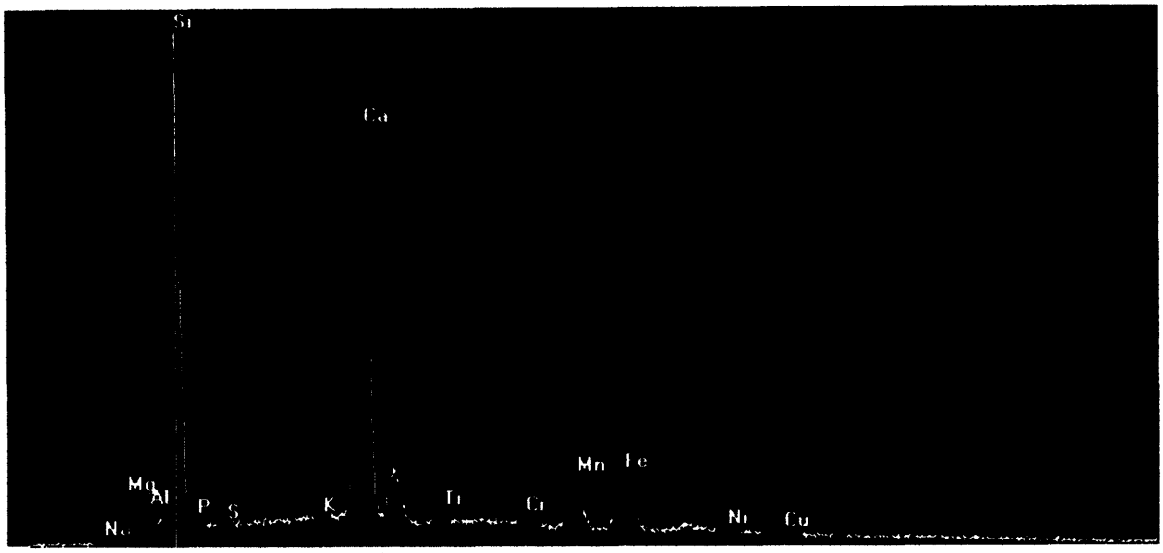

San Bartolo MIT5320-A EDS 9

San Bartolo MIT5320-A EDS 10